A Comparative Study of Stellarator and Tokamak Transport

U. Stroth

IPPIII/216

Nov. 1996

MAX-PLANCK-INSTITUT FÜR PLASMAPHYSIK

85748 GARCHING BEI MÜNCHEN

MAX-PLANCK-INSTITUT FÜR PLASMAPHYSIK
GARCHING BEI MÜNCHEN

A COMPARATIVE STUDY OF TRANSPORT IN STELLARATORS AND TOKAMAKS[1]

Ulrich Stroth

Max-Planck-Institut für Plasmaphysik, IPP-EURATOM
Association, Boltzmannstraße 2, 85748 Garching

IPPIII/216 **Nov. 1996**

[1]Submitted to Plasma Physics and Controlled Fusion

Die nachstehende Arbeit wurde im Rahmen des Vertrages zwischen dem Max-Planck-Institut für Plasmaphysik und der Europäischen Atomgemeinschaft über die Zusammenarbeit auf dem Gebiete der Plasmaphysik durchgeführt.

Contents

1 Introduction

Stellarators and tokamaks are the most advanced concepts for magnetic confinement of thermonuclear plasmas. The tokamak line has been developed to the verge of a fusion test reactor like ITER (REBUT *et al.*, 1995) and in the stellarator line, which has been pursued with less effort, the first large devices are being realized with LHD (FUJIWARA *et al.*, 1995) and W7-X (NÜHRENBERG *et al.*, 1995; GRIEGER *et al.*, 1991).

Both concepts have inherent beneficial and problematic features with respect to a fusion reactor and it is sensible to learn from comparisons about both the technical aspects and the physical processes present in the plasma. A common concern of stellarators and tokamaks on the way to a burning plasma is to obtain sufficiently good confinement properties for the stored plasma energy. The energy confinement determines the dimensions of devices and is therefore one of the key parameters in fusion research.

The scientific question relating to energy confinement is the understanding of transport in high-temperature plasmas. These plasmas are strongly driven systems far from thermodynamic equilibrium. The energy and particle transport losses are considered to be driven by turbulent processes. Although it is clearly observed that the plasma is not quiescent, the mechanism of the turbulence and its actual importance for transport are not yet known. Theoretically, the magnetic configuration influences turbulence in many aspects. Hence, a comparison of transport in devices as different as stellarators and tokamaks should reveal the importance of the magnetic field topology for transport.

A first extensive comparison was published four years ago in (WAGNER and STROTH, 1993) and is briefly summarized in the next section. This work is an extension and specifically builds upon the experimental findings collected since then. It concentrates on aspects where the author believes most progress in understanding has been made. Accordingly, the article treats the dependences of the energy confinement time on global (Section 5) and local parameters such as magnetic shear (Section 6), isotopic mass (Section 7), density (Section 8) and temperature (Sections 9, 10 and 11). An interesting question related is whether transport is exclusively determined by local plasma parameters or whether global effects can be important too (Section 12). An alternative access to anomalous transport, which is discussed in Section 13, is to measure the fluctuation amplitudes of plasma parameters.

As background for the evaluation of experimental results, short summaries are given of the differences in the magnetic configurations of stellarators and tokamaks (Section 3) and of the importance they have for theories on turbulent transport (Section 4).

2 Previous Conclusions

As a starting point, a short overview of the results from a first detailed comparison (WAGNER and STROTH, 1993) of transport in stellarators and tokamaks is given. At the end of this article some of the previous conclusions are revised, others substantiated to a greater extent.

In 1992, the results of a comparison of transport in the different devices could be summarized as follows:

Similarities in transport

- Transport processes parallel to the magnetic field lines are correctly described by neoclassical theory in both devices.
- Ion heat transport is consistent with collisional theory at least for stellarators and smaller tokamaks. An anomaly appears in larger tokamaks, where the collisionality can be lower.
- The radial electron thermal diffusivity is anomalously high compared with collisional transport and increases towards the plasma edge.
- The global energy confinement time is of comparable magnitude and shows similarities in the parametric dependence.
- The degradation of confinement with heating power is observed in all stellarator and tokamak regimes and in both devices problems are encountered in relating the observation to a local plasma parameter.

Differences in transport

- The tokamak electron temperature profile is resilient to changes in shape (*profile consistency*) and the density profile is more peaked then in stellarators. Anomalous energy and particle inward drifts (*pinches*) had to be postulated in order to explain the tokamak profiles. In stellarators, both the electron density and temperature profile respond to the particle and energy sources in a way such as expected from diffusive transport.
- Confinement in tokamaks shows a Bohm-like dependence on the gyro radius indicating the importance of long-scale turbulence. In stellarators, the electron thermal diffusivity and the confinement time scale gyro-Bohm-like, as expected from short-scale turbulence.
- Transient transport experiments in tokamaks point to the importance of energy pinches or a nonlinear dependence of the transport coefficient on the temperature gradient. For stellarators, strong pinches and a strong dependence of the transport coefficient on the temperature gradient could be excluded.

- In most tokamak regimes, a weak or no dependence of the confinement time on the density was observed. In contrast, the energy confinement time in stellarators increases with the density.
- The isotopic effect is observed in almost all tokamak regimes, whereas it is weak or absent in stellarators.

In summary, the picture of transport in stellarators seemed to be more orthodox than that of transport in tokamaks. Profile consistency, anomalous heat and particle pinches were not needed to explain the profiles and the puzzle of the isotopic effect was not present. The observed density dependence of the confinement time left room for a temperature dependence to explain the power degradation. On the other hand, there was striking similarity in the gross confinement properties and the power degradation was unexplained in stellarators too. This invited further experiments and a closer look into comparative studies.

3 Differences in the Magnetic Configurations

Determining the local parameter dependences of the transport coefficients is the goal of confinement studies in stellarators and tokamaks. The plasma density and temperature and the poloidal and toroidal magnetic fields can be varied and the influence on transport can be studied in single devices. Other parameters, however, are inherent to the device and in a single device they can only be varied in a very limited way. This is especially true of the magnetic configuration and the plasma current, the magnetic shear and the fraction of trapped particles. The configurations of stellarators and tokamaks differ very much in these parameters.

3.1 Size and Aspect Ratio

The geometrical parameters of stellarators and tokamaks are quiet different. The devices have comparable major radii (R) between 1 and 3 m but the minor radii (a) of tokamaks are much larger. In stellarators, the rotational transform is produced by external coils. In order to create sufficient twist of the field lines, the coils have to be close at the plasma and the minor radius must not be too large. For the stellarators, this results in aspect ratios R/a in the range from 5 (in CHS) to 12 (in (W7-AS). In tokamaks, the values are in the range from 2.5 (in JET) to 4 (in ASDEX). The definitions of the minor radius are different in the two devices, and in stellarator notation the aspect ratio of JET is only about 1.7. The minor radius enters confinement in a trivial way. At constant fluxes and gradients in density and temperature, the energy content increases with the size of the plasmas. But the aspect ratio also determines the number of trapped particles which are important for collisional and anomalous transport processes.

The total plasma volume of present-day stellarators is typically 1 to 3 m^3 while large tokamaks enclose a volume of 30 (TFTR) to more than 100 m^3 (JET). Hence, in a comparison of results from stellarators and tokamaks not only the magnetic configuration is different, one also compares large devices with small devices. Hence, for this study the results from smaller tokamaks like JIPP T-IIU or RTP are of special interest and the results from a collaboration between RTP and W7-AS will be emphasized.

A further geometrical difference is the shape of the plasma cross-section which is of relevance for the MHD stability of the plasma. In the 3dimensional stellarator configurations, the shape can change as a function of the toroidal angle. In heliotron/torsatrons it can be represented by an ellipse which rotates with toroidal angle. The cross-section of toroidally symmetric tokamak plasmas varies from circular to elliptical shapes with triangularity.

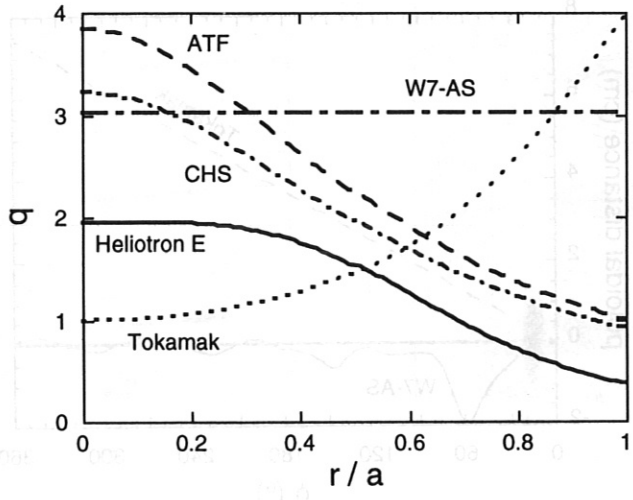

FIG. 1: Radial profiles of the safety factors of the ATF, Heliotron E and CHS heliotron/torsatrons, the W7-AS advanced stellarator and a tokamak.

3.2 Rotational Transform and Magnetic Shear

The strong toroidal plasma current and the inductive toroidal electric field in tokamaks are sources of free energy which are absent in stellarators. Tearing modes constrain the current profile which is linked to the temperature profile and the toroidal electric field is responsible for neoclassical convective transport, which is, however, small. These processes should not be dominant in transport of stellarators and can represent a major difference for the devices.

Magnetic shear has a stabilizing influence on macroscopic and microscopic instabilities. It also limits the radial extent of unstable modes. The global shear is a flux-surface-averaged parameter defined by the derivative of the safety factor q as

$$s = \frac{r}{q}\frac{\partial q}{\partial r} \; . \tag{1}$$

If shear plays a central role in the anomalous transport of high-temperature plasmas, it should lead to different levels of transport in stellarators and tokamaks. As shown in Fig. 1, the configurations have very different profiles of the rotational transform. Tokamaks normally operate with positive shear throughout the plasma cross-section. The shear in heliotron/torsatrons is reversed in relation with tokamaks, whereas it is very low in the stellarators of the Wendelstein line.

For the Wendelstein stellarators, the vacuum profile, as plotted in the figure, is modified to some extent by small contributions from ohmic, electron cyclotron resonance or neutral beam current drive and by the Pfirsch-Schlüter and neoclassical bootstrap currents. The global shear remains, however, small compared with that of tokamaks.

For the stabilization of micro-turbulence, the local shear is a critical parameter (WALTZ and BOOZER, 1993). It is related to the change of the local

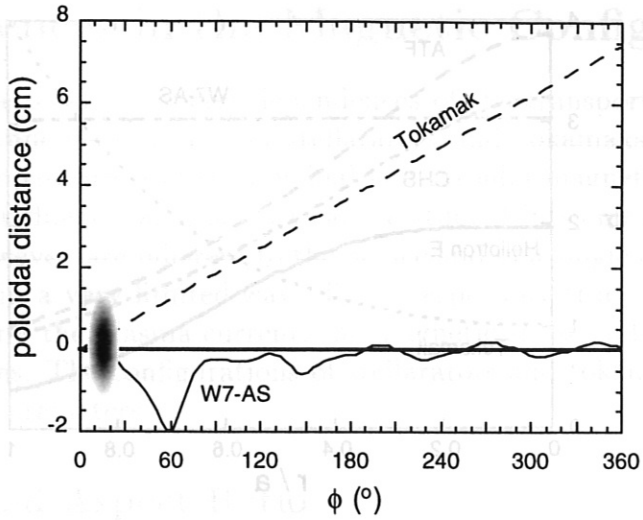

FIG. 2: Illustration of the local magnetic shear. Plotted is the the poloidal distance of two radially displaced field lines as a function of the toroidal angle. For the tokamak, a configuration equivalent to W7-AS at $\iota = 1/3$ in cylindrical approximation is used. The field lines are at $\rho \approx 0.8$ and are radially displaced by about 1 cm. A typical radial turbulence correlation length is indicated by the shaded area.

pitch angle of field lines with radius and determines the radial extension of the turbulence. In Fig. 2 the local shear of W7-AS at an rotational transform of $\iota = 1/3$ is compared with the shear of a comparable tokamak with $q = 1/\iota = 3$. Plotted is the poloidal distance of two field lines which depart at positions radially displaced by 1 cm. The local shear is related to the slope of the lines. It is shown that at some toroidal locations the local shear in W7-AS can exceed the tokamak shear. The maximum displacement of the field lines is comparable to the poloidal and radial correlation lengths of the turbulence, which are of the order of 1 cm (LIEWER, 1985). The total displacement of the field lines remains small, however, against the displacement found in tokamaks after one toroidal turn. In stellarators and tokamaks the influence of local and global shear on turbulence should be different and comparison of the different devices may yield information on the importance of shear for anomalous transport.

3.3 Trapped Particles

The three-dimensional stellarator magnetic field configurations do not only produce toroidally trapped particles, which are dominant in tokamaks, but also trapped particles in the helical ripples. In the long-mean-free-path regime, they make a major contribution to particle and heat transport. Distributed in a complicated way over regions of good and bad magnetic field curvature, they also act as a destabilizing agent of drift-wave turbulence. Details on the interaction of trapped particles and transport can be found in (CARRERAS *et al.*, 1988).

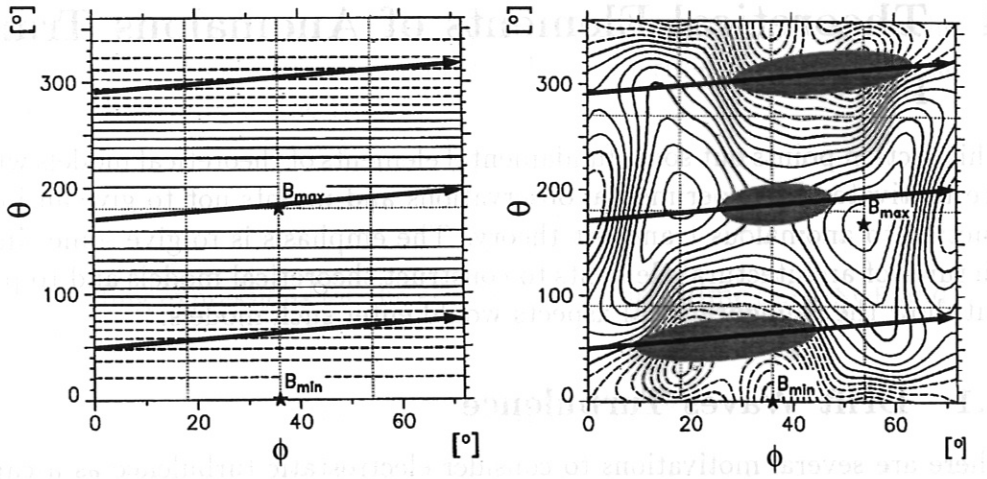

FIG. 3: Contour plots of the magnetic field strength on a $q = 3$ magnetic surface of a tokamak (left) and the W7-AS stellarator. A magnetic field line is plotted together with some regions where helically trapped particles are located. The maxima and minima of the field are marked by an asterisk.

Figure 3 shows the difference of the magnetic field on a flux surface in a tokamak and the W7-AS stellarator. Along a field line, particles in both devices can be trapped in the magnetic mirror between high- and low-field side. In W7-AS, the coils are in proximity of the plasma. They create additional helical magnetic traps. Trapped particles in these mirrors cannot travel from the upper side ($\theta = 90°$) to the lower side ($\theta = 270°$) of the plasma and can therefore be lost due to vertical drifts.

4 Theoretical Elements of Anomalous Transport

This section points out some fundamental elements of theoretical models which are motivated by experimental observations and intents not to give an introduction to anomalous transport theory. The emphasis is to give some simple pictures of architectural elements to construct theoretical models and to point out, how the configurational aspects would enter such models.

4.1 Drift Waves Turbulence

There are several motivations to consider electrostatic turbulence as a candidate for anomalous transport. From the theoretical side it is important that such modes are easy to destabilize, as they rely on free energy sources which are present in the plasma. An experimental motivation is that the empirical parametric scaling of the energy confinement time is similar to that derived from analytical drift wave models (CONNOR and TAYLOR, 1977; DOMINGUEZ and WALTZ, 1987; ROMANELLI and BRIGUGLIO, 1989). The models produce decreasing confinement times with increasing heating power through a temperature dependence. The experimentally observed current dependence is introduced through a dependence on magnetic field. Furthermore, the anomalous transport induced by $\tilde{\mathbf{E}} \times \mathbf{B}$ drifts leads to comparable diffusivities for the electron and ion heat as well as for the particle transport. This is consistent with experiments.

A comparison of the absolute values for the diffusivity gives reasonable agreements only in the plasma core. The observed increase of the diffusivities towards the plasma edge is not reproduced by the simple models. For realistic experimental testing of the theories, however, numerical simulations of the turbulent flow (SCOTT, 1992a) should be used in the future.

For the comparison of transport in different configurations, the stabilizing influence of magnetic shear and the destabilizing effect of trapped particles are important. It is, however, difficult to anticipate the influence of these parameters on results from full numerical simulations.

4.2 Beta Limit and Confinement

Due to unstable modes, the attainable ratio of plasma pressure to magnetic field pressure is limited by a critical value $\beta^{crit.}$. The β limit due to ideal ballooning modes increases with plasma current I_P and decreases with magnetic field B_t. It can be expressed in the form

$$\beta^{crit.} \sim \frac{I_P}{aB_t} \,. \tag{2}$$

It was suggested (CONNOR and TAYLOR, 1977) that the plasma takes notice of the value of $\beta^{crit.}$ already at β values at which the actually limiting instabilities

are predicted to be stable. Transport would increase as β approaches the critical value. Such a model is motivated by experiments, since an ansatz for the heat diffusivity of the form

$$\chi \sim \left(\frac{\beta}{\beta^{crit}}\right)^{3/2} \tag{3}$$

yields scaling expressions for the energy confinement time (CONNOR and TAYLOR, 1977)

$$\tau_E \sim a^{-0.1} R^{1.4} I_P^{1.4} P^{-0.7} n^{0.3}, \tag{4}$$

which are similar to the experimental ones.The model produces a weak dependence on minor radius and a strong one on major radius, it predicts the degradation of confinement with heating power P and shows only a weak dependence on density n. These properties agree with experiment.

A further corroboration of such an ansatz is the experimental observation that confinement improves when the value of $\beta^{crit.}$ increases. This was found, for example, in DIII-D where stability and confinement varied coherently in plasma shaping experiments and in discharges with more peaked current profiles (FERRON *et al.*, 1993).

A problem of such a model is that the modes, which are responsible for the β limit, should be stable in the regimes where the scaling is compared with experiment. Because of the similarities with experimental findings, however, it is worthwhile to investigate mechanisms, which can destabilize such modes below the critical value of ideal MHD. It was found, that resistivity could play this role at the plasma edge (CARRERAS and DIAMOND, 1989). A theory of self-sustained turbulence, based on micro-ballooning modes, was able to reproduce an impressive variety of the experimental confinement aspects (ITOH *et al.*, 1994a). This model has been also extended to transport in stellarators (ITOH *et al.*, 1994b) and it was found that the magnetic configuration and especially magnetic shear can have a strong impact on the obtained transport level.

4.3 Profile Consistency and Critical Gradient

The experimental observation that the electron temperature profile shape is strongly constrained in fusion plasmas is discussed in Section 10. Figure 4 illustrates the so-called profile consistency. It can be reduced to the observation, that the heat flux across the magnetic field can change dramatically in the absence of strong changes in the thermodynamic variables. This is reminiscent of the heat transport in fluids heated from below as investigated first by Benard (for an overview see (CHANDRASEKHAR, 1961)).

In these experiments, the heat transport mechanism changes at some critical parameter from conduction to convection. For liquids with different values of the viscosity this happens at different values for the temperature gradient,

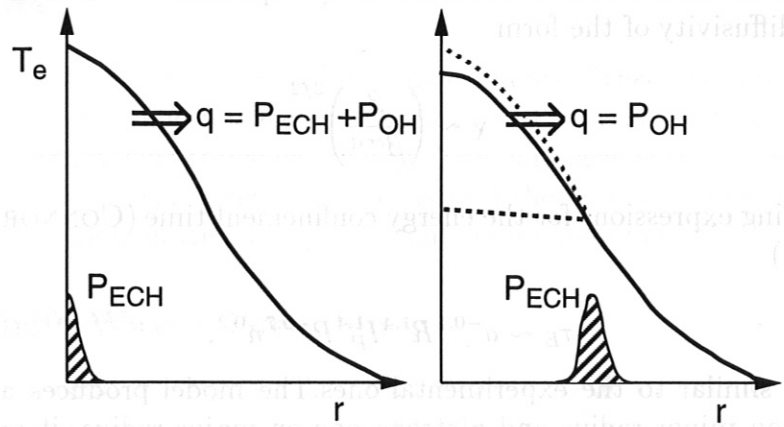

FIG. 4: Illustration of profile consistency. The profile on the left corresponds to central auxiliary heating P_{ECH} on a background of a small amount of inductive heating P_{OH}. The profile is radially peaked. On the basis of a typical diffusive model, the profile should flatten in the plasma center (represented by the dashed curve) when the heating location is moved outward. The observation is, in the contrary, only a minor change in the profile from the dotted to the solid line.

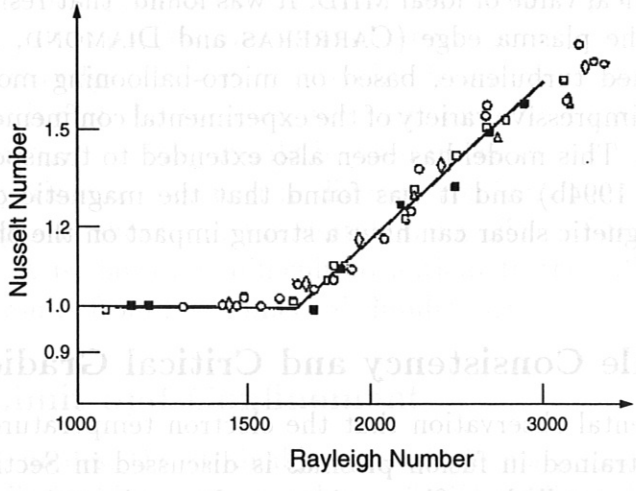

FIG. 5: The dimensionless heat flux (in terms of the Nusselt number) versus temperature gradient (in terms of the Rayleigh number) for a variety of liquids with very different physics parameters (different silicone oils, ethylene, glycol, heptane and water). Convective flow sets consistently in when the value of the critical Rayleigh number of 1700 is surpassed (adapted from (CHANDRASEKHAR, 1961)).

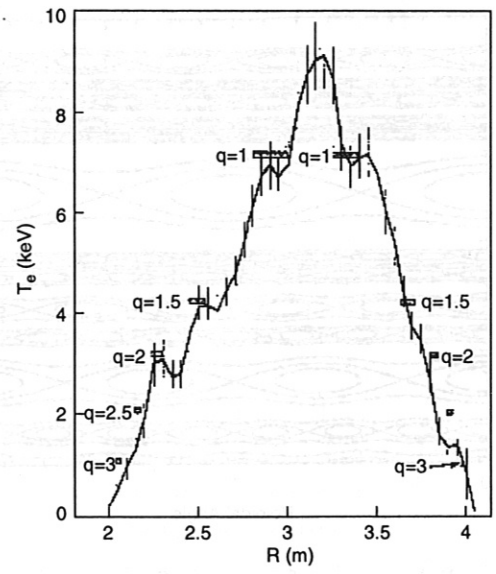

FIG. 6: Temperature profile from JET measured with the LIDAR system. The location of major rational values of the safety factor are indicated by boxes (adapted from (NAVE *et al.*, 1992)).

taken as the difference in temperature from above and below the liquid. If all data are plotted in terms of appropriate dimensionless parameters, they can be described in terms of two variables, the Nusselt number (proportional to the heat flux normalized to its value in the conductive regime) and the Rayleigh number (proportional to the temperature gradient). This is illustrated in Fig. 5.

The nonlinear dependence of the heat flux on temperature gradient leads to the desired resilience of the temperature profile. The comparison with fluid dynamics leads to the question whether high-temperature plasmas can be described in a similar way in terms of dimensionless parameters and whether the magnetic flux surfaces can be destroyed to some extent in order to allow for a convective flux (MONTGOMERY *et al.*, 1989).

A semi-empirical model along this line has been developed (REBUT *et al.*, 1989). The important element of this model is a critical temperature gradient above which anomalous transport is active. At gradients below the critical value, transport should be reduced to the neoclassical level. This results in a similar behavior of the heat flux in plasmas as shown in Fig. 5 for liquids. Since the model is related to rational q values and magnetic shear, it would predict an improved confinement level for shearless stellarators compared to tokamaks and can therefore be tested in a comparative study.

4.4 Structures in Profiles and Magnetic Islands

The magnetic flux surfaces can be destroyed most easily at locations with rational values of the safety factor q. Experimental indications for partial

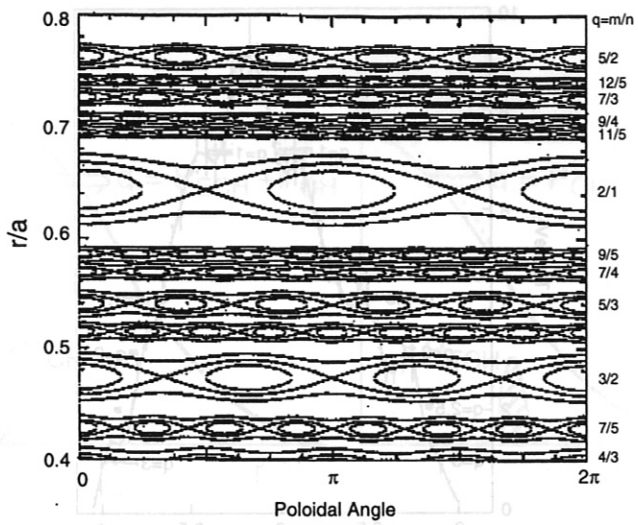

FIG. 7: A model with radial regions of good confinement alternated with regions with magnetic islands and low confinement (adapted from (CALLEN *et al.*, 1993)). Plotted are the obtained island chains as a function of minor radius.

destruction were deduced from dips in the light from the ablation clouds of pellets (PEGOURIE and DUBOIS, 1989) and from structures in the electron temperature profile as shown in Fig. 6 (NAVE *et al.*, 1992). Motivated by these observations, a model has been developed (CALLEN *et al.*, 1987b), which describes the magnetic configuration as alternating zones of good flux surfaces and magnetic island chains. Fig. 7 shows an example with island chains at the locations of rational q values.

Similar as the model of (REBUT *et al.*, 1989), the concepts using coupled chains of magnetic islands at rational values of the safety factor is cannot be directly applied to W7-AS where low-order rational q values can be avoided.

5 Scaling of the Energy Confinement Time

The energy confinement time is a global transport parameter which is very readily accessible by experiment. Defined as the plasma energy content W divided by the absorbed heating power P, it can be related to the thermal diffusivity χ through

$$\tau_E = \frac{W}{P - \frac{\partial W}{\partial t}} \approx \frac{a^2}{< \chi >}. \tag{5}$$

The electron and ion thermal diffusivities are combined in the radially averaged parameter $< \chi >$. At present, there is no theory which allows the energy confinement time to be deduced from first principles. Hence, empirical scaling expressions for τ_E are used as a normalization of the confinement quality of discharges. This allows one to compare discharges from different experiments and also to predict the performance of future devices. The expressions are derived from confinement databases with global parameters from different devices taken from discharges in comparable confinement modes. Typical parameters used are the minor and major radii a and R (in meters), line-averaged density $\bar{n}_e$ ($10^{19}\mathrm{m}^{-3}$), total absorbed heating power P (megawatts) and magnetic field strength B_t (tesla). For Tokamaks the total plasma current I_P (megamperes) is used, which is replaced by the rotational transform ι_a at the plasma edge in the case of currentless stellarators. The plasma shape is often described by the ratio κ of the elliptical half-axes.

5.1 Scaling of Tokamak Confinement

The most comprehensive sets of tokamak data in the different confinement regimes are stored in the ITER L- and H-mode global confinement databases. An updated version of the scaling expression for confinement in the low confinement mode (L-mode) (GOLDSTON, 1984) will be published in the near future (ITER DATABASE GROUP, 1995). At present, the ITERL89-P expression (YUSHMANOV *et al.*, 1990) is used as reference for this confinement mode:

$$\tau_E^{ITERL89P} = 0.038 \times a^{0.3} R^{1.2} P^{-0.5} \bar{n}_e^{0.1} B_t^{0.2} I_P^{0.85} M^{0.5}\,, \tag{6}$$

where the dependence on the isotopic mass M was added artificially. Under high confinement (H-mode) conditions (WAGNER *et al.*, 1982; BURRELL *et al.*, 1995), the global energy confinement time is also influenced by the ELM activity at the plasma edge. The intrinsic confinement is therefore best represented by the expressions for the thermal confinement time in the quiescent H-mode (ITER DATABASE GROUP, 1994), which is given by

$$\tau_E^{ITERH93P} = 0.036 \times a^{-0.11} R^{1.79} \kappa^{0.66} P^{-0.67} \bar{n}_e^{0.17} B_t^{0.32} I_P^{1.06} M^{0.41}\,. \tag{7}$$

The minor radius of tokamaks is defined as the small half-axis of the plasma cross-section and the plasma volume can be approximated by $V = 2\pi^2 a^2 \kappa R$. Typically, tokamak confinement strongly depends on major radius and not on the minor radius. The density and magnetic field dependences are weak and the current dependence is almost linear.

5.2 Scaling of Stellarator Confinement

The first inter-machine scaling expression for stellarators, the LHD scaling (SUDO *et al.*, 1990), was deduced from a rather limited number of data. A recent extended study published was based on a database comprising a total of 859 discharges from the ATF, CHS and Heliotron E heliotron/torsatrons and the W7-A and W7-AS shearless stellarators.

Within the stellarator line the differences are more pronounced than within the tokamak line. As discussed in Section 3, the devices differ most notably in the profile of the rotational transform and hence in the magnetic shear. Further differences are the fraction of trapped particles, the magnetic hill and the shape of the plasma cross-section. In spite of these differences, a common scaling for the stellarator L-mode confinement is given by the ISS95 expression (STROTH *et al.*, 1996b)

$$\tau_E^{ISS95} = 0.079 \times a^{2.21} R^{0.65} P_{tot}^{-0.59} \bar{n}_e^{0.51} B_t^{0.83} \iota_{2/3}^{0.4} \,. \tag{8}$$

This expression consistently describes the parameter dependences of heliotron/torsatrons and shearless stellarators. In order to obtain this fit, the heliotron/torsatrons have been allowed to lie on the average below the fit, and the shearless stellarator above it. The deviation which occurs is not larger than that in typical tokamak scaling studies.

A difference to tokamaks is the way in which the minor radius is calculated. For stellarators, it is defined via the plasma volume $V = 2\pi^2 a^2 R$. Because of the fundamental difference in the profile of the rotational transform (see Fig. 1) for heliotron/torsatron devices the radial position at which ι is calculated is important. For the ISS95 expression, the normalized radius of 2/3 was used, which lies in the confinement-relevant region of the steepest profile gradients. The scaling result did not depend crucially on this choice, but this value is important for the comparison with tokamaks. Stellarator confinement depends about quadratically on the minor radius and shows stronger density and magnetic field dependences.

5.3 Comparison of Global Confinement

In the form in which the scaling expressions for stellarators and tokamaks are traditionally written, the dependences on the geometrical parameters, the magnetic field and the plasma current are apparently different. A current dependence in the form used for tokamaks would predict vanishing confinement times for stellarators. Obviously, this is not true and for a realistic comparison the plasma current has to be rephrased by using (I_P in megamperes)

$$I_P = 5 \frac{a^2 B_t}{R} \frac{1+\kappa^2}{2} \frac{1}{q} \,. \tag{9}$$

If the current in the tokamak expressions is replaced by Eq. 9 in terms of q, the scaling expressions for stellarators and tokamaks become similar. Table 1 lists

Scaling	α_a	α_R	α_P	α_n	α_B	α_q	Ref.
Goldstone	1.63	0.75	-0.50	0.00	1.00	-1.00	(GOLDSTON, 1984)
Kaye-Goldstone	1.99	0.41	-0.58	0.26	1.15	-1.24	(KAYE and GOLDSTON, 1985)
ITER89P	2.00	0.35	-0.50	0.10	1.05	-0.85	(YUSHMANOV *et al.*, 1990)
ITERH90P	2.04	0.58	-0.47	0.00	1.17	-1.02	(CHRISTIANSEN *et al.*, 1992)
ITERH90P′	1.64	1.05	-0.57	0.10	1.46	-0.86	(CHRISTIANSEN *et al.*, 1992)
ITERH93P	2.01	0.84	-0.67	0.17	1.38	-1.06	(ITER DATABASE GROUP, 1994)
LHD	2.00	0.75	-0.58	0.69	0.84	0.00	(SUDO *et al.*, 1990)
ISS95	2.21	0.65	-0.59	0.51	0.83	-0.40	(STROTH *et al.*, 1996b)

TABLE 1: Coefficients of the most common scaling expressions for the energy confinement time in the tokamak L-mode (upper), tokamak ELM-free H-mode (middle) and stellarator L-mode (lower).

the dependences on the modified parameters for the most common stellarator and tokamak confinement expressions. Taking the variation of the coefficients from one tokamak scaling to another as a measure of accuracy, the stellarator expression reproduces most of the trends shown by the tokamaks.

Some differences remain in this global comparison. The confinement time of tokamaks depends less on the plasma density. This feature is the subject of Section 8. Both the q and the B_t-dependences are somewhat stronger in tokamaks. A stronger degradation of confinement with q in tokamaks is just the opposite of what one would expect from the reduced sawtooth transport at high q as well as from a more peaked current profile at high q values. On the other hand, the edge value of the safety factor is a crude parameter if the local magnetic field is relevant for confinement. Using q at a more transport-relevant radial position might also change the parameter dependence.

For the comparison of the absolute value of the confinement time, too, the radius at which q is evaluated is a crucial question. If the edge value q_a were used, scalings would predict an improvement in confinement of a factor of about 3 to 10 from a comparable q_a=5 tokamak in relation to Heliotron E with $q_a \approx 1/3$. Since confinement is not produced exclusively at the plasma edge, this is not realistic and the use of q at 2/3 of the radius seems more appropriate. For tokamaks, it is calculated from a profile of the form

$$q(\rho) = \frac{\rho^2}{1-(1-\rho^2)^4} q_a \,, \tag{10}$$

and for stellarators from

$$\iota(\rho) = \iota_a + (1-\rho^\gamma)(\iota_0 - \iota_a) \,, \tag{11}$$

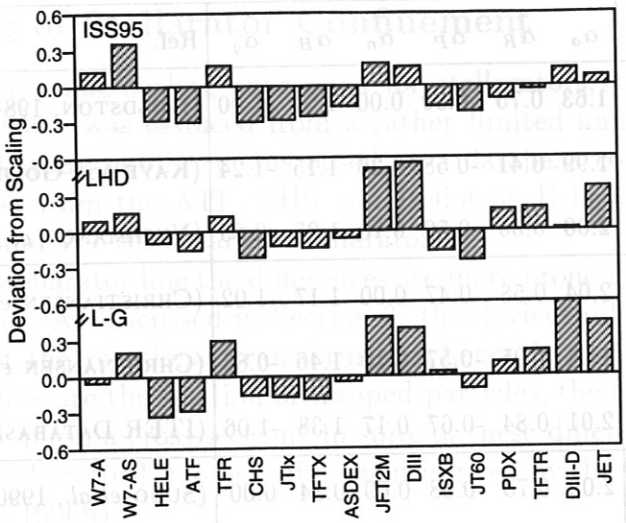

FIG. 8: $(\tau_E - \tau^{scal})/\tau^{scal}$ averaged over all discharges of each device from the databases in (STROTH *et al.*, 1996b). For τ^{scal} the predictions from the scaling expressions ISS95, LHD and L-G are used. The devices are ordered by ascending inverse aspect ratio. JTlx refers to JT60 with lower x-point and TFTX to aspect-ratio experiments in TFTR (adapted from (STROTH *et al.*, 1996b)).

with $\gamma = 2$, 3 and 4 for ATF, CHS and Heliotron E, respectively.

A further difference is the definition of the minor plasma radius. Since τ_E depends about quadratically on a, it will be crucial for the comparison to use the appropriate values. If stellarator data are used in a tokamak scaling expression, $a/\sqrt{\kappa}$ should be inserted instead of a. And if tokamak data are used in the stellarator expression ISS95, $a\sqrt{\kappa}$ has to be used.

A sensible comparison can be done on the basis of the Lackner-Gottardi (L-G) expression (LACKNER and GOTTARDI, 1990), where τ_E scales with $a^2\kappa$. In this case it is consistent to use $\tau_E \sim a^2\kappa$ for tokamaks and $\tau_E \sim a^2$ (with $\kappa = 1$) for stellarators. The Lackner-Gottardi expression in the alternative notation reads

$$\tau_E^{L-G} = 0.68 \times 0.0627 \times a^2 R P_{tot}^{-0.6} \bar{n}_e^{0.6} B_t^{0.8} q_{2/3}^{-0.4} \,. \qquad (12)$$

The additional factor 0.68 was obtained by adjusting the scaling expression to the center of gravity of a combined stellarator-tokamak dataset (STROTH *et al.*, 1996b). Since $q_{2/3}$ was used instead of q_a, this adjustment was necessary.

A comparison of stellarators and tokamaks on the basis of different scaling expressions is shown in Fig. 8. Plotted is the average for each device on the basis of various scaling expressions. The data are from L-mode stellarator and tokamak databases. On the average, the different expressions describe both stellarators and tokamaks with similar quality. The LHD expression reproduces almost exactly the center of gravity of the combined dataset. On the basis of the L-G expression, the quality of W7-AS confinement is similar to the average tokamak confinement. The heliotron/torsatron devices are on the level of the lowest tokamaks.

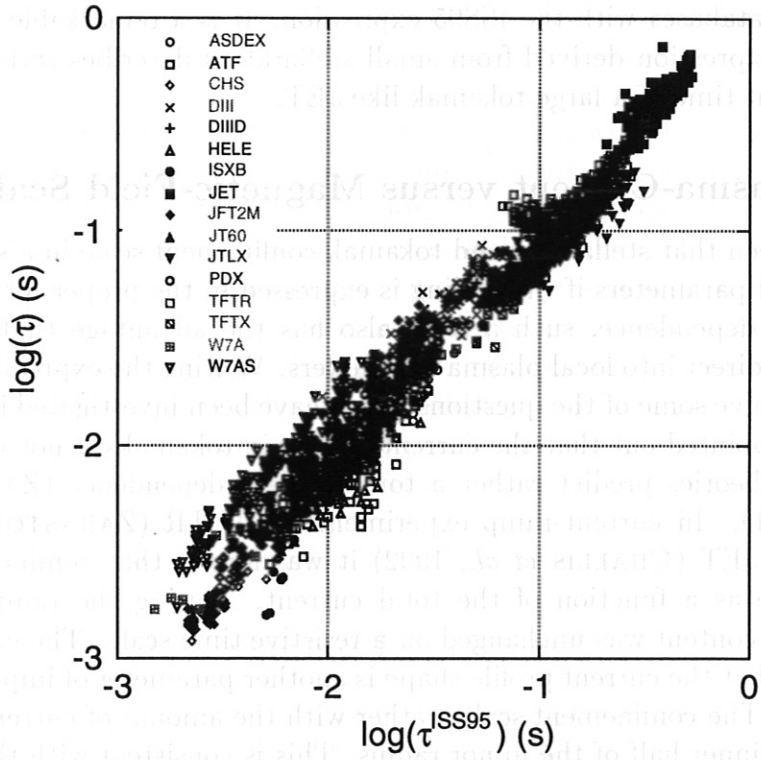

FIG. 9: τ_E versus the prediction from the ISS95 expression (Tab. 7) for this database and tokamaks from the ITER L-mode database (adapted from (STROTH *et al.*, 1996b)).

The stellarator expression ISS95 describes stellarators and tokamaks equally well. Deviations from the scaling expressions of up to 40% of the energy confinement time are observed. Similar deviations are also present if the ITERL89-P expression is applied to this tokamak L-mode dataset. The scatter of the stellarators around the fit is about the same as for the tokamaks. The difference between the ISS95 and the L-G expressions can be expressed as an additional aspect ratio dependence like $(R/a)^{0.25}$. This favors the tokamaks in relation to the stellarators and can also be seen in the figure, where the devices are arranged by aspect ratio. The aspect ratio ranges from 2.5 in JET to about 12 in W7-AS.

Figure 9 shows a detailed comparison of all data from the stellarator and tokamak databases with the ISS95 expression. It is a remarkable result that a scaling expression derived from small stellarators describes rather well the confinement time of a large tokamak like JET.

5.4 Plasma-Current versus Magnetic-Field Scaling

We have seen that stellarator and tokamak confinement scale in a similar way with global parameters if the scaling is expressed in the proper form. Besides the power dependence, such a form also has the advantage that it can be translated direct into local plasma parameters. Writing the expressions in this form can solve some of the questions which have been investigated in the past:

It was pointed out that the current scaling in tokamaks is not understood and that theories predict rather a toroidal field dependence (ZARNSTORFF *et al.*, 1991). In current-ramp experiments in TFTR (ZARNSTORFF *et al.*, 1991) and JET (CHALLIS *et al.*, 1992) it was found, that confinement does not change as a function of the total current. During the ramping phase the energy content was unchanged on a resistive time scale. The experiments indicated that the current profile shape is another parameter of importance for transport. The confinement scales rather with the amount of current enclosed within the inner half of the minor radius. This is consistent with the poloidal magnetic field being the relevant local parameter. Other evidence can be found from experiments in DIII-D, where confinement increases with a peaking of the current profile (l_i) (FERRON *et al.*, 1993).

According to simple considerations leading to Eq. 5, a quadratic dependence of the confinement time on the minor radius is expected. In order to clarify the strong major and weak minor radius dependences in tokamaks, dedicated size scans were carried out in TFTR (GRISHAM *et al.*, 1991). The results confirmed the weak dependence of the common scaling expressions. However, the parameters a, R, I_P, B_t and q cannot be decorrelated. The actual confinement scaling one observes depends on the direction of the scan through this five-dimensional parameter space. A major radius scan was done at constant a, q and I_P. The observed strong dependence on R can therefore also be described as a sum of the dependences on R and B_t. In the DITE tokamak, the minor radius was varied by a movable limiter (COTTRELL *et al.*, 1984). This

was done at constant plasma current. Hence, it was a combined a and q scan and the effects of both dependences can cancel in a way to produce a confinement time, which seems independent of minor radius, as it was observed in DITE.

It is therefore useful to include stellarator data in the comparison in order to decorrelate q from I_P and B_t, and an expression of the form of Eq. 8 seems to be a more natural parameterization of global confinement.

5.5 Stellarators in Tokamak Operation

In small stellarators, the transition from stellarator to tokamak operation was carried out explicitly. During ohmically heated discharges at constant plasma current the external contribution to the rotational transform was modified. Experiments of this type in Cleo (ATKINSON *et al.*, 1977) and W7-A (W7-A TEAM, 1977) showed that the energy content increases with increasing external transform. Discharges with the same amount of plasma current but with higher values of the external rotational transform have longer energy confinement times. In W7-A, the stellarator discharges with an external contribution of about 50% showed longer confinement times than the almost pure tokamak discharges with an external contribution to the transform of about 10% (W7-A TEAM, 1977). In terms of a tokamak scaling expression, which depends only weakly on the magnetic field, this is contradictory. But the results confirm the expression in stellarator notation, which predicts improvement of confinement with increasing toroidal field and rotational transform or decreasing q. The poloidal field seems to improve confinement in the same way independently of whether it is generated by external coils or by a plasma current.

5.6 Dimensionless Scaling Expressions

The above analyses were done in terms of engineering variables. For comparing with theoretical models, it would be desirable to have also the parametric dependences on physics variables. In particular, one would like to see the heating power replaced by a local quantity such as the temperature, which can be expressed in terms of the plasma energy content. The leading dimensionless variables used in such studies are the gyro-radius normalized to the machine size ρ_*, the collisionality ν_* and β.

The transformation of a scaling expression of the form $\tau \sim a^{\alpha_a} P^{\alpha_P} n^{\alpha_n} B^{\alpha_B}$ (to use this formula, the plasma current dependence must be transformed into a q dependence) into a dimensionless expression of the form $\tau/\tau^B \sim a^{\alpha^a} \rho_*^{\alpha^\rho} \beta^{\alpha^\beta} \nu_*^{\alpha^\nu}$ can be done with the help of

$$\alpha^a = \frac{\frac{1}{2}\alpha_P - 2\alpha_n - \frac{5}{4}\alpha_B + \alpha_a + \alpha_R}{1+\alpha_P} - \frac{5}{4}, \tag{13}$$

$$\alpha^\rho = \frac{-3\alpha_P - 2\alpha_n - \frac{6}{4}\alpha_B}{1+\alpha_P} + \frac{1}{2}, \tag{14}$$

scaling	α_a	α_ρ	α_β	α_ν
Goldstone	0.51	0.50	-0.75	-0.25
Kaye-Goldstone	-0.89	-0.70	-0.52	-0.24
ITER89P	-0.08	-0.05	-0.53	-0.28
ITERH90P	-0.49	-0.15	-0.53	-0.36
TERH90P'	-0.37	-1.08	-0.66	-0.44
ITERH93P	0.11	-0.71	-1.23	-0.28
LHD	-1.17	-1.64	0.32	-0.06
ISS95	-0.01	-0.71	0.16	-0.04

TABLE 2: The most common scaling expressions for the energy confinement time in the tokamak L-mode (upper), tokamak ELM-free H-mode (middle) and stellarator L-mode (lower) in terms of dimensionless parameters.

$$\alpha^\beta = \frac{\frac{3}{2}\alpha_P + \alpha_n + \frac{1}{4}\alpha_B}{1+\alpha_P} + \frac{1}{4}, \tag{15}$$

$$\alpha^\nu = \frac{-\frac{1}{2}\alpha_P - \frac{1}{4}\alpha_B}{1+\alpha_P} - \frac{1}{4}. \tag{16}$$

The obtained expressions are normalized to the Bohm confinement time τ^B. A scaling expression is dimensionally correct if the dependence on the minor radius vanishes ($\alpha^a = 0$). Bohm or gyro-Bohm constraints can be constructed out of $\alpha^\rho = 0$ or $\alpha^\rho = -1$, respectively. A comparison of some scaling expressions in terms of the dimensionless parameters is given in Table 2.

As a general trend, tokamaks L-mode confinement scales more Bohm-like and tokamak H-mode and stellarator confinement more gyro-Bohm like. It can be seen from Eq. 14 and Table 1 that the differences in the dependence on ρ^* is primarily due to the different density scalings. As long as the B and P scalings prevail, the gyro-Bohm-like dependence vanishes as soon as the density dependence becomes weaker.

The scatter in the coefficients is larger than in terms of engineering parameters. This is due to the fact that ρ_* is not sufficiently varied in the databases. It has been attempted to break the collinearity in dimensionally similar discharges. First experiments with neutral beams in a tokamak (WALTZ *et al.*, 1990) did not bring the envisaged result. In pairs of discharges with different ρ_* and with all other dimensionless parameters similar the thermal diffusivity changed dramatically. This was due to the fact that in one discharge the beam deposition was strongly off-axis but the temperature profiles were similar to those of the other one, where the power was centrally deposited. This effect is known as profile consistency, and the data can only be explained by strong

nonlinear dependences on the local plasma parameters which would not be consistent with the parametric form of the scaling laws.

Similar experiments on ECH discharges in W7-AS revealed a gyro-Bohm-like scaling of the electron thermal diffusivity (STROTH *et al.*, 1993c). The experiments in DIII-D were repeated and this time the power deposition profile was kept similar in the discharge pairs (LUCE *et al.*, 1995). It was found that also in tokamaks the electron thermal diffusivity scales gyro-Bohm-like. The scaling of the ion channel was observed to depend on the confinement mode and the combination of both determines the scaling of the confinement time.

Although a similar picture seems to emerge for stellarators and tokamaks, it remains unclear why the power deposition profile has to be similar in pairs of dimensionally similar discharges. In the experiments, there is no dimensionless parameter considered, which is related to the power deposition profile. As long as the question of the impact of the power deposition profile on transport is not answered, the experimental approach to investigating anomalous transport in terms of dimensionless parameters has to be interpreted with caution in respect of a valid transport model.

6 The Role of Magnetic Shear

The magnetic shear is one of the main differences between stellarator and tokamak magnetic configurations. If it is a key parameter in anomalous transport, the confinement behavior should be very different in the two different concepts. In the previous section it was pointed out that this is not the case. On the other hand, reversed shear in tokamaks can appear simultaneously with a strong reduction in energy transport. Reversed shear in tokamaks refers to a profile of the safety factor which is non-monotonic with minor radius. The shear is negative in the plasma center and positive at the edge. The sign of shear in the center is the same of that of the normal heliotron/torsatron shear.

Negative shear can have several beneficial effects on stability (KESSEL *et al.*, 1994). Short-wavelength ballooning modes are stable in the negative shear region and access to the second ballooning stability regime is possible. Hence, the pressure profile gradient is not limited by these instabilities and can develop. A strong pressure gradient itself generates bootstrap current which again is favorable for increasing the q value on the magnetic axis. This in turn has a stabilizing effect on short and long-wavelength instabilities.

Since a large fraction of bootstrap current is also favorable for steady-state operation, the concept of confinement improvement by reversed shear is also a central element of the advanced tokamak concepts as suggested in the TDX (NEVINS *et al.*, 1993) and SSTR (SEKI *et al.*, 1991) studies.

6.1 Reversed Shear in Tokamaks

Prior to the theoretical investigations in (KESSEL *et al.*, 1994), a reduction of transport together with a non-monotonic q profile was indeed found experimentally in JET (HUGON *et al.*, 1992; SMEULDERS *et al.*, 1995). Reversed shear was generated by injecting pellets into a discharge with a small amount of ion cyclotron resonance heating (ICH). The achieved PEP confinement mode is illustrated in Fig. 10. This transient phase is characterized by a hollow current profile with reversed shear up to one-third of the minor plasma radius. Strong gradients in the electron density and pressure profiles develop in the region where the shear is slightly negative. Electron and ion thermal diffusivities are reduced to the level of the neoclassical electron diffusivity. Similar results were obtained by off-axis lower-hybrid current drive during the initial current ramp-up phase of discharges (SÖLDNER *et al.*, 1995).

In DIII-D (LAZARUS *et al.*, 1992; MANUEL *et al.*, 1995), the reversed shear was obtained in the current ramp-up phase by injecting the neutral beams already in the early phase of the discharge, when the density was still low. By this technique, the hollow current profile from the ramp-up phase can be conserved for a few seconds. If the injection was delayed, the discharge progressed in an ordinary VH-mode (JACKSON *et al.*, 1991). In DIII-D, the reversed-shear discharges are characterized by central peaking of the ion temperature and the toroidal rotation velocity profile. The magnetic shear is reversed in the inner

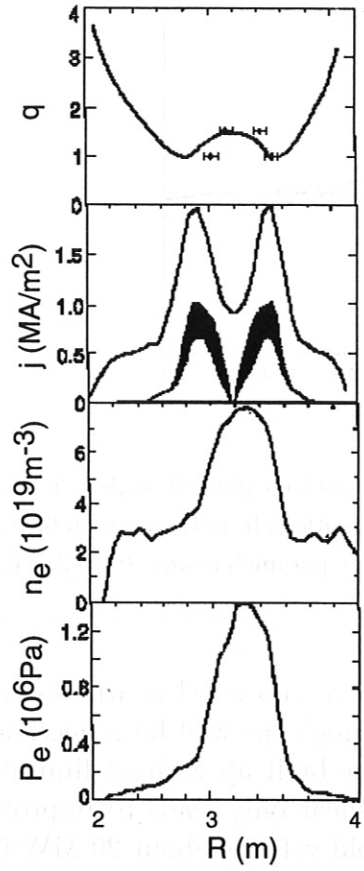

FIG. 10: JET discharge with reversed magnetic shear and improved confinement (adapted from (HUGON *et al.*, 1992)).

half of the minor radius. The strongest gradients in the ion temperature and toroidal rotation profiles occur near the outer edge of the reversed magnetic shear region. At this location, the shear is negative and it has a small value. In spite of the high central β values, no strong MHD activity was observed. This is in agreement with ballooning stability under conditions of reversed shear.

In Tore Supra indications of reversed shear under steady-state conditions were found (HOANG *et al.*, 1994). In these discharges strong lower hybrid current drive was applied to flatten the q profile. During this so-called LHEP mode, the central electron energy transport is strongly reduced and the temperature profile peaks. The authors stress that the observations are in qualitative agreement with the shear dependence of the RLW model (REBUT *et al.*, 1989).

High-β_p-mode discharges in JT-60 have a strong contribution of bootstrap current. The broad current profiles can be driven hollow by means of off-axis neutral-beam current drive (KAMADA *et al.*, 1994). Indications are found that a reversed-shear region develops and that, similarly to the observations in the other experiments, the pressure profile peaks.

Recently, also from TFTR improved confinement was reported in a reversed shear region (BATHA *et al.*, 1995). It was achieved in the current ramp-up phase with early NBI or ICH heating. The transition to improved confinement required a power threshold of about 20 MW.

In summary, a relation between improved confinement and reversed shear

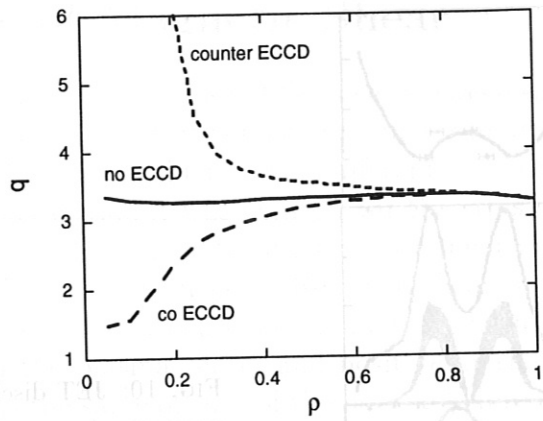

FIG. 11: Profile of the safety factor for discharges with co (launch angle 8°), ctr. (launch angle -8°) and no ECCD. The profiles contain contributions from the vacuum field and from ECCD, ohmic and bootstrap currents. The discharge parameters are: $B_t = 2.5$ T, $\iota \approx 1/3$, $\bar{n}_e = 6.5{\times}10^{19}\,\mathrm{m}^{-3}$, $T_e(0) = 0.9$ keV, $P = 0.4$ MW.

is established for many tokamaks. It is, however, no yet clear whether reversed shear is the origin of the improvement. It might as well be a necessary condition which allows a pressure gradient to be built up without limitation due to ballooning modes. In TFTR, reversed shear only leads to improved confinement if the NBI power exceeds a threshold value of about 20 MW (BATHA *et al.*, 1995) and in DIII-D discharges with reversed shear can exist for 1 s before a confinement transition occurs (MANUEL *et al.*, 1995).

6.2 Magnetic Shear Variations in Stellarators

In contrast to the observations in tokamaks, heliotron/torsatron shear, which is reversed to the tokamak shear, does not give rise to strong transport improvements. Figure 8 shows that energy confinement in heliotron/torsatrons is not superior to that in shearless stellarators or tokamaks. It is rather the other way round. This is true on the basis of all scaling expressions investigated. However, a moderate influence of the sign of the magnetic shear on global confinement cannot be ruled out from a comparison on the basis of scaling laws. Furthermore, it was shown (COOPER,) that the same amount of magnetic shear which stabilizes ballooning modes in tokamaks has not such a beneficial effect in torsatrons.

In W7-AS, the influence of the magnetic shear on confinement has been studied by means of electron-cyclotron-resonance current drive (ECCD). Experiments were carried out with ECCD in the co and ctr. directions with respect to the toroidal field (MÜLLER *et al.*, 1995). In the co and ctr. directions the driven current, which was of the order of 5 to 10 kA, increases and decreases the rotational transform, respectively. The direction of the driven current was changed by the toroidal launching angle and the launched power was 0.4 MW in all cases. An ohmic transformer was used to control the total

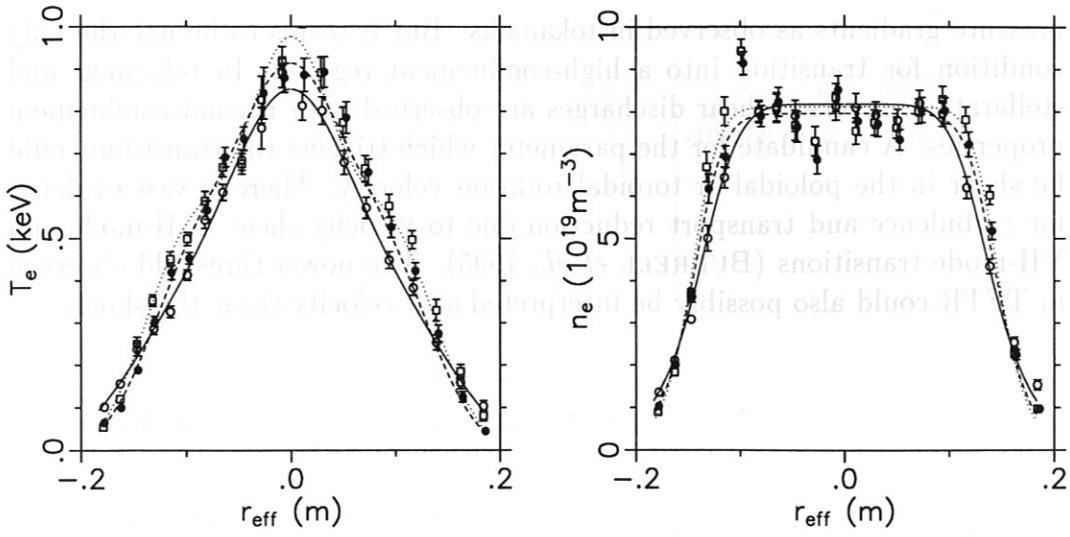

FIG. 12: Influence of magnetic shear on confinement. Compared are the electron density and temperature profiles for discharges with no (dashed), co (solid) and ctr. ECCD (dotted line). See Fig. 11 for the corresponding q profiles.

current to values below 100 A. The total current is composed out of a bootstrap current, the ohmic current and the ECCD current. The bootstrap current in W7-AS runs in the co direction. In Fig. 11, the q profiles as calculated from the total current are plotted for the cases with co, ctr. and no current drive. Due to the central deposition of ECH, the q profile is appreciably modified up to one-third of the minor plasma radius.

Figure 12 shows the electron temperature and density profiles for the three cases. The profiles are very similar and strong modifications of the gradients are not detected in the reversed shear situation (ctr. current drive).

In W7-AS, magnetic shear can have an effect if global modes or destruction of magnetic surfaces at major rational ι values degrade the plasma. The observed flattening of the temperature gradient in such a region can be radially limited if magnetic shear is added (RINGLER *et al.*, 1990; ERCKMANN *et al.*, 1995). In the W7-A stellarator, the same effect was observed with shear from inductively driven current (WOBIG *et al.*, 1987). Discharges with degraded confinement due to rational ι values recovered to the high confinement quality when moderate shear was introduced. The same amount of shear, however, did not change the confinement if it was added to a discharge which was in the vicinity of rational ι values and, therefore, not degraded. Hence, a strong reduction of anomalous transport by reversed magnetic shear in stellarators is not observed.

6.3 Summary

There is experimental evidence of the beneficial effect of reversed magnetic shear on MHD stability. It seems to be the pre-condition to obtain steep

pressure gradients as observed in tokamaks. But it seems to be not the only condition for transition into a high-confinement regime. In tokamaks and stellarators, reversed-shear discharges are observed with normal confinement properties. A candidate for the parameter which triggers the transition could be shear in the poloidal or toroidal rotation velocity. There is vast evidence for turbulence and transport reduction due to velocity shear in H-mode and VH-mode transitions (BURRELL *et al.*, 1995). The power threshold observed in TFTR could also possibly be interpreted as a velocity shear threshold.

Device	LOC	SOC	L mode	H mode	Ref.
ASDEX	1.3	1.5	1.3	2.0	(STROTH *et al.*, 1995b)
ASDEX-Upgrade	-	-	1.4	1.4	(RYTER *et al.*, 1995)
DIII	1.0	1.4	1.4	2.0	
FTU	1.1	1.4	-	-	
ISX-A	1.4	1.4	-	-	
ISX-B	1.4	1.4	-	-	
JET	-	1.4	1.2	-	
JFT-2M	1.1	1.4	1.4	1.4	
T11	1.3	1.3	-	-	
TEXTOR	1.4	1.4	-	-	
TFTR	-	-	1.2	-	(HAWRYLUK *et al.*, 1991)
W7-AS	1.1	-	-	-	(STROTH *et al.*, 1995a)

TABLE 3: The ratio of the confinement time of deuterium and hydrogen discharges from various devices and for different confinement regimes. The values are from (BESSENRODT-WEBERPALS *et al.*, 1993) if not indicated otherwise.

7 The Isotopic Effect

There is overwhelming evidence that at otherwise comparable discharge parameters deuterium discharges have improved confinement properties compared with hydrogen ones. The improvement is attributed to the ion isotopic mass and was termed the isotopic effect (MURMANN *et al.*, 1988). It has received revived interest because if it scales with the mass of the primary ion it would be beneficial for the D-T operation in ITER. Experiments in TFTR have shown that the confinement indeed improves if tritium is added to deuterium discharges (HAWRYLUK *et al.*, 1994).

From the theoretical point of view the isotopic effect is difficult to explain. The step size of collisional transport increases with the ion mass, and drift wave turbulence creates transport through flow cells which increases with the normalized gyro-radius and, hence, mass.

7.1 Isotopic Effect in Tokamaks

The isotopic effect has been observed in many tokamaks and in improved as well as degraded confinement regimes. It is therefore a universal characteristic of high-temperature plasmas. Table 3 gives a selection of the effects observed in different devices. As a general trend, a weaker effect is observed in the linear ohmic confinement regime (LOC) than in the saturated regime (SOC) or in L-mode discharges. In the H-mode it can be stronger. Deuterium discharges in the ELMy H-mode have a lower ELM frequency than hydrogen discharges.

This additionally improves the global confinement for the higher isotopic mass and can lead to an artificially enhanced confinement improvement of up to 100%. In quiescent H-modes in ASDEX the estimated effect was only $M^{0.46}$ (BESSENRODT-WEBERPALS *et al.*, 1993).

In ohmic regimes, the isotopic effect is amplified because of the link between the heating power and electron temperature: An observed effect of $\tau_E = W/P \sim M^{0.5}$ is connected with a change in the heating power according to $P_{OH} \sim T^{-3/2} \sim W^{-3/2}$. This leads to an isotopic effect in the heating power of the order $P_{OH} \sim M^{-3/10}$. Assuming a realistic coefficient for the power degradation of confinement, the intrinsic isotopic effect α_M is given by $\tau_E \sim M^{\alpha_M} P^{-1/2} \approx M^{\alpha_M + 3/20}$. Hence, if an isotopic effect of $M^{0.5}$ is observed in ohmic plasmas, the intrinsic effect connected with confinement improvement is only $M^{0.35}$. Taking this into account, the intrinsic isotopic effect in ohmic plasma seems to be smaller than in additionally heated ones.

The experimental features of the isotopic effect have been extensively studied in ASDEX (WAGNER *et al.*, 1990; BESSENRODT-WEBERPALS *et al.*, 1993). Deuterium compared with hydrogen discharges showed higher electron temperatures in the plasma center, lower edge densities and stronger density peaking. The improved ohmic confinement regime (IOC), characterized by peaking in the density profile, was not accessible in hydrogen. The η_i-mode (ROMANELLI, 1989) is often referred to as a candidate which could explain the confinement improvement via density peaking and one could try to explain the isotopic effect also as a consequence of a change in density profile. But the isotopic effect was also present in pellet injection discharges with very peaked density profiles. In these discharges, the η_i-mode should be stable, nevertheless a reduction in transport is observed with deuterium.

Pellet fueled discharges have a very low impurity content and $Z_{eff} \approx 1$. This rules out that the improvement is introduced through a change in Z_{eff}, as has been conjectured in (COPPI *et al.*, 1993).

The isotopic effect was also observed in all transport channels in ASDEX. It was present in the electron heat transport dominated LOC regime and lower-hybrid heated discharges. It was observed in the angular momentum transport which is carried by the ions. From gas modulation experiments and from the higher gas consumption of hydrogen discharges it was concluded that the isotopic mass enters particle confinement too. In ohmic discharges it was shown that the electron transport coefficient reduces with isotopic mass across the entire plasma cross-section.

The isotopic effect of mixed ion contributions is of an additive nature. The relevant parameter could be an effective mass, defined as

$$M_{eff} = \frac{\sum_i M_i n_i}{\sum_i n_i}. \tag{17}$$

This is shown in Fig. 13, where L-mode discharges in ASDEX with different combinations of neutral beam and plasma isotopes are compared. Relatively to the ASDEX scaling without a mass dependence, D-into-D injection produced

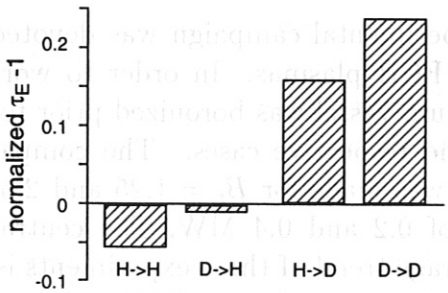

FIG. 13: Energy confinement time normalized to the ASDEX scaling expression for NBI heated L-mode discharges with varied composition of plasma and NBI isotopes. Plotted is the average of values from the large dataset published in (STROTH *et al.*, 1995b).

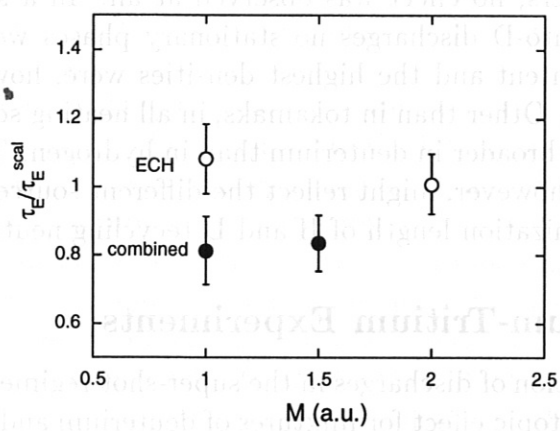

FIG. 14: The confinement time normalized to the W7-AS scaling versus the effective isotopic mass number. Plotted are average values for discharges with ECH heating and combined heating. The error gives one standard deviation of the distribution of the averaged points.

better confinement than the mixed cases and these are better than the H-into-H injection case.

7.2 Isotopic Effect in Stellarators

Up to now, no isotopic effect has been found in stellarators. The effect has been studied in ATF (MURAKAMI *et al.*, 1991). The negative result has been confirmed by a recent analysis of the international stellarator database (STROTH *et al.*, 1996b). It has been noted, however, that there are no data from D-into-D injection available. In the database, the isotopic effect is only tested on discharges with ECH heating or on discharges with NBI where the injected isotope is different from the plasma isotope. In the latter case, the isotope mix has to be precisely known to quantify the effect on confinement. Since this is not the case, the result is only preliminary. ECH, on the other hand, has been restricted to moderate densities. The regime of these discharges might be similar to the tokamak LOC regime, where also a reduced isotopic effect is present and the mentioned amplification due to ohmic heating is lost in stellarators.

In W7-AS, an experimental campaign was devoted to a careful study of the isotopic effect in ECH plasmas. In order to work with a pure isotopic composition, the vacuum vessel was boronized prior to the experiments using H_6B_2 and D_6B_2 in the respective cases. The comparison of hydrogen and deuterium discharges was made for $B_t = 1.25$ and 2.5 T at $\iota = 1/3$ and $1/2$ and an ECH power of 0.2 and 0.4 MW. The central density was $n_e(0) \approx 4\times10^{19}\ \mathrm{m}^{-3}$. The average trend of these experiments is depicted in Fig. 14.

The absence of an isotopic effect in ECH plasmas is confirmed by these experiments. The trend, however, is not uniform for all parameters. In the more separatrix-dominated case at $\iota = 1/2$, an effect of the order of $M^{0.2}$ was observed in the global confinement time as well as in a heat pulse analysis. At other parameters, no effect was observed at all. In a series of NBI with H-into-H and D-into-D discharges no stationary phases were achieved. The highest energy content and the highest densities were, however, obtained in the hydrogen case. Other than in tokamaks, in all heating schemes the density profile tends to be broader in deuterium than in hydrogen. The density profile in small plasmas, however, might reflect the different source distributions due to the different ionization length of H and D recycling neutrals.

7.3 Deuterium-Tritium Experiments

Detailed investigation of discharges in the super-shot regime in TFTR have revealed a strong isotopic effect for mixtures of deuterium and tritium (HAWRYLUK *et al.*, 1994; SCOTT *et al.*, 1995; ZARNSTORFF *et al.*, 1995). In the plasma center, the tritium content was up to 50%. If the effective mass is used as parameter, the confinement time increases as $M^{0.85}$. The strongest effect of $M^{-1.8}$ is found both in the ion thermal and momentum diffusivities. A somewhat weaker effect of $M^{-1.4}$ was observed in the density transport and no clear effect was present in the electron thermal diffusivity. In comparison with the effect observed under L-mode conditions (see Table 3), this shows, that the isotopic effect can strongly vary from one discharge condition to another.

7.4 Larmor Radius versus Turbulence Scale Length

Although the isotopic effect in confinement is clearly established, its strength varies depending on the regime and the features are not as robust as other scaling properties. An ordering of the strength of the isotopic effect might be possible in terms of the ion temperature. In ohmic discharges, and in most stellarator discharges, the ions are relatively cold and the effect is smaller or absent. When the ions are heated directly by auxiliary heating, the effect seems to be stronger. In line with this it is interesting to note, that in TFTR discharges, with ion temperatures in the range of 30 keV, the thermal ion diffusivity can even be reduced with increasing ion temperature (MEADE *et al.*, 1991).

The ion Larmor radius can enter the turbulent transport in two respects.

Ion transport would be reduced if orbit averaging, which increases with the Larmor radius, reduces the influence of the turbulence on the ions. This could explain the strong effect observed in the ion thermal diffusivity of TFTR tritium discharges. But a reduction of particle and electron heat transport can only be explained if the ions also have a stabilizing effect on turbulence in general, as was considered in (SCOTT, 1992b).

Possibly both mechanisms are superimposed. In both cases, the relevant parameter is the ratio of the Larmor radius to the radial turbulence scale length. This interplay might describe the facets of the observed effects. If the ion Larmor radius has a critical size in relation to the turbulence, a change in the Larmor radius might have a strong effect. In the case of supershots, the confinement is improved and the radial correlation length of turbulence might be reduced. Since the ion temperature is high the Larmor radius is large and the isotopic effect is large too.

The other extreme, where the Larmor radius is small but the turbulence scale length is small too, might be related to the L-to-H transition. The power threshold in hydrogen is twice the threshold in deuterium (RYTER and THE H-MODE DATABASE WORKING GROUP, 1996).

A result from an analysis of the ELM-free H-mode discharges from the ITER database might also give a hint on the importance of temperature: In this analysis, a stronger isotopic effect has been observed for discharges with higher injected power per particle (H-MODE DATABASE GROUP, 1993). This is due to the observation that the data in this database show a weaker effect for JET and DIII-D, which are operated with lower power density than other devices which show a stronger effect. High power densities are related to higher temperatures and larger Larmor radii for the ions. Higher heating power, on the other hand, produces larger transport and might be related to longer correlation lengths. It would be this interplay which determines the value of the isotopic effect.

8 Density Dependence of Confinement

In Section 4 it is stated that a transport coefficient which depends on temperature leads to a confinement time scaling of the form:

$$\chi \sim T^{3/2} \Rightarrow \tau_E \sim \left(\frac{n}{P}\right)^{0.6} . \tag{18}$$

In other words, if the degradation of confinement with power is explained by the dependence of the transport coefficient on temperature, this automatically leads to a dependence of confinement on density. The reason for this is that the confinement time is not written as a function of temperature but as a function of heating power. The temperature of a discharge heated at constant power decreases as the density increases. According to this model, the increase in confinement results from the changing temperature and not from the increase in density. Hence, this form of density dependence is linked to the problem of temperature dependence and therefore to the one of power degradation, as discussed in the subsequent sections in detail.

Since the temperature drops towards the plasma edge, a major conjecture against the model is that it produces decreasing transport coefficients with increasing radius. This is in contradiction to experimental findings in stellarators and tokamaks (WAGNER and STROTH, 1993). A direct dependence of the transport coefficient on density, on the other hand, appears as density dependence in the confinement time without introducing dependences on other parameters:

$$\chi \sim \frac{1}{n} \Rightarrow \tau_E \sim n \tag{19}$$

A model of this type, reproduces the correct increase of the transport coefficient towards the plasma edge.

8.1 Density Scaling of Tokamak Confinement

In early experiments in small tokamaks like Pulsator (KLÜBER *et al.*, 1975) and Alcator *A* (GAUDREAU *et al.*, 1977) it was observed that the energy confinement time increases with plasma density. An empirical scaling expression of the form (PARKER *et al.*, 1985)

$$\tau_E \sim a^2 R \bar{n}_e. \tag{20}$$

was deduced from ohmically heated discharges. This *neo-Alcator* scaling expression predicted very favorable confinement times for large experiments and dense plasmas. Subsequently, in larger devices like Doublet III (EJIMA *et al.*, 1982) and ASDEX (GRUBER, 1984; KEILHACKER *et al.*, 1986), these expectations were not fulfilled and a saturation of confinement with density was observed.

At present, the following ohmic confinement regimes can be distinguished: The linear ohmic confinement regime (LOC) is characterized by a linear increase of τ_E with density. At higher density it is superseded by the saturated

regime (SOC). In some cases, the saturation is overcome when the plasma can access to the improved confinement regime (IOC) as in ASDEX (SÖLDNER *et al.*, 1988) or JIPP T-IIU (TOI *et al.*, 1991). This is possible under low-recycling conditions and is triggered by turning off the external gas flux to the plasma. Related to the IOC regime are the enhanced regimes which are obtained after injecting pellets into ohmically heated plasmas. Examples are the pellet regimes in Alcator *C* (GREENWALD *et al.*, 1984) and ASDEX (KAUFMANN *et al.*, 1988).

A survey of ohmic confinement in different tokamaks showed (SIMMET and STROTH,) that the critical line averaged density $\bar{n}_e^{sat}$ at which saturation sets in approximately scales as

$$\bar{n}_e^{sat} \sim V^{-0.45} P^{0.55} M^{0.6} Z_{eff}^{-0.4}. \tag{21}$$

Accordingly, confinement in devices with larger volume V saturates at lower densities. P stands for the ohmic heating power. If the expression can also be used for other electron heating schemes like ECH, it would also describe why strongly electron-heated discharges like the ECH plasmas in T10 (ESIPTCHUK and RAZUMOVA, 1986) saturate at higher density than those with ohmic heating.

With auxiliary heating, generally the observed density dependence is weak. First indications of this were found in early experiments with neutral beam heating in ISX-B (SWAIN *et al.*, 1981). The weak density dependence can also be seen from the tokamak scaling expressions in Table 1, which are dominated by neutral-beam-heated discharges.

Because of the importance of a temperature dependence of the transport coefficient for anomalous transport theory, it was conjectured (ROMANELLI, 1989; LACKNER *et al.*, 1989) that the expected density dependence of the confinement time might be masked by other effects with opposite trends. The properties of neutral beam injection could play this role: (i) The energy contributed by the fast ions to the total energy increases at lower density. If the fast ions are better confined than the thermal ones, this would lead on the average to an improvement of confinement which becomes stronger with decreasing density. (ii) Shine-through of the beams reduces the available heating power at low density. If this effect is not correctly taken into account in the calculation of the confinement time, the confinement time is overestimated. (iii) At higher density the neutral beam particles are already ionized in the outer plasma region and the power deposition profile becomes broader and, according to a diffusive transport model, less efficient in building up the temperature.

In scaling studies of the thermal energy confinement time, these effects are partly taken into account by the use of approximate expressions for shine-through and fast particle content. As reproduced in Table 1, the thermal confinement time depends more strongly on density than the total ones.

In ASDEX, the density dependence of L-mode confinement was studied in the low-density region (STROTH *et al.*, 1991b). Discharges at $\bar{n}_e = 1.3$, 2.0 and 2.6×10^{19} m^{-3} were heated with NBI of 1.8 MW. The discharges were

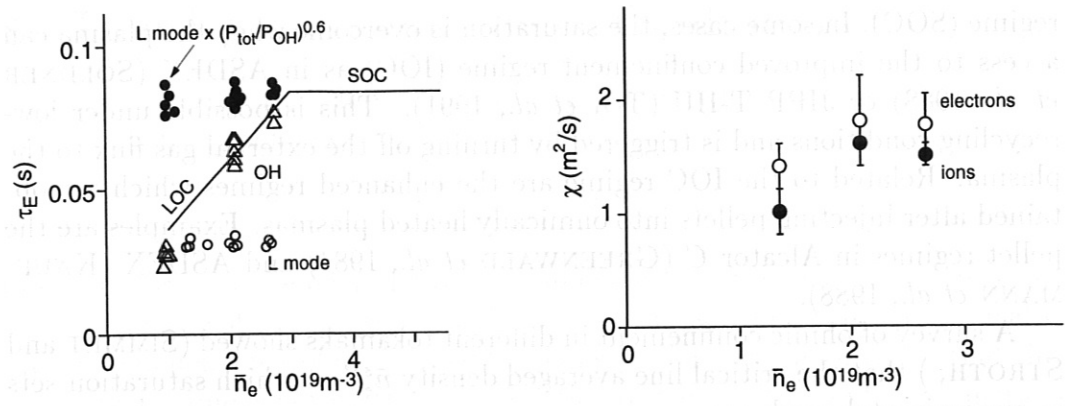

FIG. 15: Left: Energy confinement time for the ohmic and L-mode phases of a density scan in ASDEX. The solid circles are calculated from the L-mode confinement time by multiplication of $(P_{tot}/P_{OH})^{0.6}$. This is a correction of the power degradation due to NBI. The lines are along the LOC and SOC confinement of ASDEX (see Fig. 17). Right: Electron and ion thermal diffusivities in the core region for the density scan.

analyzed using the TRANSP transport code. In Fig. 15, the global energy confinement times from the ohmic pre-phases and the L-mode phases are depicted. While the ohmic confinement shows the usual density dependence, the L-mode confinement is constant with density. At the lowest density, the difference between ohmic confinement and L-mode confinement is surprisingly small. It is much less then expected from the usual power degradation coefficient $P^{-0.5}$. Apparently, the L-mode confinement does not originate from the LOC ohmic confinement but rather from the SOC level of ohmic confinement. In Fig. 15 it is shown that the L-mode confinement times indeed correspond to the level given by the saturated ohmic confinement. With the usual coefficient for power degradation of $P^{-0.5}$, the confinement time can be scaled back to the value of the ohmic power level. In this way, values are obtained on the level of the SOC regime. Figure 15 confirms the absence of an intrinsic density dependence. The right hand side shows the thermal electron and ion diffusivities, which are both almost constant. The somewhat smaller value at the lowest density can be explained by the reduction in absorbed power.

In Fig. 16 the power deposition profiles are shown for the density scan. The effect of shine-through is evident at the lowest density. But there is no strong profile broadening observed as the density is increased.

In conclusion, the energy confinement time of tokamak discharges does not strongly depend on density. An exception occurs in strongly electron-heated discharges. They must be regarded as degraded regimes compared with the SOC confinement level. And they are also degraded with respect to the L-mode confinement, which seems to originate from the SOC level of confinement via power degradation.

For the comparison with stellarators, the density-dependent LOC regime will be of special interest. The transition from LOC to SOC was studied in

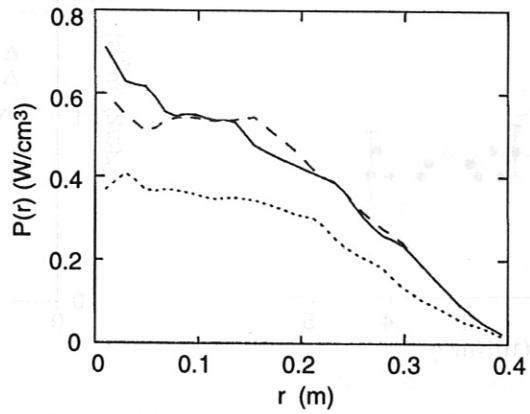

FIG. 16: Total power deposition profiles calculated by TRANSP for the density scan in Fig. 15. The line-averaged densities are 1.3 (dotted), 2.0 (solid) and $2.6\times10^{19}\,\mathrm{m}^{-3}$ (dashed line).

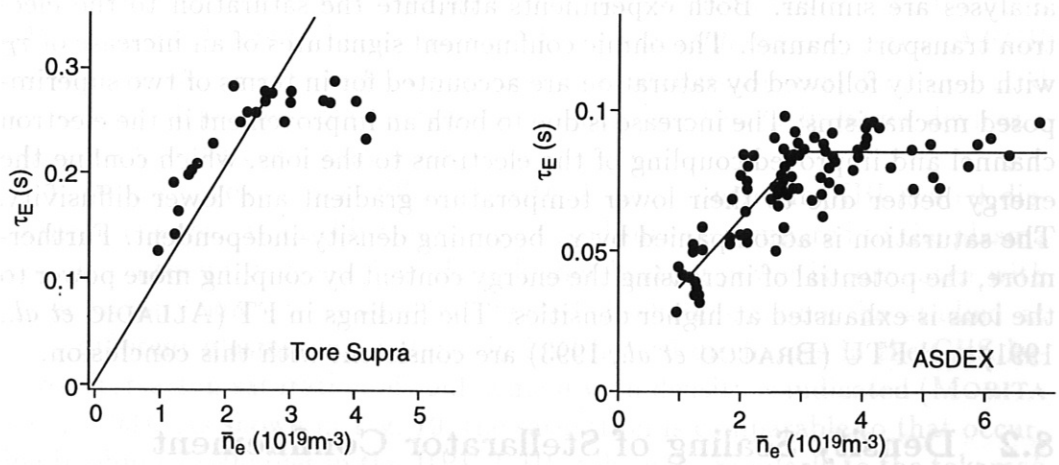

FIG. 17: Energy confinement time as a function of line-averaged density for ohmically heated discharges in Tore Supra (adapted from (GARBET *et al.*, 1992)) (left) and ASDEX (right) (adapted from (SIMMET and THE ADSEX TEAM, 1996)).

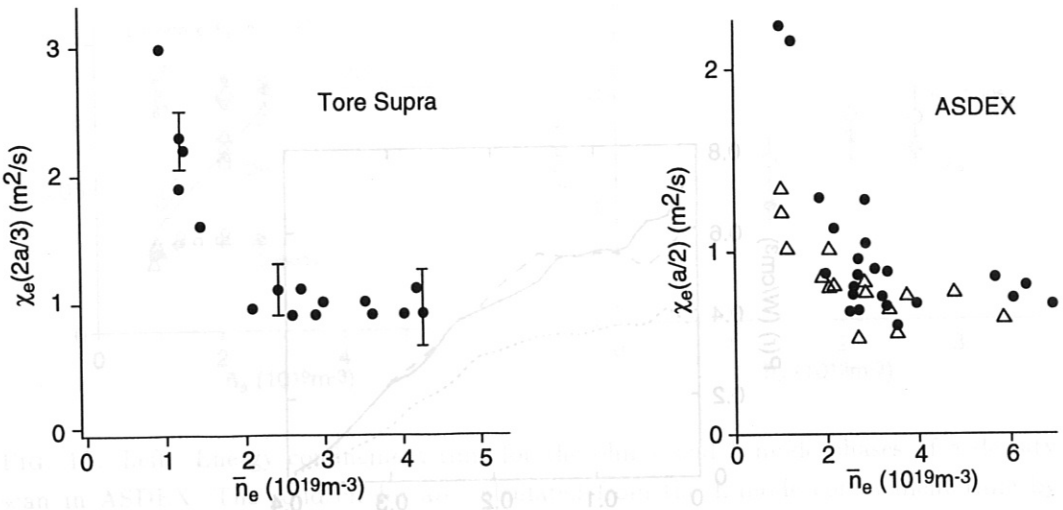

FIG. 18: Electron thermal diffusivity as a function of line-averaged density for ohmically heated discharges in Tore Supra (left,adapted from (GARBET *et al.*, 1992)) and ASDEX (right, adapted from (SIMMET and THE ADSEX TEAM, 1996)). For ASDEX, circles and triangles correspond to plasma currents of 380 and 320 kA.

several tokamaks. The results from ASDEX (SIMMET, 1994; SIMMET and THE ADSEX TEAM, 1996) and Tore Supra (GARBET *et al.*, 1992) are reproduced in Figs. 17 and 18. The energy confinement time in Fig. 17 saturates and the saturation is reflected in the electron thermal diffusivity shown in Fig. 18. Although the ion transport is consistent with neoclassical theory in ASDEX and is anomalous in Tore Supra, the conclusions drawn from the transport analyses are similar. Both experiments attribute the saturation to the electron transport channel. The ohmic confinement signatures of an increase of τ_E with density followed by saturation are accounted for in terms of two superimposed mechanisms: The increase is due to both an improvement in the electron channel and improved coupling of the electrons to the ions, which confine the energy better due to their lower temperature gradient and lower diffusivity. The saturation is accompanied by χ_e becoming density-independent. Furthermore, the potential of increasing the energy content by coupling more power to the ions is exhausted at higher densities. The findings in FT (ALLADIO *et al.*, 1991) and FTU (BRACCO *et al.*, 1993) are consistent with this conclusion.

8.2 Density Scaling of Stellarator Confinement

For stellarators, in contrast, a clear density dependence of confinement is detected in many devices for both ECH and NBI-heated discharges. Comparable density dependences are reported from ATF (COLCHIN *et al.*, 1990) ($\alpha_n = 0.67$), Heliotron E ($\alpha_n = 0.66$) (ZUSHI *et al.*, 1988; SANO *et al.*, 1990) and W7-AS (RINGLER *et al.*, 1990) ($\alpha_n = 0.66$).

Direct comparison of these results with tokamak confinement calls for caution. Tokamak L and H-mode databases are dominated by NBI-heated dis-

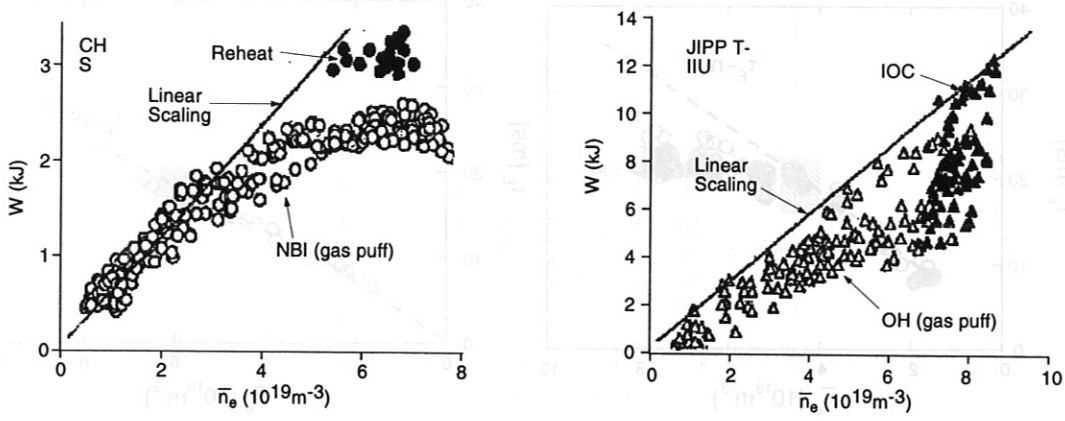

FIG. 19: Energy content as a function of density of NBI heated discharges in the CHS heliotron/torsatron (left) and of ohmically heated discharges in the JIPP T-IIU tokamak (right). The reheat and IOC improved confinement modes are indicated by solid symbols. (Adapted from (MORITA *et al.*, 1993).)

charges from devices which are typically larger than the existing stellarators. Stellarator scaling expressions are usually deduced from both ECH and NBI heated discharges. Both the heating method and machine size could introduce a bias. Since there is no plasma current available for plasma start-up, ECH plays the role of a basic heating in stellarators. Ohmic heating and ECH have in common that only the electrons are heated direct. Energy is coupled to the ions by electron-ion collisions. The importance of this term increases with density: $Q_{ei} \sim n_e^2(T_e - T_i)/T_e^{3/2}$. Due to density cut-off, ECH has been limited to low densities in the past. We have seen that in small devices the tokamak LOC regime extends to high densities. If the confinement properties of ECH and OH discharges are comparable, the present stellarators may have operated in a density-dependent regime while at higher densities or in larger devices a transition to saturation may occur.

A second caveat is the difficulty with density control in NBI-heated discharges. The reason for this is the large vessel surface compared to the plasma volume in present devices. Therefore, higher heating power is correlated with higher density and stationary NBI-heated discharges cannot be studied at many different plasma parameters. In NBI-heated discharges in the CHS heliotron/torsatron saturation of confinement with density is indicated (MORITA *et al.*, 1993). As shown in Fig. 19, the saturation is comparable to that occurring in ohmic discharges in the JIPP T-IIU tokamak. Similarly to the tokamak IOC regime, in CHS an improvement above the saturated confinement level can be achieved in the NBI reheat mode (MORITA *et al.*, 1993), which has similar characteristics to those of the IOC regime: it is triggered by switching off the gas flux and a steepening of the density gradient.

More recently, high-frequency ECH at 140 GHz has become available. This made it possible for the first time to study transport in electron-heated stellarator plasmas up to a density of $\bar{n}_e \simeq 10^{20}$ m^{-3}: In W7-AS, the density

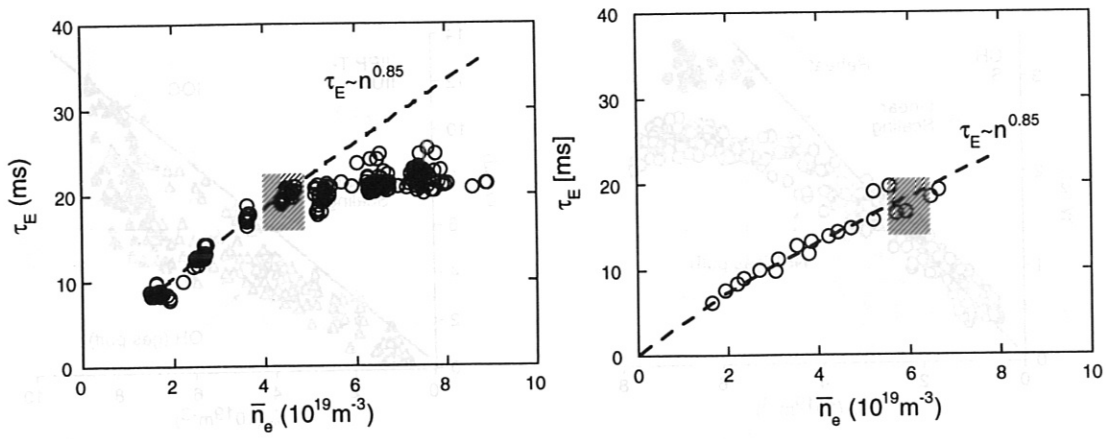

FIG. 20: Left: Evolution of the energy confinement time in a density scan in W7-AS. The discharges at $B_t = 2.5$ T and $\iota = 1/3$ were heated with 0.45 MW ECH. The dashed line is a result from a regression analysis restricted to $\bar{n}_e \leq 4.5{\times}10^{19}$ m^{-3}. Right: Discharges from density ramps with $P = 0.68$ MW. The hatched areas indicate the predictions for the saturation density according to Eq. 21.

dependence of confinement was studied in a density range from $\bar{n}_e = 1$ to 10×10^{19} m^{-3} (STROTH *et al.*, 1995a). The global energy confinement time of this series of discharges is shown in Fig. 20. It increases up to a line-averaged density of $\bar{n}_e \simeq 5{\times}10^{19}$ m^{-3}. A regression of the data in Fig. 20 up to this density yields a strong density dependence of $\tau_E \sim \bar{n}_e^{0.85}$. At densities $\bar{n}_e \geq 5{\times}10^{19}$ m^{-3} a saturation of the confinement time similar to that in ohmically heated tokamaks is observed. Surprisingly, the value of the density at which saturation occurs is correctly predicted by the tokamak expression (Eq. 21). As predicted, the saturation sets in at higher density if the heating power is increased. On the right-hand side of Fig. 20, the data from density ramps heated with 0.68 MW are plotted. The hatched areas indicate the prediction of Eq. 21.

Power balance analyses were carried out for the discharges of the density scan. As in ohmically heated ASDEX discharges, the ion thermal diffusivity is of the order of the neoclassical one. The results for the electron thermal diffusivity are depicted in Fig. 21. The values in the figure represent radial averages around normalized radii in the core and the edge of the plasma. At both radial locations, the electron and ion channels can be separated with sufficient accuracy. The electron thermal diffusivity drops with density until a density is reached at which saturation in confinement sets in too. At the inner location the saturation seems to set in somewhat earlier than at the outer one and there is an indication of an increase at the highest densities. The saturation of the diffusivity coincides with that in the electron energy content and must be considered as its origin.

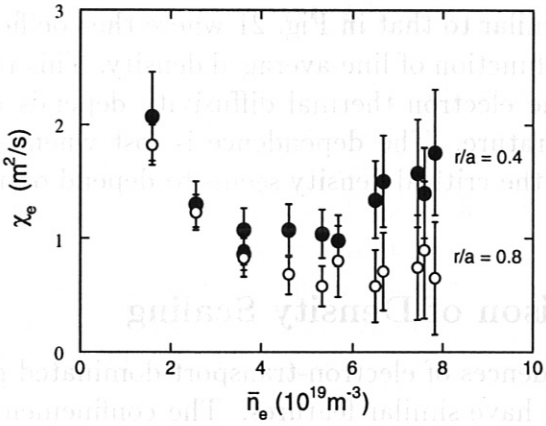

FIG. 21: Evolution of the electron thermal diffusivity at two radii in the density scan of Fig. 20. Plotted are radial averages in the core at $r/a = 0.4$ ($5 \leq r \leq 8.5$ cm) and the edge at $r/a = 0.8$ ($12 \leq r \leq 15$ cm) (adapted from (STROTH *et al.*, 1995a)).

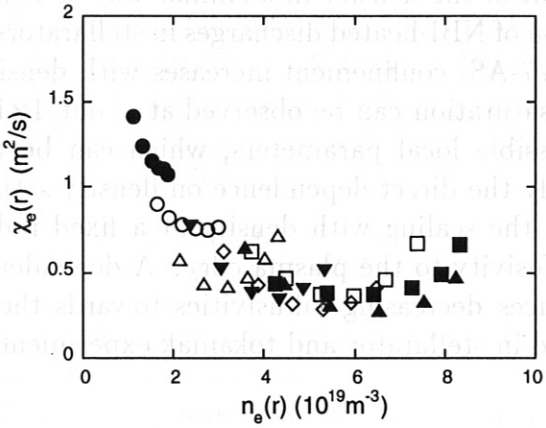

FIG. 22: Local electron thermal diffusivity as a function of the local electron density for the discharges of Fig. 20 (left part). The different symbols mark the individual discharges and the region represented extends from the edge to the onset of the flat part of the density.

8.3 Radial Profile of the Diffusivity

We have studied the transport coefficient as a function of the line-averaged density, which, as a global parameter, is inversely linked to the electron temperature. According to the ansatz in Eq. 18, the discussed density dependence could, therefore, be caused by a temperature dependence of the diffusivity. The density, however, also varies as a function of radius and decreases towards the plasma edge together with the temperature. If the density dependence also describes the radial course of the transport coefficient the temperature is ruled out as a candidate. Generally, an increase of the diffusivity with radius is observed in stellarators and tokamaks.

In Fig. 22 the electron thermal diffusivity of the discharges from the density scan in Fig. 20 is plotted versus the local density at the same location. The

behavior is very similar to that in Fig. 21 where the coefficient is plotted at a fixed location as a function of line-averaged density. This result indicates that at low densities the electron thermal diffusivity depends on density directly and not on temperature. The dependence is lost when a critical density is surpassed whereas the critical density seems to depend on the applied heating power.

8.4 Comparison of Density Scaling

The density dependences of electron-transport-dominated plasmas in stellarators and tokamaks have similar features. The confinement time saturates at comparable critical densities. In both devices, the saturation is related to the electron thermal diffusivity.

The density dependence found in stellarator scaling expressions might be due to peculiarities of small devices. In larger devices, the confinement might become independent of the density in a similar way as it is observed in tokamaks. The situation of NBI-heated discharges in stellarators, however, remains inconclusive. In W7-AS, confinement increases with density to values above $10^{20}\mathrm{m}^{-3}$, in CHS, saturation can be observed at about $4\times10^{19}\ \mathrm{m}^{-3}$.

Of the two possible local parameters, which can be responsible for the density scaling, only the direct dependence on density satisfactorily describes both observations, the scaling with density at a fixed radius and the radial increase of the diffusivity to the plasma edge. A dependence of transport on temperature produces decreasing diffusivities towards the edge, whereas an increase is observed in stellarator and tokamak experiments.

9 Power Degradation of Confinement

The heating process in high-temperature fusion plasmas is tempered by the corollary of enhanced turbulent transport and the energy confinement time becomes shorter with increasing heating power. This so-called power degradation is a robust feature observed to be of the order of $\tau_E \sim P^{-0.5}$ in both stellarator and tokamak plasmas. The inherent physics of power degradation is not understood. A common approach to understanding the problem is to find local plasma parameter dependences of the thermal diffusivity consistent with power degradation. This is the subject of this and the three subsequent sections.

Power degradation is also observed in experiments where the temperature T, temperature gradient ∇T and the local power flux q are the only local parameters which vary with changes in the global parameter P. Therefore, these parameters are the obvious candidates through which the transport coefficients could be connected with the heating power. T is favored by collisional as well as drift-wave-type theories (ROMANELLI *et al.*, 1986; DOMINGUEZ and WALTZ, 1987; CONNOR and TAYLOR, 1977), and ∇T by models using marginal stability of modes at some critical temperature gradient (REBUT *et al.*, 1989).

The two different forms of transport coefficients result in the same power dependence of the confinement time:

$$\left.\begin{array}{rcl} \chi & \sim & \nabla T \\ \chi & \sim & T \end{array}\right\} \Rightarrow \tau_E \sim P^{-0.5} \,. \tag{22}$$

These are local models where the diffusivity changes only as a function of the plasma parameters at the same location.

Alternatively, the heating power could be thought of as a global parameter which could directly influence the transport behavior of the plasma, e.g. by distortion of the particle distribution function:

$$\chi(r) \sim \int^r d^3r' P^{0.5}(r') \Rightarrow \tau_E \sim P^{-0.5} \,. \tag{23}$$

This will be called a global or a non-local model. The diffusivity at a certain radius changes simultaneously with the power deposited at any smaller radius. It is an analytical representation of the physical idea that transport can change on a faster time scale than that given by diffusive propagation of perturbations. One could think that the heating power acts as a local source of energy for turbulence, which can then propagate on a different time scale as the perturbation in the temperature and cause enhanced transport also at distant plasma radii.

A fundamental question connected with the power degradation problem will therefore be whether transport is governed by local plasma parameters or whether a change in plasma parameters at one position can modify the diffusivity at another position.

Experimentally, it is difficult to distinguish the impact of the three parameters on transport. In general they are changed only in a correlated way. If the

power is increased, the temperature and temperature gradient increase along with it.

In this section, power degradation is investigated on the basis of the energy confinement time and the local power balance. But a valid model must also describe the temporal development of perturbation in the plasma, such as heat pulses or the evolution of the temperature after stepping the heating power. Both techniques allow the three parameters to be decorrelated to some extent and are discussed in the subsequent sections.

9.1 Power Degradation in Tokamaks

Power degradation is observed in tokamaks under L and H-mode conditions and with all heating methods (WAGNER and STROTH, 1993). It first emerged when auxiliary heating became available in tokamaks (SWAIN *et al.*, 1981; GOLDSTON, 1984). In ohmically heated discharges, the decrease of confinement with power was balanced by an improvement with the concurrently increasing plasma current. From the beginning, it has been attempted to attribute the degradation of confinement to enhanced turbulence with increasing temperature (HUGILL, 1983).

The degradation of confinement is present in all transport channels. It is observed in electron-transport-dominated ECH plasmas (TFR GROUP and FOM ECRH TEAM, 1988) and in ion-transport-dominated NBI discharges (SCOTT *et al.*, 1991), in the momentum (KALLENBACH *et al.*, 1991) and in the particle transport. In power scans at constant density, an increase of the electron and ion thermal diffusivities with the electron and ion temperatures, respectively, was observed (SCOTT *et al.*, 1991).

In ASDEX, experiments were conducted (STROTH *et al.*, 1991a) to study the role of the electron temperature in NBI-heated L-mode discharges. Two types of power scans were carried out. In a scan at constant density, the electron temperature increased with heating power. This is the normal case of a power scan. In a scan at constant temperature, the density and heating power were increased simultaneously. For the two scans, the evolutions of the energy confinement time with heating power are illustrated in Fig. 23. The degree of power degradation is the same in the two cases. Also in the case of constant temperature, the confinement time decreases with heating power. Hence, electron and ion temperatures cannot be a leading local plasma parameter in power degradation.

Density and temperature (or power) enter the local transport equation in different forms. This also leads to different β values in the two scans. The constant-temperature scan is at higher local β and shows less variation in β than the constant-density scan. Therefore, the local β is not a good parameter either to describe power degradation. It would also yield diffusivities which strongly decay towards the plasma edge. This is incompatible with experiment.

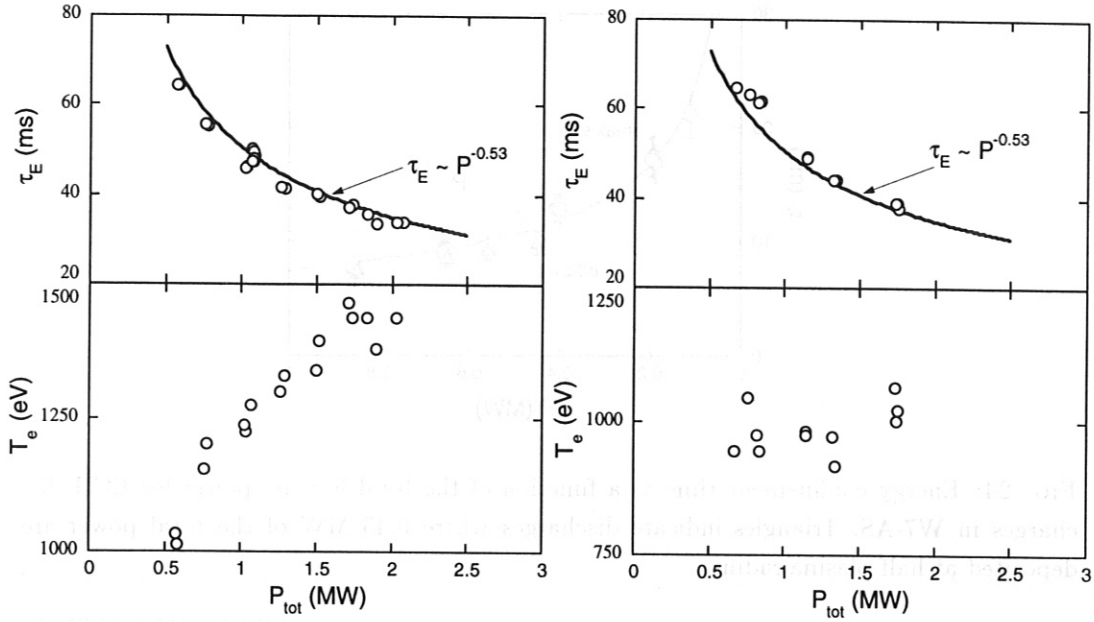

FIG. 23: Energy confinement time and central electron temperature from power scans in ASDEX at constant density (left) and constant electron temperature (right). The constant temperature discharges were achieved by increasing the density together with the heating power. The other parameters were $I_P = 380$ kA and $B_t = 2.2$ T. The ohmic heating power was about 0.3 MW.

9.2 Power Degradation in Stellarators

Stellarator plasmas are well suited for investigating power degradation. Other than in tokamaks, the change of ohmic heating whenever the temperature is changed does not blur the investigations. In the absence of ohmic heating, discharges can be compared, where the temperature profiles are modeled with the help of well localized ECH.

Also in stellarators, the degradation of confinement with power is well documented (SUDO *et al.*, 1990; STROTH *et al.*, 1996b). In present-day stellarators, the ion energy transport is mostly consistent with neoclassical theory. Increased ion thermal energy losses are expected in the low-collisionality regime, where neoclassical theory predicts increasing convective losses due to ripple-trapped particles. At present, stellarator discharges access this regime only marginally. In the plateau regime an increase with $T_i^{3/2}$ should occur. But power degradation is also observed under conditions which are clearly dominated by electron losses (RINGLER *et al.*, 1990).

In ECH discharges in stellarators, there is no connection between plasma current and heating power. Other than in tokamaks, electron-heated plasmas can be studied where only the temperature is changed and all the other parameters, such as the magnetic field and rotational transform, are kept fixed. ECH power scans are therefore very well suited to disentangling the role played by the different parameters in power degradation.

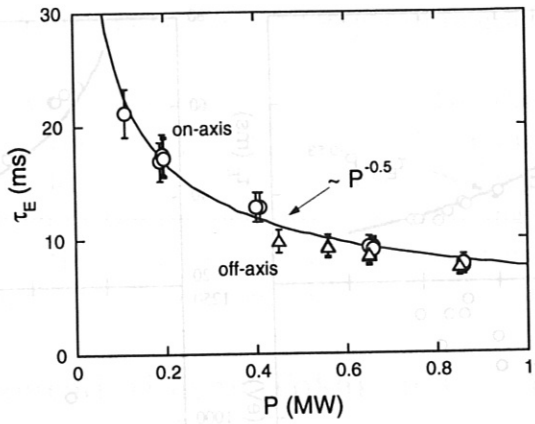

FIG. 24: Energy confinement time as a function of the total heating power for ECH discharges in W7-AS. Triangles indicate discharges where 0.45 MW of the total power are deposited at half plasma radius.

In the W7-AS stellarator, such power scans were carried out at $B_t = 2.5$ T, $\iota = 1/3$ and $\bar{n}_e = 2.5{\times}10^{19}$ m^{-3}. The ECH power was varied from 0.1 to 0.85 MW by using two gyrotrons at about 0.2 MW power each and one at 0.45 MW. By central heating only the electron temperature at a normalized radius of $r/a = 0.4$ increased from 250 to 1150 keV and its gradient from 33 to 120 eV/cm.

The discharge conditions were such that the ions are almost decoupled from the electrons. The global energy confinement time shown in Fig. 24 is dominated by electron heat transport. It can be described by a power law of the form $\tau_E \sim P^{-0.5}$ over the entire power range of almost a factor of 10. The change in heating position from the plasma center to half minor radius only influences the central part of the profiles, which does not contribute much to the total energy content.

As mentioned above, in power scans the parameters T, ∇T and P are strongly linked. Combinations of on- and off-axis heating were employed to decorrelate T and ∇T. The technique, which is illustrated in Fig. 25, can only be applied because of the narrow power deposition of ECH. A comparison of temperature profiles obtained from on-axis heating only (solid line) and a combination of on- and off-axis heating (dashed line) at position 1 can decorrelate the temperature from the temperature gradient. At location 1 the temperatures are the same but the gradients and local power fluxes are different. This case is difficult to realize because the reduction in central heating has to be compensated by off-axis power which is less efficient in building up the temperature. The other case can be realized more easily, where the role of temperature at constant temperature gradient can be studied. Discharges with the same amount of on-axis power and different off-axis power are compared. At positions 1, the profile represented by the dashed line has the same gradient as the one of the dotted line at position 2 but the have different temperatures.

A decorrelation, however, takes place only if the temperature profiles diffu-

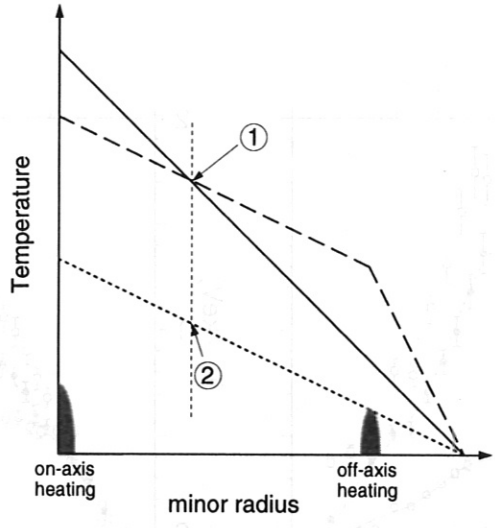

FIG. 25: Decorrelation of electron temperature and temperature gradient by use of combined on- and off-axis heating.

sively follow the power deposition profile. Profile resilience and strong energy pinches will not allow this procedure.

Of course, the experimental profiles do not exactly follow this idealized picture. The electron temperature profile shapes obtained are represented in Fig. 26. For example, the discharge with 0.1 MW on-axis power can be compared with that where 0.45 MW is additionally deposited at half plasma radius. The power flux through the radial region between the two deposition zones (at $r \simeq 6$ cm) is 0.1 MW in both cases but the temperature increases from 0.4 to 1 keV.

In the power scan with additional off-axis heating only the central power was changed from 0 to 0.4 MW. The off-axis power contribution was fixed at 0.45 MW. A transition from a flat temperature profile (0 MW on-axis) to a peaked one (0.4 MW on-axis) is observed. The extreme resilience of the electron temperature to changes in the profile shape, as found in the DIII-D tokamak (LUCE and PETTY, 1994), is not observed in W7-AS. Some indications of profile consistency might be indicated by the fact that 0.1 MW on-axis heating power suffices to build up an appreciable temperature gradient which is not much different from that obtained with 0.4 MW on-axis power.

The dependences of the local transport coefficient on the plasma parameters are investigated by means of a power balance analysis carried out during the stationary phases of the discharges. The results presented in Figs. 27-29 concern averages of small radial regions ($\pm$ 1.7 cm) in the inner part inbetween the two deposition zones and in the outer part of the plasma, outside the off-axis position.

Figure 27 illustrates the dependence of the electron thermal diffusivity in the outer plasma region on the total heating power. The discharges with the lowest powers are omitted because the density profile changes too much in the

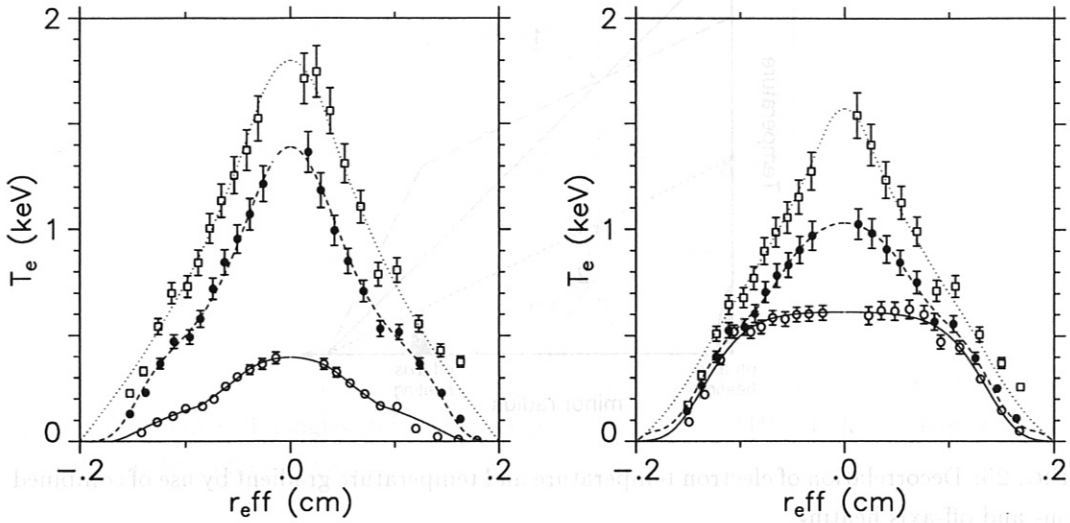

FIG. 26: Electron temperature profiles from ECE measurements for different ECH power deposition profiles in W7-AS. Left: on-axis heating with $P = 0.1$, 0.4 and 0.85 MW (open circles, solid line; solid circles, dashed line; squares, dotted line); right: off-axis heating with $P = 0.45$ MW plus an on-axis contribution of $P = 0$, 0.1 and 0.4 MW (same symbol sequence).

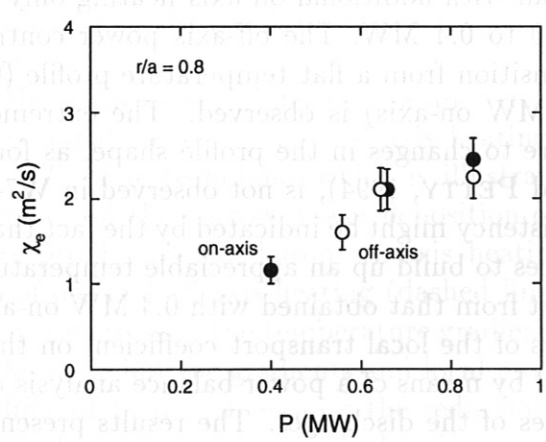

FIG. 27: Electron thermal diffusivity at $r/a = 0.8$ as a function of the total heating power. Open symbols denote conditions where 0.45 MW was deposited off-axis and the remainder on-axis.

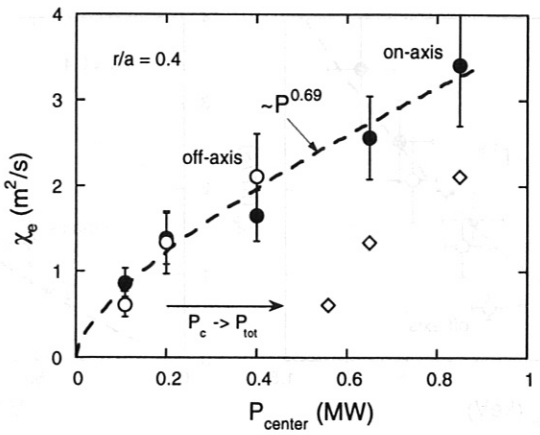

FIG. 28: Electron thermal diffusivity at $r/a = 0.4$ as a function of the on-axis heating power. Open symbols denote conditions where 0.45 MW was deposited off-axis and the remainder on-axis. If the data were plotted as a function of the total power, only the open symbols would move to the position of the squares (adapted from (STROTH *et al.*, 1995a).

outer plasma region. The diffusivities for on and off-axis heated discharges can be represented by an up to almost linear dependence on heating power. The temperature gradient at the plasma edge does not depend on how the power is distributed further in. This result is expected from a purely diffusive model. It also shows that quantities related to the deposited power density, such as the non-thermal particle fraction, which is very different in on- and off-axis heated discharges, do not sensitively determine the transport level.

Figure 28 shows that it is indeed the power deposited inside a flux surface which determines χ_e on the flux surface. The values of the diffusivity at r/a = 0.4 of the two scans can be well represented as a function of the on-axis power only. If the values are plotted versus the total heating power, the off-axis data move to the positions indicated by the diamonds and cannot be cast in a unique analytic form together with the on-axis data.

Hence, the degradation of the confinement time is also found in the electron transport coefficient. At both radial positions it increases as the power deposited inside the respective flux surface. As indicated in Fig. 28, the central value of the diffusivity can be represented by a power law similar to that valid for the confinement time. In the edge, the degradation seems to be stronger.

In Fig. 29 the evolution of the diffusivity in the plasma center with the electron temperature and temperature gradient is shown. A detailed discussion of the local dependences is not possible on the small database available. But some clear trends can be detected. As expected, an increase of the diffusivity with temperature and temperature gradient is observed and the degradation of the confinement time can also be interpreted by a dependence on the local plasma parameters. However, the local parameters do not parameterize the diffusivity as well as the global heating power. The dashed lines represent the fits to this restricted dataset. They are a very poor representation of the data

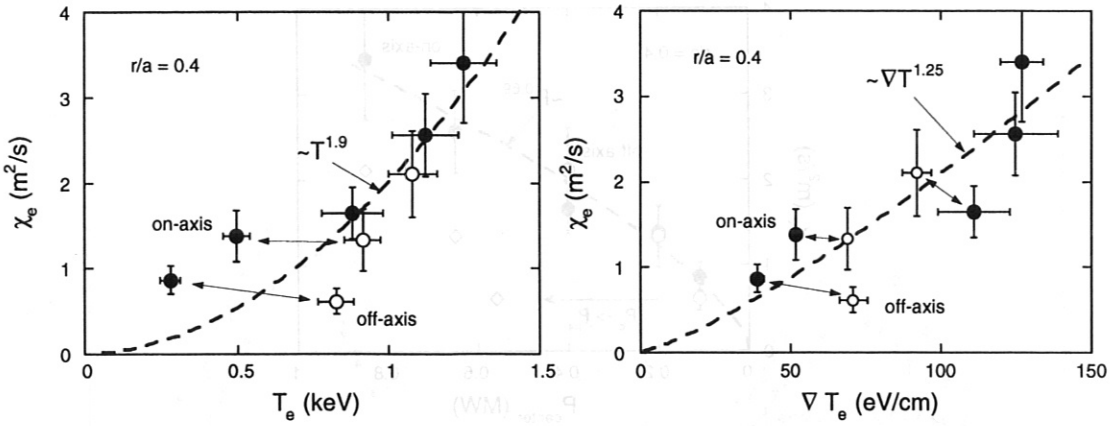

FIG. 29: Electron thermal diffusivity at $r/a = 0.4$ as a function of the the local electron temperature (left) and the gradient (right) for power scans in W7-AS. Open symbols denote conditions where 0.45 MW was deposited off-axis and the remainder on-axis.

and lead to dependences of the form $\chi \sim T^{1.9}$ or $\chi \sim \nabla T^{1.25}$. The strong scatter of the data is a result of the efforts to decorrelate the temperature and temperature gradient. Points connected by arrows are from discharges with the same amount of on-axis heating. In Fig. 29 it can be seen that although the diffusivities are similar the temperatures are very different. It is therefore not possible to describe the diffusivity as a function of the temperature only. If transport is local and does not depend on the temperature at all, then the temperature gradients of the connected data points should be the same. At least at the lowest heating powers this is not the case. Although the local heat fluxes are similar (electron-ion coupling makes only a small contribution) the gradients are different. This cannot be accounted for in a sole dependence on the temperature gradient or heating power. Hence there are other important effects which cannot easily be explained by simple dependences.

Especially the off-axis data point with 100 kW on-axis power is interesting. The produced gradient is steeper than that built up with 200 kW on-axis power only. This is reminiscent of the profile resilience observed in tokamaks and will be discussed in the next section.

In summary, the confinement time in electron-transport-dominated stellarator discharges degrades with increasing heating power. The degradation is found in the electron thermal diffusivity, which scales with the heating power deposited at smaller plasma radii. A simple description as a function of local parameters gives a much poorer representation of the data. The comparison with local parameters indicates, however, that in power degradation there are interesting processes involved which have to be studied on a larger dataset. They might be related to profile resilience, which is discussed in the next section.

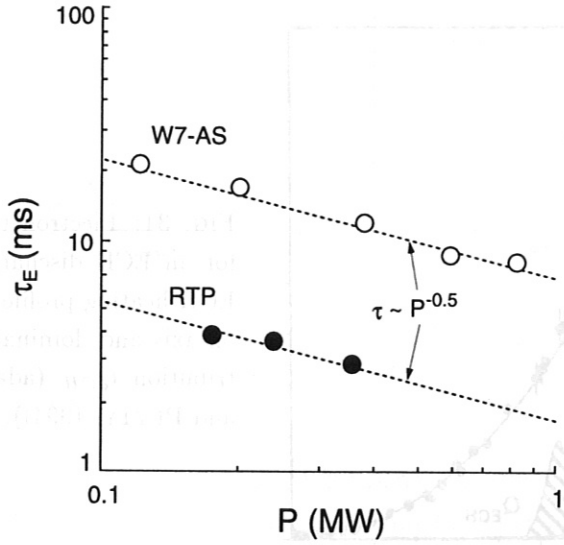

FIG. 30: Energy confinement time of ECH power scans at constant density in the RTP tokamak and the W7-AS stellarator (adapted from (PETERS *et al.*, 1994)).

9.3 Comparison of Power Degradation

Power degradation in stellarators and tokamaks and in electron and ion-transport-dominated plasmas is observed to be of the same order of magnitude. A direct comparison of ECH plasmas in the RTP tokamak and the W7-AS stellarator (PETERS *et al.*, 1994) is shown in Fig. 30. In both devices, the degradation is related to an increase in the local diffusivities which can be parameterized in terms of the heating power.

Since stronger heating usually results in higher temperatures and temperature gradients, it will always by possible to relate the increase in the diffusivity to the local temperature. A stringent test of the relevant parameter in terms of a local power balance is therefore only possible if T, ∇T and P can be decorrelated. In ASDEX this was done by increasing the density together with P and in W7-AS by modeling the temperature profile with the help of the power deposition profile. Both experiments showed that it is not meaningful to relate power degradation to the electron temperature as a leading agent.

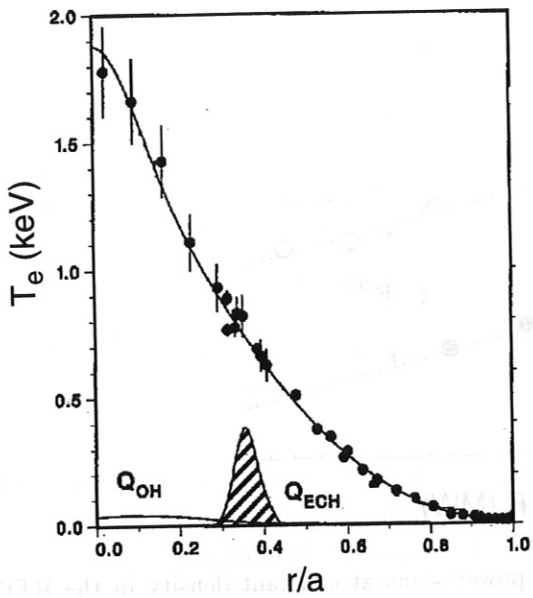

FIG. 31: Electron temperature profile for an ECH discharge in DIII-D. The ECH heating profile Q_{ECH} is centered off-axis and dominates the ohmic contribution Q_{OH} (adapted from (LUCE and PETTY, 1994)).

10 Profile Consistency

The absolute value of the electron temperature varies with the amount of heating power and, for tokamaks, the shape of the profile changes with the safety factor q (MURAKAMI *et al.*, 1986). At high q values the profile is more peaked. At a constant q value, however, it is difficult to modify the profile shape through variations in the power deposition profile. This stiffness of the electron temperature profile is known in the literature as profile resilience or profile consistency (COPPI, 1980) and is observed in many tokamaks (MURAKAMI *et al.*, 1986; WAGNER *et al.*, 1986; FREDRICKSON *et al.*, 1987). As illustrated in Fig. 4, the electron temperature gradient changes only little with large changes in the power flux. Hence, in a diffusive model the dependence of the diffusivity on temperature must be highly nonlinear. This links the problem of profile consistency to the problem of power degradation.

The electron temperature in tokamaks is linked through the electrical conductivity to the plasma current. Changes in the current profile can result in instabilities such as tearing modes. Hence, instabilities could put a restriction on the current profiles allowed and this in turn would also restrict the variability of the temperature profile. If the strong plasma current is the cause of this phenomenon, it should be absent in stellarators. And this is indeed the case. ECH-heated stellarator discharges with off-axis power deposition show flat temperature profiles within the deposition region (see Fig. 26).

One of the most extreme cases of profile consistency is observed in ECH-heated discharges in DIII-D (LUCE and PETTY, 1994). The electron temperature profile obtained by strong off-axis heating is reproduced in Fig. 31. Although the ECH power is absorbed at 1/3 of the plasma radius, the profile is similar to that obtained if the ECH is absorbed in the plasma center. By moving to the off-axis location, only a small decrease in the central temperature is

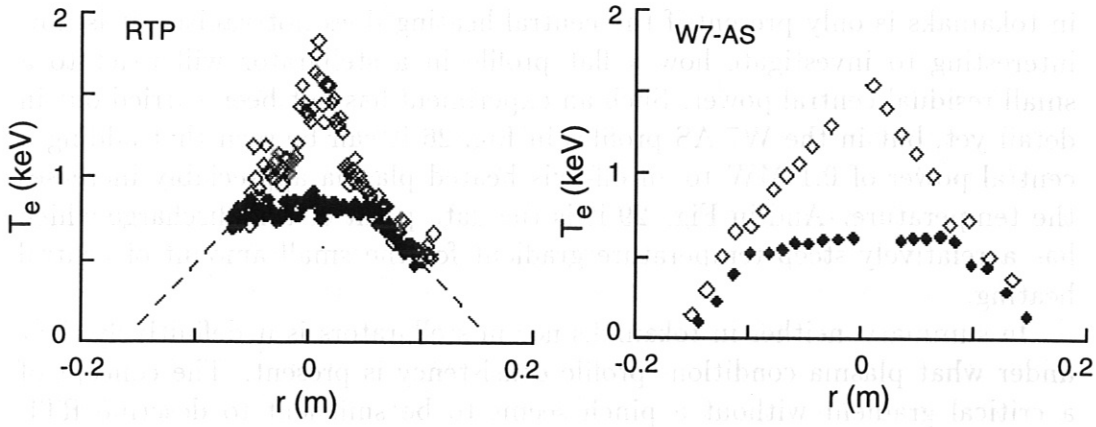

FIG. 32: Electron temperature profiles from RTP (left) and W7-AS (right) with on-axis (open symbols) and off-axis ECH (solid symbols) (adapted from (PETERS *et al.*, 1994)).

observed. In the center, the electron energy loss through collisional coupling to the ions is larger than the gain from ohmic heating. Hence, there must be an inward flow of heat in the electron channel. The observed heat pinch is much stronger than that predicted by neoclassical theory and an anomalous heat pinch (NORDMANN *et al.*, 1992; WEILAND and NORDMAN, 1993) would be required to explain the profile.

Experiments in JET have shown that the temperature profile can be forced to change its shape (BALET *et al.*, 1992). This was achieved by a combination of pellet injection and off-axis ICH. The electron temperature profile undergoes a transition from a hollow shape to one which is peaked in the final stage. It is shown that the evolution can be modeled without a heat pinch. This analysis was done in a one-fluid model. It shows that the total energy flux is directed down the gradients and that the entropy does not increase in the plasma center. However, since electron and ion channels cannot be separated, the experiment cannot rule out a pinch in the electron channel.

More recently, similar experiments in the RTP tokamak lead to a different result. In RTP and W7-AS, discharges were performed at similar plasma parameters (PETERS *et al.*, 1994). The temperature profiles obtained in both devices are depicted in Fig. 32. Discharges with on- and off-axis ECH are compared. In the case of off-axis heating the profiles are flat in RTP and W7-AS. For both experiments, strong pinches must be excluded in the discharges with the low central temperature gradient.

Other than in DIII-D, the RTP data could be interpreted in terms of a critical-gradient model. If there is heating in the plasma center the temperature is above a critical value and transport increases nonlinearly with the temperature gradient. This makes the profile resilient to changes. If the central heating is completely switched off, the temperature gradient falls below the critical value and transport is reduced to the neoclassical level.

The finding that there is no profile consistency in stellarators was based on the flat profiles during off-axis heating. We have now seen that the consistency

in tokamaks is only present if the central heating does not vanish. It is now interesting to investigate how a flat profile in a stellarator will react to a small residual central power. Such an experiment has not been carried out in detail yet, but in the W7-AS profiles in Fig. 26 it can be seen that adding a central power of 0.1 MW to an off-axis heated plasma appreciably increases the temperature. And in Fig. 29 it is the data point of this discharge which has a relatively steep temperature gradient for the small amount of central heating.

In summary, neither in tokamaks nor in stellarators is it definitively clear under what plasma conditions profile consistency is present. The concept of a critical gradient without a pinch seems to be sufficient to describe RTP and W7-AS. Under heating conditions with peaked profiles, of course, a pinch cannot be ruled out. In the steady-state profiles of RTP and W7-AS, there is only room for a pinch if it is *switched on* by the heating itself. It is difficult, however, to reconcile these results with the strong pinch found in DIII-D. It has been proposed that the pinch acts only at lower collisionality as in the DIII-D discharge (NORDMANN *et al.*, 1992; WEILAND and NORDMAN, 1993).

More information about the possible presence of pinches and nonlinear dependences on the temperature gradient can be acquired by heat pulse analyses discussed in the next section.

11 Transient Transport

Perturbative transport studies are an elegant tool for investigating the parameter dependences of the transport coefficients. The first experiments were done with short microwave pulses in a spheromak (EJIMA *et al.*, 1974) and on sawtooth propagation in the ORMAK tokamak (CALLEN and JAHNS, 1976). Later, the technique was extended to study particle and impurity transport. But most of the work treats the electron thermal diffusivity as well as off-axis elements of the electron heat transport. A recent review of the vast experimental data which is now available can be found in (LOPES CARDOZO, 1995).

It is not the objective of this section to give a full account of perturbative transport. We concentrate on experiments of importance for the stellarator-tokamak comparison.

The results from the different devices can be summarized briefly as follows: Electron temperature perturbations in tokamaks propagate faster than one would expect from the steady-state thermal diffusivity. In the W7-AS stellarator, on the contrary, the propagation takes place at a speed consistent with the steady state value. The difference between the diffusivities as determined from a steady-state power balance and the perturbative transport is very sensitive to the parameter dependences of the transport coefficient. Especially, the role of the temperature and the temperature gradient can be studied with good sensitivity. This allows us to continue the discussion started in the context of power degradation.

As a basis for this discussion, it is helpful to revisit some elementary equations.

11.1 Perturbative versus Power Balance Analysis

In general, a local power balance and a perturbative analysis yield transport parameters which are different from each other and which are usually both different from the actual thermal diffusivity. But in this difference lies the power of the method which compares the two results.

In a local power balance, the local heat flux q for each particle species is calculated from integrals over all sources and sinks. The value is then corrected for temporal changes in the energy content $\frac{3}{2}\frac{\partial}{\partial t}nT$ and for energy carried by convective particle fluxes $\frac{5}{2}nT\Gamma$. The transport coefficients are then calculated from the heat flux by

$$q = -n\chi\nabla T - u_{in}nT\,. \tag{24}$$

The convective velocity u_{in} comprises all off-diagonal elements of the transport matrix. Since the contribution from particle transport has already been subtracted, this term is a convective heat transport mechanism which is not connected with a net radial particle flow. In the literature it is referred to as a heat pinch (CALLEN *et al.*, 1987a).

In a power balance analysis, the heat flux is usually interpreted in terms of the diagonal term only. The calculated thermal diffusivity is therefore only

equal to the real thermal diffusivity χ if the pinch can be neglected. The relation between the power balance diffusivity and the real one is

$$\chi^{PB} = \chi - u_{in}\frac{T}{|\nabla T|} \,. \tag{25}$$

In order to simulate the propagation of a perturbation, the time-dependent form of Eq. (24) has to be solved. The analysis principles, however, can be very well seen in the linearized equation (GENTLE, 1988; LUCE *et al.*, 1993). The relation between the small perturbations (marked by a twiddle) and the unperturbed quantities (indexed with $_0$) is

$$\tilde{q} = -n\chi_0\nabla\tilde{T} - n\tilde{\chi}\nabla T_0 \,. \tag{26}$$

It is assumed that the pinch term does not change during the perturbation. If the process is analyzed in terms of a diagonal transport element only, again the calculated diffusivity is different from the real one. We refer to this quantity as the heat pulse value for the diffusivity and it is related to the real diffusivity of the unperturbed state χ_0 through

$$\chi^{HP} = \chi_0 + \tilde{\chi}\frac{\nabla T_0}{\nabla\tilde{T}} \,. \tag{27}$$

The two values for the diffusivity will only be the same if no changes in the diffusivity occur when the plasma parameters change ($\tilde{\chi} \equiv 0$). In heat pulse experiments, it is primarily the temperature and temperature gradient that will change. Hence, the heat pulse diffusivity gives the correct value only if the real diffusivity is independent of the local parameters. Otherwise, corrections have to be applied. For the models based on Eqs. (22) and (23) one obtains

$$\begin{aligned}
T: \;& \chi = \chi_0\left(\tfrac{T}{T_0}\right)^{\alpha} \;\Rightarrow\; \tilde{\chi} = \tfrac{\partial\chi}{\partial T}\big|_{T_0}\tilde{T} &&= \alpha\chi_0\tfrac{\tilde{T}}{T_0} \,, \\
\nabla T: \;& \chi = \chi_0\left(\tfrac{\nabla T}{\nabla T_0}\right)^{\beta} \;\Rightarrow\; \tilde{\chi} = \tfrac{\partial\chi}{\partial(\nabla T)}\big|_{\nabla T_0}\nabla\tilde{T} &&= \beta\chi_0\tfrac{\nabla\tilde{T}}{\nabla T_0} \,, \\
P: \;& \chi = \chi_0\left(\tfrac{P}{P_0}\right)^{\gamma} \;\Rightarrow\; \tilde{\chi} = \tfrac{\partial\chi}{\partial P}\big|_{P_0}\tilde{P} &&= \gamma\chi_0\tfrac{\tilde{P}}{P_0} \,.
\end{aligned} \tag{28}$$

With the perturbative method, the measured values will deviate from chi_0 if the diffusivity depends on the various parameters. For the three models, the measured value can be related to the real diffusivity through

$$T: \qquad \chi^{HP} = \chi_0\left(1 + \frac{\alpha c}{\sqrt{f_m}}\right) \,, \tag{29}$$

$$\nabla T: \qquad \chi^{HP} = \chi_0\left(1 + \beta\right) \,. \tag{30}$$

A temperature dependence acts in the same way as a convective term. It produces a term which does not depend on the perturbation of the temperature gradient. The enhancement depends on α, the power modulation frequency f_m and the plasma parameters (summarized in c). A dependence on the temperature gradient leads to an enhancement by a constant factor. It is important

to stress that any model which explains power degradation in terms of a diffusivity depending on the local plasma parameters (as in Eqs. 22) automatically leads to enhanced values for χ^{HP}. In the case of a temperature dependence, the correction is small at high modulation frequencies.

The global model is the only one in which the true thermal diffusivity is reproduced by a perturbative experiment:

$$P: \qquad \chi^{HP} = \chi_0 \,. \tag{31}$$

The global dependence, however, changes the transport equation (JACCHIA *et al.*, 1995). In the linearized form, this model produces an extra term which does not depend on the perturbed temperature or temperature gradient. It can therefore be treated as an additional source or sink term in the equation which determines the heat flux:

$$\nabla\tilde{q} = \tilde{p} - \frac{3}{2}n\frac{\partial\tilde{T}}{\partial t} = -\nabla n\chi_0\nabla\tilde{T} + \gamma\frac{\tilde{P}}{P_0}Q_0(r) \,. \tag{32}$$

The additional term instantaneously follows the temporal evolution of $\tilde{P}$. But $\tilde{P} = \int \tilde{p}(r)dr$ is a global parameter taking into account the change in the radially integrated power deposited inside the radius at which the transport equation is evaluated. The size of the additional source term is given by the exponent of the power dependence of the diffusivity, the percentage of modulated power and the sum of all local sinks and sources in the stationary unperturbed state Q_0. The sign of Q_0 determines whether the additional term is a source or a sink. In the region of strong heating the term is negative and, moved to the other side of Eq. (32), reduces the available modulated power $\tilde{p}$. In the edge region, where radiation and coupling to the ions dominate, the extra term is positive and acts as if some power was synchronously modulated at this location together with the centrally modulated power.

The term is generated by the second derivative of the temperature profile, which is the consequence of sources and sinks in the volume element. If the transport coefficient changes according to Eq. 28 without changing the local plasma parameters, a second derivative leads to a lack or excess of energy in the volume element.

In summary, the comparison of results from perturbative and power balance analyses for the diffusivity is a very useful technique to disentangle the parametrical form of the electron thermal diffusivity. If pinches are absent, a power balance gives the true value for the diffusivity, and the ratio to the value obtained from the perturbative analysis is a direct indication of the importance of the local parameters. If $\chi^{HP} > \chi^{PB}$ with a constant value for the ratio, a dependence on temperature gradient follows; if the ratio depends on the modulation frequency, a temperature dependence can be concluded. If a strong inward energy pinch is present, the χ^{PB} would be reduced and the ratio would again be larger than one with the tendency to decrease with increasing temperature (or heating power). The global model will allow for $\chi^{HP} = \chi^{PB}$.

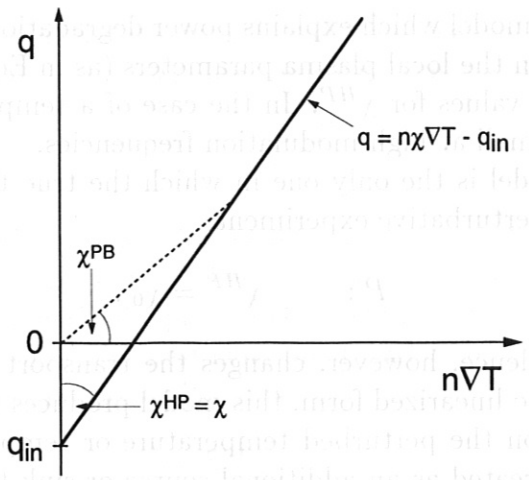

FIG. 33: Anomalous electron heat transport according to a electron thermal diffusivity which does not depend on temperature together with a heat pinch q_{in} (MANTICA *et al.*, 1996)

11.2 Transient Transport in Tokamaks

As a general trend in tokamaks, a larger value for the diffusivity from perturbative experiments than from the power balance is observed (LOPES CARDOZO *et al.*, 1990). The ratio can be as large as 10, as in TFTR (FREDERICKSON *et al.*, 1986). In JET, the enhancement factor was about 2.5 in ohmic discharges and became smaller when auxiliary heating was applied (TUBBING *et al.*, 1987). The findings were consistent with a critical temperature gradient model. Most analyses were done on sawtooth propagation and it has been argued that MHD perturbation produced by the sawtooth let the heat pulse propagate through a bed of enhanced turbulence which is not representative of the stationary level (MCGUIRE *et al.*, 1988). Taking into account the realistic redistribution of heat by the sawtooth crash can reduce the enhancement to one (FREDRICKSON *et al.*, 1990; FREDRICKSON *et al.*, 1993).

However, in ECH modulation experiments in RTP an enhancement factor in the range of of 2-4 was also measured (LOPES CARDOZO *et al.*, 1993). In RTP it is possible to describe the heat pulses from sawteeth and from power modulation with the same diffusivity (GORINI *et al.*, 1993; JACCHIA *et al.*, 1994). The value for χ^{HP} does not change as a function of the temperature, temperature gradient and heating power (HOGEWEIJ *et al.*, 1995) and therefore the ratio to the value from the power balance decreases with heating power. This is consistent with a heat pinch being important in RTP, and a model as described in Fig. 33 (HOGEWEIJ *et al.*, 1994) was developed for the description of anomalous transport in tokamaks. In the absence of a temperature gradient, there is a net heat flux in the inward direction. The diffusivity is assumed to be independent of the local parameters. Therefore, one has $\tilde{\chi} = 0$ in Eq. 26 and the heat pulse diffusivity is equal to the true one, which is represented by the slope of the solid line in the figure. The power balance analysis includes

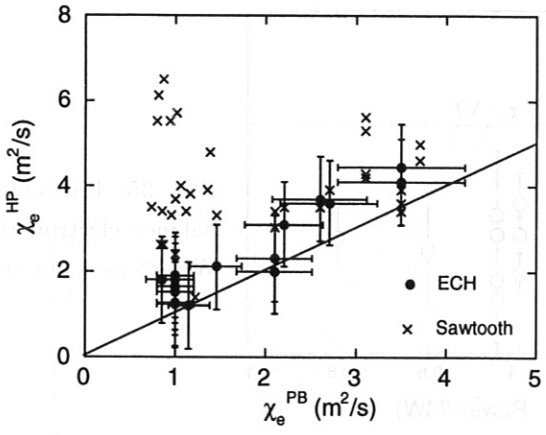

FIG. 34: Electron thermal diffusivity derived from sawtooth propagation and ECH modulation compared with the power balance diffusivity in ASDEX Upgrade (adapted from (RYTER *et al.*, 1996)).

the pinch in the diagonal term and yields a smaller value. As the temperature gradient increases with the heating power, the pinch becomes a small correction and both values approach each other. Direct evidence of a heat pinch was also found in off-axis power modulation experiments in DIII-D (LUCE and PETTY, 1994).

Recent results from ASDEX Upgrade indicate that sawtooth propagation could nevertheless be atypical of the thermal transport in tokamaks. In an analysis of heat pulses induced by sawteeth the heat pulse diffusivity was up to a factor of 5 larger than the power balance value (GIANNONE *et al.*, 1995; RYTER *et al.*, 1996). Interestingly, the difference depends on the size of the sawtooth. Analyses for different sawtooth amplitudes $\tilde{T}_e$ showed (KÖLLERMEYER, 1995) that the ratio between χ^{HP} and χ^{PB} decreases with the size of the perturbation. For small amplitudes, the value from sawtooth propagation roughly coincides with that estimated from a bower balance analysis. In contrast, ECH power modulation experiments were carried out and a value comparable with the power balance diffusivity was found in a wide range of values for the diffusivity (RYTER *et al.*, 1996). Fig. 34 shows the agreement between the two diffusivities in the case of ECH modulation and the large scatter in the case of sawtooth propagation studies.

To draw final conclusions on perturbative transport in tokamaks, further experiments are required. The results from ASDEX Upgrade question the applicability of sawtooth propagation for analysis of the heat transport and the differences in the results from ECH modulation have to be resolved.

11.3 Transient Transport in Stellarators

In stellarators, the sawtooth instability does not occur and ECH power modulation was used from the beginning to study the perturbative transport. In torsatrons, the magnetic topology complicates the use of ECH and ECE for

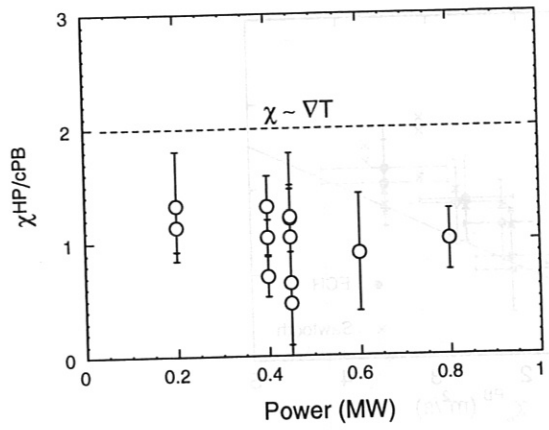

FIG. 35: Ratio of heat pulse to power balance electron thermal diffusivity in W7-AS as a function of heating power.

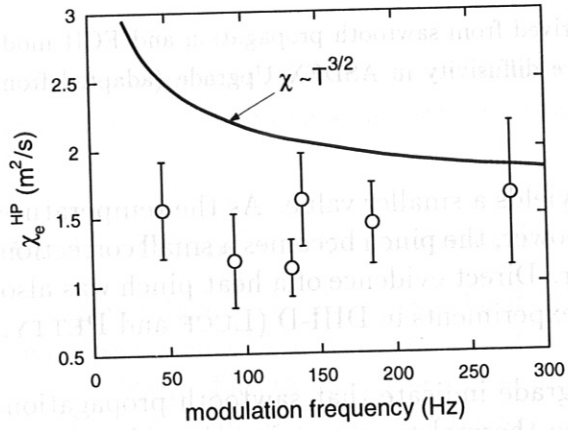

FIG. 36: Electron thermal diffusivity from heat pulse propagation as a function of ECH power modulation frequency. The line represents the predictions expected from a dependence of the diffusivity as $T^{3/2}$.

heat pulse analysis, which rely on accessible regions with a well-defined gradient in the magnetic field. Therefore, only results from the W7-A (HARTFUSS *et al.*, 1986) and W7-AS stellarators (GIANNONE *et al.*, 1992) are available. Both devices have locations around the major circumference where the toroidal magnetic field decays monotonically in the direction of the major plasma radius. This is an important asset for localized heating and localized temperature measurements with ECE.

From W7-AS, detailed studies based on ECH power modulation are available. The results can be summarized as follows (GIANNONE *et al.*, 1992; HARTFUSS *et al.*, 1994): The same value for the electron diffusivity is found from power balance and perturbative analyses, and the two estimates scale in the same way with the magnetic field, rotational transform, density and heating power. This is at variance with the diffusivity being a function of the electron temperature or temperature gradient. And it also rules out the existence of strong heat pinches in W7-AS. The heat pulse value of the diffusivity does not depend on the modulation frequency, which is also against a temperature dependence of the diffusivity.

In Fig. 35, the ratio of the heat pulse and the power balance diffusivity is shown as a function of the heating power. The values scatter around one and a dependence stronger than $(\nabla T)^{0.5}$ is inconsistent with the data. In Fig. 36, the values obtained from heat pulse analyses are plotted as a function of the

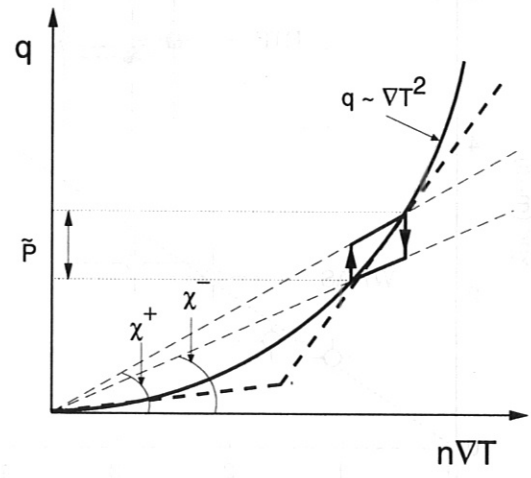

FIG. 37: Anomalous electron heat transport according to models which depend nonlinearly on the temperature gradient (solid and dashed lines) and the hysteresis which describes the plasma in a heat pulse cycle according to a global model (indicated by arrows) (adapted from (STROTH *et al.*, 1996a)).

ECH power modulation frequency. The modulation frequency varies from 50 to 280 Hz, but the value for the heat pulse diffusivity remains the same. Comparison with a temperature model rules out a dependence of the form $\chi \sim T^{3/2}$. Hence, a local model is inconsistent with the transient transport studies in W7-AS. Only the global model allows the two diffusivities to have the same value.

Together with the observed power degradation, these results can be interpreted in terms of the global model in Eq. 28, which is illustrated in Fig. 37. Under stationary conditions, represented by the solid line, the heat flux is approximately equal to the heating power deposited inside the flux surface. The diffusive relation to the temperature gradient is then given by $q \sim nq^{0.5}\nabla T$. This leads to the quadratic dependence of q on ∇T as plotted in the figure and it is in fair agreement with the power balance analysis of the power scan in Fig. 29. The exact functional dependence of the diffusivity on the heating power is not the critical element in the global model. Elements such as a critical temperature gradient as indicated by the dashed line could be incorporated. The critical element of the global model is that the diffusivity changes instantaneously with the heating power.

In the figure the global model resembles a local model. The difference occurs during a power modulation cycle. The relation between the heat flux and temperature gradient follows the hysteresis along the arrows. When the power is reduced, q decreases at constant ∇T. The diffusivity assumes the value χ^-, that corresponds to the reduced heating power. The distortion in the temperature gradient then relaxes to the steady-state gradient. This process is described as diffusive relaxation. The discharge passes through the second half of the hysteresis when the power is increased again, and the perturbation

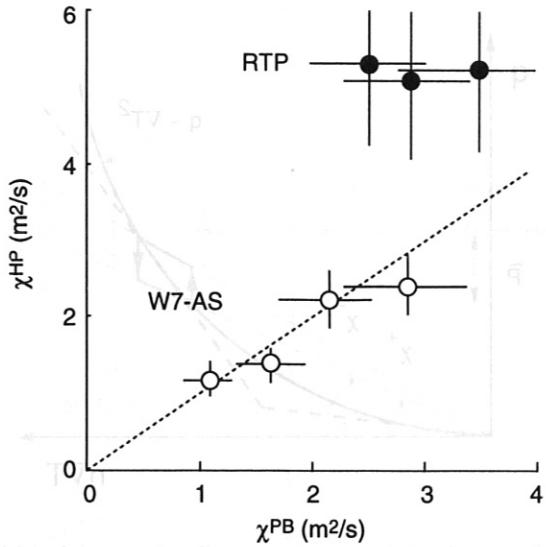

FIG. 38: Heat pulse and power balance electron thermal diffusivity from RTP and W7-AS (adapted from (PETERS *et al.*, 1994)).

propagates now with the value χ^+ of the diffusivity. In average, the heat pulse propagates according to a diffusivity close to the value measured by the power balance.

11.4 Comparison of Transient Transport

A direct comparison of ECH power modulation experiments in the RTP tokamak and the W7-AS stellarator was undertaken in (PETERS *et al.*, 1994; PETERS, 1995). Figure 38 summarizes the different results of tokamak and stellarator transport. It shows the comparison of the two diffusivities for the ECH power scans from Fig. 30. In the case of RTP, a constant value for the heat pulse diffusivity is found. The value is larger than the power balance value and the difference decreases with heating power. In W7-AS, in contrast, the two methods yield the same value and the same scaling with heating power.

Unification of the models for RTP (see Fig. 33) and for W7-AS (see Fig. 37) was suggested in Ref. (MANTICA *et al.*, 1996). A link is obtained by a heat pinch which increases with plasma current. In the currentless W7-AS the heat pinch would vanish and in RTP the power balance diffusivity would have to decrease with current. This is in line with experimental observations in RTP (PETERS, 1995), which can, however, also be interpreted by an improvement of confinement with current. On the other hand, a strong pinch in RTP is difficult to reconcile with the flat temperature profiles shown in Fig. 32.

In recent ECH power modulation experiments in ASDEX Upgrade results similar to those in W7-AS were found. The diffusivities from power modulation and from a power balance have the same value. The observation that heat pulses from the sawtooth instability propagate at a pace different to those from power modulation questions this method as a perturbative analysis method.

At present, the ASDEX Upgrade and W7-AS results are consistent with the global model. Since the ASDEX Upgrade results are different from other tokamaks, however, before drawing final conclusions, further power modulation experiments in tokamaks should be awaited.

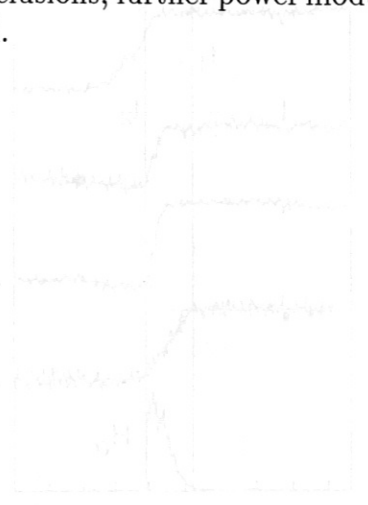

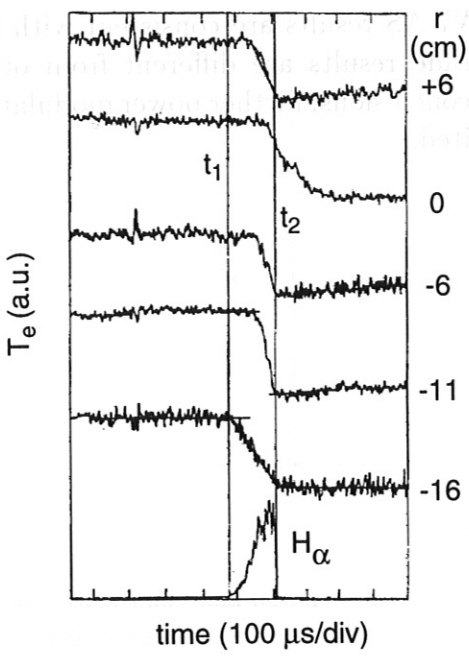

FIG. 39: Electron temperature evolution at different radii (indicated on the right) during pellet ablation in TFR. The H_α trace shows the light from the ablation cloud and indicates the end of the process at t_2 (adapted from (LAURENT and EQUIPE TFR, 1986)).

12 Non-local Effects in Transport

Recent observations in stellarators and tokamaks which point to the importance of non-local effects have shattered to some extent the belief in the local nature of transport . The experiments described below have in common that the local energy flux changes in the absence of a change in the thermodynamic variables. The change can be triggered from the plasma center and from the plasma edge, externally by the heating power, by impurity ablation or by pellets and intrinsically through L-to-H-mode transitions

12.1 Pellet Ablation

The pellet ablation experiment in Fig. 39 was carried out in the TFR tokamak (LAURENT and EQUIPE TFR, 1986). Two different aspects in the electron temperature evolution cannot be described by the transport coefficients valid before the discharge was perturbed: The cold front of the pellet penetrates at twice the pellet velocity. More importantly, at the end of the ablation process, the slope in the temporal evolution of the temperature changes within 10 μs at all plasma radii outside the q=1 surface. In terms of a thermal diffusivity this means a change from 0.5 to 10-100 m^2/s in the short time interval.

The authors put forward the concept of canonical profiles which minimize transport. Local distortion of these profile enhance transport everywhere. Since the density changes only on a time scale of milliseconds, the distortion of $\nabla T/T$ seems to be the relevant parameter. As soon as the local heat sink represented by the pellets vanishes, the diffusivity relaxes to the normal level.

Similar fast relaxation processes were also observed in ASDEX (VLASES *et al.*, 1983) and Alcator *C* (GREENWALD *et al.*, 1985). The results from TFR

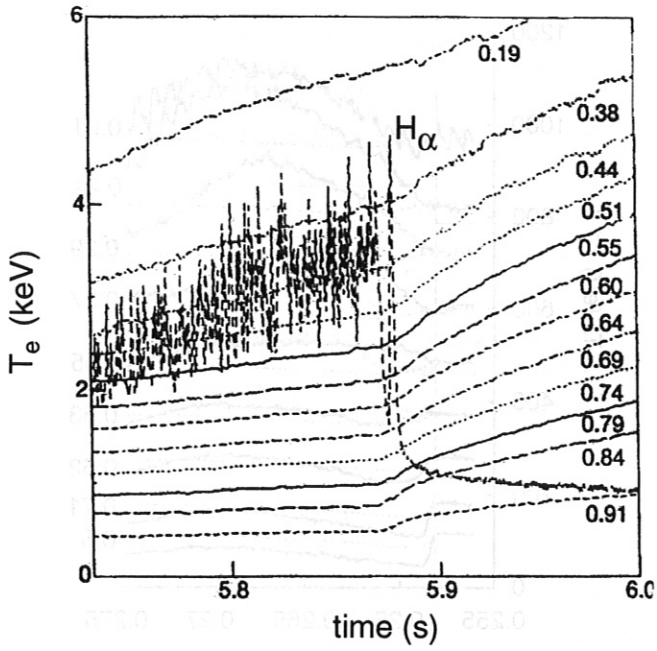

FIG. 40: Electron temperature versus time for different radii during an L-to-H transition in JET. The superposed H_α signal indicates the time point of the transition. The normalized radii of the temperature measurements are given on the right (adapted from (CORDEY *et al.*, 1995b)).

were recently confirmed in Tore Supra (LIU and TALVARD, 1994).

12.2 L-to-H Transition

The transition of a discharge from L to H-mode confinement occurs on a time scale of 100 μs. The initial confinement improvement is concentrated in a narrow edge region about 1 cm wide. The subsequent increase in density and temperature can propagate radially inward and be analyzed in the spirit of a perturbative experiment. The temperature changes which are observed in the plasma core can occur, however, on a much faster time scale than according to a diffusive propagation of the perturbation. This effect was observed in low-density discharges in JET (NEUDATCHIN *et al.*, 1993). In Fig. 40, an example from JET is shown (CORDEY *et al.*, 1995b). The transition time is indicated by the sharp decay in the H_α trace. Already after a delay which is very short compared with the confinement time of $\approx$0.5 s, the slope in the electron temperature evolution in the core responds to the change in the edge. Similar effects were also observed in the ion energy and momentum transport channels (CORDEY *et al.*, 1995a). The electron temperature evolution can be modeled best if the thermal electron diffusivity is changed everywhere from L to H-mode level within $\approx$4 ms (CORDEY *et al.*, 1995b). The authors claim that it is difficult to describe the data by a local model, unless a highly nonlinear dependence of the heat diffusivity on the temperature or temperature gradient

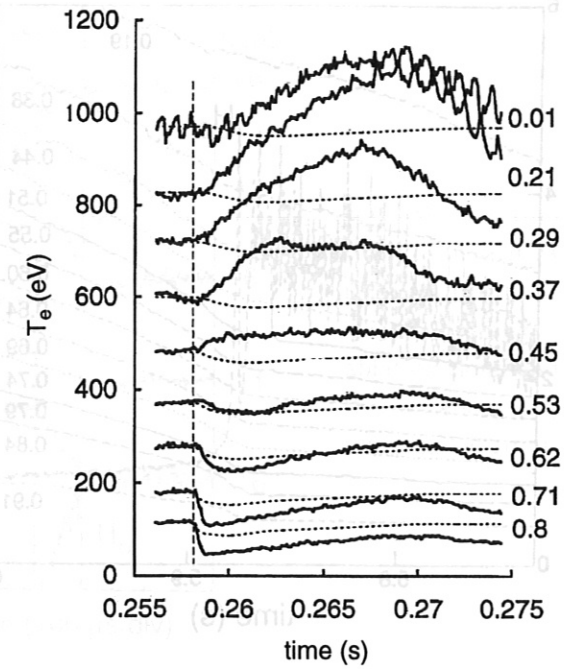

FIG. 41: Electron temperature evolution at different radii (indicated on the right) after carbon impurity injection in the plasma edge of TEXT. The dashed lines correspond to diffusion based on a local transport model (adapted from (GENTLE *et al.*, 1995)).

is assumed.

Radial mode coupling and fast propagation of turbulence is suggested as a possible process to explain the fast communication of the edge with the core plasma. Confirmation for this approach is found in a fast response of the density fluctuation amplitude (CORDEY *et al.*, 1995b).

12.3 Cold Pulse Propagation

Impurity injection into the plasma edge was proposed as an alternative method to generate perturbations in the electron temperature for transient transport studies. Results from first experiments in TFTR (KISSICK *et al.*, 1994) were similar to those from heat pulse propagation experiments discussed in Section 11. The *cold pulse* propagation is consistent with a diffusivity which is four times larger than the power balance value.

Experiments in the TEXT tokamak (GENTLE *et al.*, 1995), which were also in JET (JET TEAM, 1995), revealed, however, the importance of non-local effects in the response of transport to impurity injection. Figure 41 shows a very clear violation of local transport in TEXT (GENTLE *et al.*, 1995). Carbon was introduced by the laser ablation technique in order to cool the plasma edge. The radiation is limited to the outer 10% of the plasma radius. The cold produced pulse propagates diffusively inward. The surprising feature appears in the plasma core, where the temperature rises, though outside it drops. The

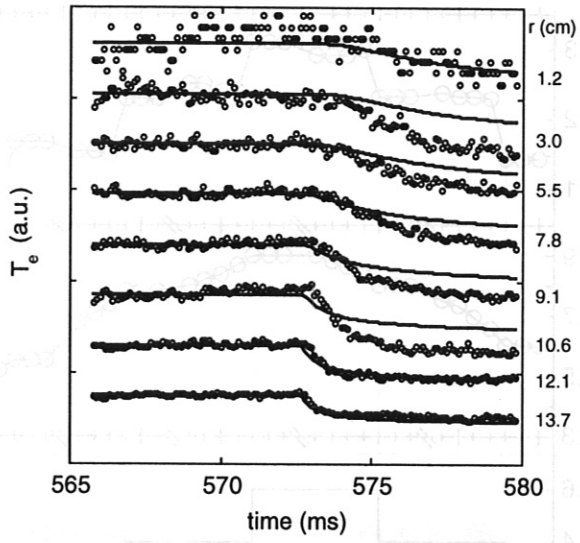

FIG. 42: Electron temperature evolution at different radii (indicated on the right) after aluminum impurity injection in the plasma edge of W7-AS. The discharge was heated by localized ECH at $r \approx 9$ cm (WALTER *et al.*,).

temporal evolution can be modeled if the thermal diffusivity increases by a factor of three to four in the outer 25% of the plasma radius on a time scale of about 100 μs and everywhere else by a factor of 2 in less than 1 ms. Since the ohmic heating power cannot change on this time scale, the reduction in the diffusivity generates an increasing temperature in the core.

Similar experiments were carried out in W7-AS (WALTER *et al.*,). Carbon was ablated by a laser and produces a dip in the edge temperature, which propagates inward. From impurity transport simulation with the SITAR code the radiation profile is determined to peak around 13 cm. In a period of 10 ms after ablation, the plasma inside 10 cm should not be affected by the additional carbon radiation. In Fig. 42 the time traces of the electron temperature are depicted at various radii and are compared with results from a time-dependent transport code. In the simulation, a stationary value for the heat diffusivity is used as obtained from a power balance analysis. No pronounced deviation from a diffusive propagation is observed. However, the observed temperature decay is faster than the one obtained from the simulations. This could point to a sudden increase of the diffusivity after carbon injection in the plasma core.

12.4 Dynamic Phases after Power Steps

The signature of non-local transport phenomena in the previous experiments was a fast response of the electron temperature. In experiments with power steps in W7-AS, the non-local transport was concluded from a too slow response of the temperature (STROTH *et al.*, 1993a; STROTH *et al.*, 1993b). After major changes in the centrally absorbed ECH power, the temporal evolution of the electron temperature profile is analyzed by means of a power

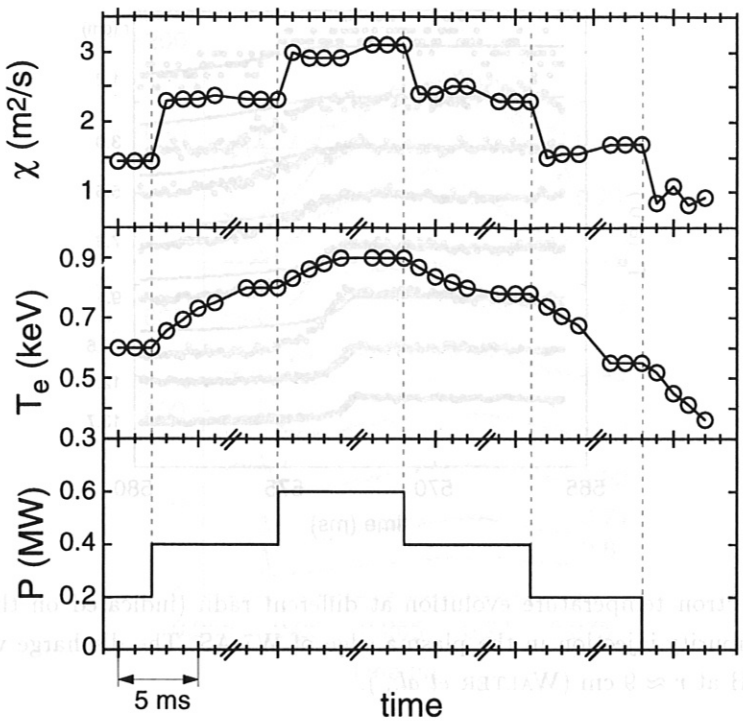

FIG. 43: Time evolution of the radially averaged ($0.35 \leq r/a \leq 0.85$) electron thermal diffusivity and temperature during the dynamic phases after changes in heating power.

balance. The slowing-down time of the non-thermal electron population produced by ECH is shorter than 0.1 ms. Hence, changes in power occur almost instantaneously.

Figure 43 shows the diffusivity from a power balance analysis outside the deposition zone. The response to power steps from 0.2 to 0.4 to 0.6 and back to 0 MW is instantaneous and decoupled from the temperature evolution. Right after changes in the power, the diffusivity jumps to the value, which corresponds to the new power level. When the power is decreased to zero, the diffusivity assumes a low non-zero value.

The analysis of the dynamic phases needs as important input the radial power deposition profile. A mechanism which could make the power deposition profile broader than expected from theory is related to suprathermal electrons produced by ECH. Due to the gradient in the magnetic field, particles which are trapped in a helical magnetic mirror suffer vertical drifts leading to radial displacements and power deposition outside the central heating location. In order to investigate this effect, experiments have been carried out in a configuration with a local magnetic field maximum at the heating location to be compared with the standard configuration, which has a small magnetic mirror.

A time-dependent simulation code was used to model the dynamic phases of the experiments in the two configurations (GIANNONE *et al.*, 1996). In Fig. 44, the ECE electron temperature drop for the phase after the power was decreased

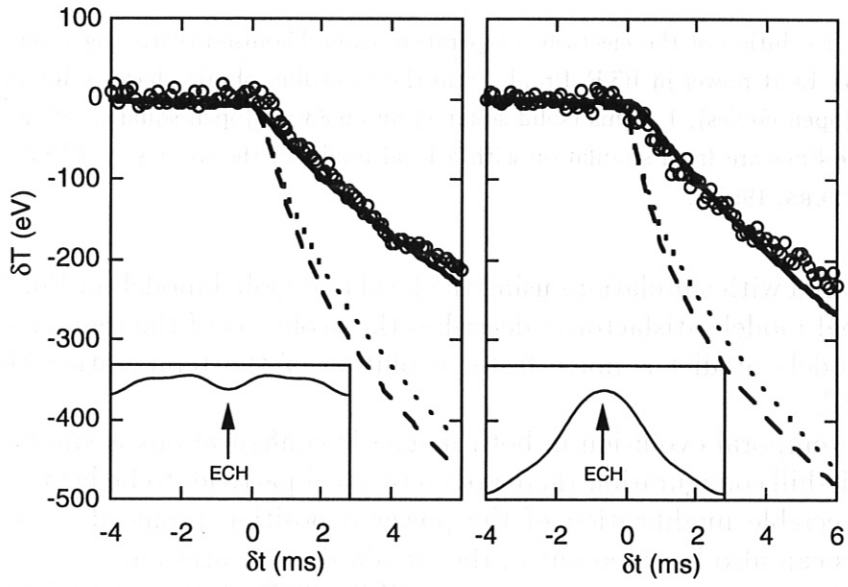

FIG. 44: Simulations of the dynamic phase after decreasing the ECH power at $\delta t = 0$ by 0.45 MW. Three models are used: $\chi(r)$ changes instantaneously with P (solid line), $\chi(r) \sim T(r)$ (dashed) and $\sim \nabla T(r)$ (dotted). The simulated changes in T are compared with ECE data at r/a = 0.22. The experiments were carried out in the standard magnetic configuration (left) and a hill configuration (right), where the ECH is absorbed in a local minimum and maximum of the magnetic field, respectively (see inserts). (Adapted from (STROTH *et al.*, 1996a))

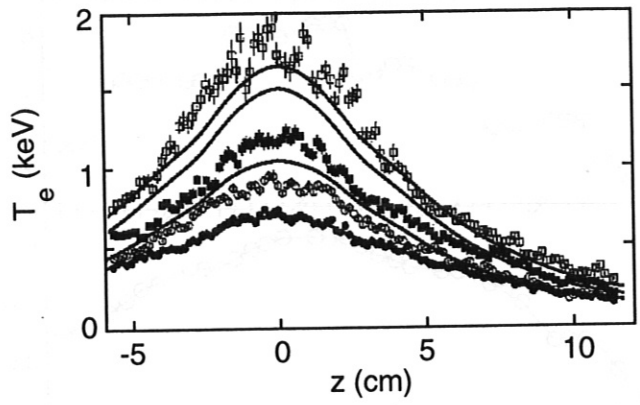

FIG. 45: Evolution of the electron temperature from Thomson scattering after switch-on of 330 kW ECH power in RTP. Profile from the preceding ohmic phase (solid circles) and 0.25 ms (open circles), 1.33 ms (solid squares) and 9.83 ms (open squares) after the power step. The lines are from simulation with a local model of the form $\chi \approx T^{3/2}/n$ (adapted from (PETERS, 1995)).

is compared with simulations using the local and global models of Eq. 28. Only the global model satisfactorily describes the evolution of the temperature. All local models predict a much faster evolution of the temperature than that measured.

The temporal evolution in both magnetic configurations is similar. In the magnetic-hill configuration there are no trapped particles to be heated. Hence, an appreciable modification of the power deposition profile due to trapped particles can also be ruled out in the standard configuration.

Similar results are reported from the TFR (TFR GROUP and FOM ECRH TEAM, 1988) and RTP (PETERS, 1995) tokamaks. As an example, Fig. 45 shows the increase in the electron temperature profile in RTP after switching on 330 kW ECH power in an ohmically heated discharge. The results are inconsistent with a local model of the form $\chi \approx T^{3/2}/n$. The data can be successfully described with a global model similar to the one used for W7-AS but also with a local model in which a heat pinch varies on a time scale of 5 ms.

12.5 Discussion

Although the signatures in the various experiments are similar, it is difficult to find a unifying picture for the observations. A picture where a local distortion of the temperature profile leads to immediate turbulence everywhere, as suggested by the pellet experiment, is in variance with the observation that transport is reduced when the edge temperature gradient is changed. This can be done in L-to-H transitions or by impurity ablation. Although the distortion in the temperature gradient goes into different directions in the two tokamak experiments, transport is reduced in both cases. In the case of W7-AS, in the

contrary, transport seems to be increased by cooling the edge.

Nevertheless, the concept of a canonical profile remains attractive because of its link to profile consistency. A working hypothesis could be that the canonical profile shape constrains only the temperature in the plasma core. If the profile is distorted, the plasma responds with enhanced turbulence. This is the case in the pellet experiment. Also in experiments with very localized heating power one tries to push the temperature profile into a non-canonical shape, and turbulence immediately increases or decreases as soon as this driving force is increased or decreased, respectively.

In this speculative picture, the plasma edge could play a role as the region where the turbulence is damped (e.g. through sheared rotation velocity, as in the H-mode). One would have an interplay between turbulence driving mechanisms in the core and damping ones in the edge.

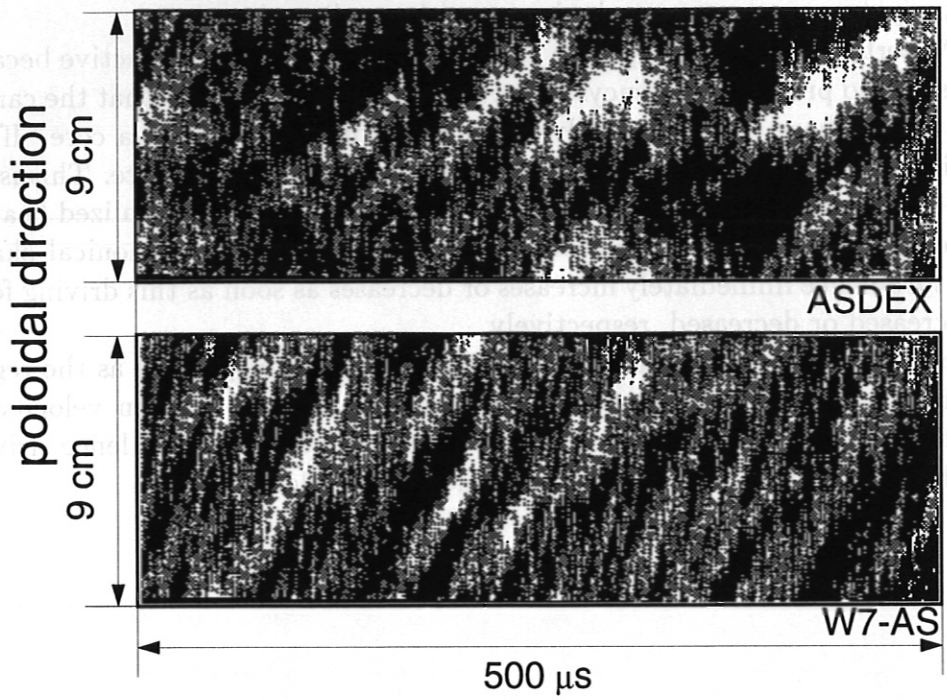

FIG. 46: H_α light intensity from the scrape-off layer of ASDEX (upper figure) and W7-AS (lower figure) measured in 16 channels covering 9 cm in the poloidal direction versus time (adapted from (ENDLER *et al.*, 1995) and courtesy of M. Endler).

13 Turbulence and Transport

Measuring the amplitudes of fluctuating plasma parameters is an alternative approach to explore anomalous transport. The strategy is to relate the measured fluctuations to the measured fluxes. For electrostatic turbulence it is not sufficient to measure the diffusivity and the density fluctuation amplitude. For a rigorous comparison, also the potential fluctuations, the phase to the density fluctuations and the radial correlation length have to be measured. Since this is only possible in the plasma edge, a rigorous comparison is restricted to this region. In the bulk, mostly a comparison with just one fluctuating quantity, the density $\tilde{n}$, is done.

Magnetic fluctuations are a sign of partial distortion of magnetic surfaces. They are also very difficult to measure in the plasma core. The influence on confinement of destroyed flux surfaces can also be studied on structures in temperature and density profiles or by pellet ablation.

13.1 Turbulence in the Scrape-off Layer

The plasma edge, and specially the scrape-off layer, is the plasma region which is best accessible to fluctuation measurements. In ASDEX and W7-AS, the fluctuation in the H_α light, which in this region is a good estimate of the density fluctuations, was measured with photomultipliers (ENDLER *et al.*, 1995).

Figure 46 shows grey-scale plots of the measured light in the two devices. The observed structures could be related to transport events as detected with Langmuir probes, which measure density, temperature and potential fluctuations. The analysis showed that the structures seen in the plots are due to single events which propagate in the ion-diamagnetic drift direction. Measurements along the field lines indicate correlation lengths of several meters along this direction in both devices (RUDYI *et al.*, 1989; BLEUEL *et al.*, 1996). The observed signatures are in qualitative agreement with a drift-wave type of model. With the observed amplitudes and phase shifts such a model would be able to explain a significant part of the anomalous transport in the scrape-off layer (ENDLER *et al.*, 1995).

This is one of the rare examples, where fluctuations are measured with signatures in agreement with drift-wave turbulence and with amplitudes and phases which could account for the anomalous transport. The structures seen in Fig. 46 are similar although they are taken from scrape-off layers with very small (W7-AS) and very strong (ASDEX) magnetic shear.

13.2 Turbulence in the Bulk

In the plasma core, density fluctuation amplitudes can vary in a correlated way with the thermal diffusivities. An example is the concurrent increase of the density fluctuation amplitude and the electron diffusivity towards the plasma edge as observed in the TFTR tokamak (FONCK *et al.*, 1992) or in the W7-AS stellarator (GIANNONE *et al.*, 1994).

For the density and power scans in W7-AS which are described in Sections 8 and 9 it was also attempted to relate the parameter dependence of the diffusivity to changes in the plasma turbulence level. Both density and temperature fluctuations were measured. For the density fluctuations, a heterodyne reflectometer was used. In order to obtain radial profiles, the frequency was varied during the discharge. Correlated ECE radiometers were used to measure the temperature fluctuations in the core region at $r/a \approx 0.5$ (SATTLER *et al.*, 1994).

In Fig. 47, the behavior of the density fluctuations in Tore Supra and W7-AS are compared. The evolution with density is similar and in both cases it correlates with the evolution of the electron thermal diffusivity as plotted in Figs. 18 and 21. We have seen that a density-dependent diffusivity explains the density dependence of confinement and the radial increase of the diffusivity to the plasma edge. Furthermore, the density fluctuation amplitude follows this evolution of the diffusivity in both respects. And it was shown that the measured density fluctuation amplitude in the scrape-off layer could be a sign of electrostatic turbulence which is able to account for the radial transport outside the separatrix. This connection via the turbulence from the edge to the core might indicate that the density dependence of the diffusivity is related to electrostatic turbulence.

Unlike in the density scan, in the power scan in W7-AS both the tempera-

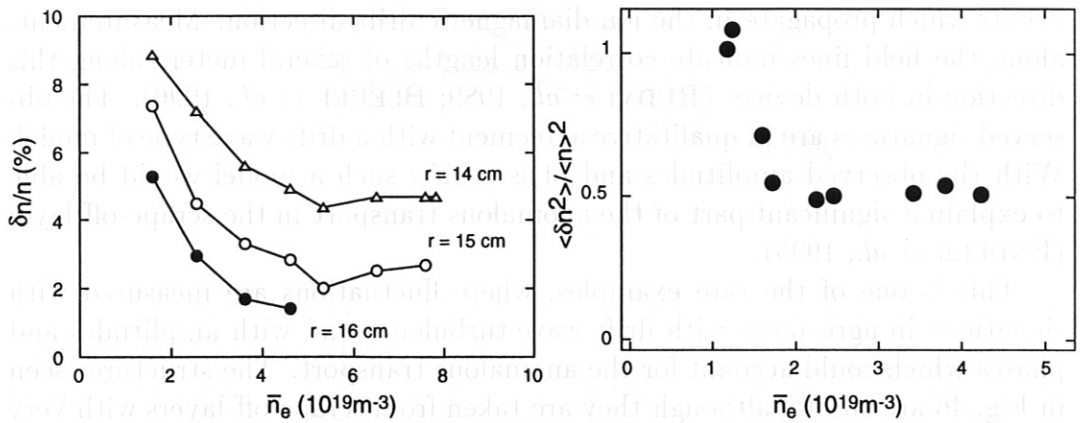

FIG. 47: Evolution of the density fluctuation amplitude during density scans in W7-AS and Tore Supra (adapted from (GARBET *et al.*, 1992)).

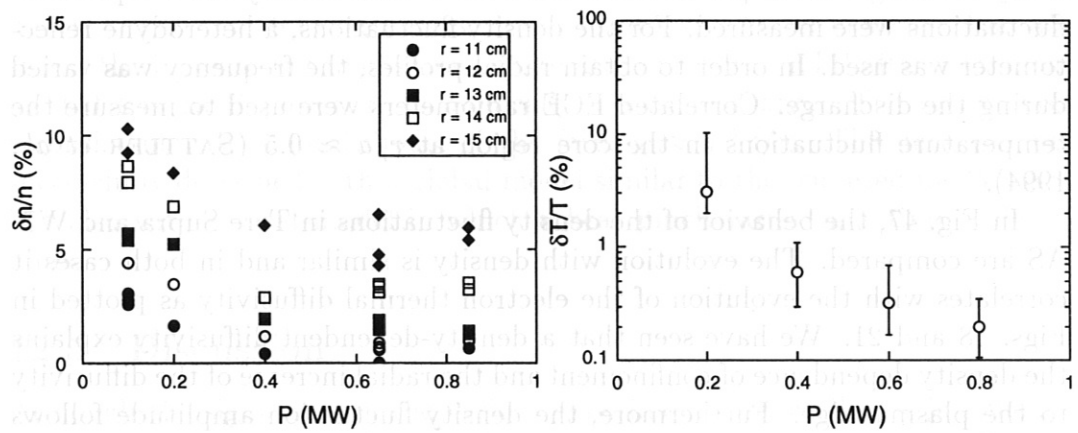

FIG. 48: Evolution of the density (left) and temperature (right) fluctuation amplitudes during a power scan in W7-AS.

ture fluctuations in the core region and the density fluctuations in the plasma edge do not follow the diffusivity. Figure 48 shows that the fluctuation amplitudes drop while the diffusivity in Fig. 27 increases. This might indicate that the dependence of confinement on the heating power has a origin different from that of the dependences on other plasma parameters. For a power scan in Tore Supra similar results are reported for the edge density fluctuations (GARBET *et al.*, 1995). In the core, however, the magnetic fluctuation level increases with increasing diffusivity.

Flat radial regions in the electron temperature profile like those in the JET profile in Fig. 6 are often interpreted as a sign of destroyed flux surfaces. Flux surfaces may be destroyed primarily at locations with rational values of the safety factor. In TFTR such structures were also seen in the profiles from Thomson scattering. A search of these structures with ECE diagnostics was, however, not successful (ZARNSTORFF *et al.*, 1993).

14 Summary and Conclusions

A comparative study of stellarator and tokamak confinement was conducted with the objective to elucidate about the importance of the magnetic configuration for anomalous transport. Plasma current, magnetic shear, rational values of the safety factor and, to a lesser extent, trapped particles are fundamental ingredients for many anomalous transport theories. If these parameters are leading ones in turbulent transport, one should observe different signatures of confinement in stellarators and tokamaks.

A comparison of global confinement on the basis of scaling expressions shows, however, that absolute value and parameter dependences of the confinement time are similar. The apparently different scaling expressions for stellarators and tokamaks become very similar if in tokamak scalings the plasma current is replaced by magnetic field parameters. This might trace the origin of the current scaling back to a magnetic-field dependence of the thermal diffusivities. The difference in the density dependence was studied in detail.

The density dependence of confinement in stellarators turns out to vanish in the case of ECH at high densities. Close similarity is observed between ECH discharges in stellarators and ohmically heated ones in tokamaks. In both regimes, the increase of confinement with density saturates at a critical density of comparable values. In stellarator and tokamak, a direct density dependence of the electron thermal diffusivity can account for the density dependence of the global confinement time.

An investigation of tokamak ohmic data shows, that the critical density, at which saturation sets in, decreases with increasing machine size. From experiments in smaller tokamaks too, a favorable density dependence was deduced in the neo-Alcator scaling. In larger devices, this had to be revised. Also in stellarators, transport might, in general, be independent of the density and the low-density electron-heated regime could be an exception. At present, this assumption is not entirely supported by NBI-heated discharges. In CHS, the saturation of the confinement time with density is observed, but in W7-AS the confinement time of NBI heated discharges increases up to the highest densities.

Very interesting remains the comparison of transient transport. New results from ASDEX Upgrade indicate that sawtooth propagation might not be the adequate tool to investigate thermal transport. The obtained value of the diffusivity depends on the size of the perturbation which is introduced by the sawtooth. This might explain the large differences, which are observed in some experiments between the diffusivity as deduced from sawtooth heat pulse and the power balance analyses. In ECH power modulation experiments in ASDEX Upgrade and W7-AS, the heat pulse and power balance diffusivities are about equal. This observation is difficult to reconcile with a local model for the diffusivity, which at the same time could account for the power degradation of the confinement time. It is an interesting question whether a heat pinch, which depends on the discharge parameters, can consistently explain these

features together with the ECH power modulation experiments in RTP, where an enhancement of the heat pulse diffusivity of a factor of 2 to 3 is found, or those in DIII-D, which provide direct evidence for a heat pinch. With further ECH power modulation experiments in larger tokamaks and at different plasma parameters it should be possible to clarify this point in the near future.

The heat pulse experiments in W7-AS were described by a model which relates the local diffusivity to the global heating power. This implies that local distortions of the plasma can instantaneously change the transport at distant locations. Such a model can also describe the transient response of the electron temperature after large changes in the heating power in RTP and W7-AS. Similar conclusions emerge from observations in tokamaks of the response of the plasma to L-to-H transitions or to pellet or impurity ablation. The diffusivity in the core changes prior to changes in the local thermodynamic variables. Although the observations in theses experiments are similar, it is not clear how they can be unified in a physics model. They all show that turbulence can communicate on shorter than the transport time scales. If the observations in stellarators and tokamaks have the same origin, this would rule out models, which explain the short time scale on the basis of radial coupling of modes which are located at major rational q values.

The observed confinement improvement with reversed magnetic shear discharges in tokamaks is contrasted with the observation in stellarators that reversed shear does not lead to a dramatic reduction in transport. Reversed shear might only be a prerequisite for the stability of steep pressure gradients. The confinement improvement, however, might be related to another mechanism such as the stabilization of turbulence by a sheared velocity flow.

Unresolved remains the difference in the isotopic effect. The magnitude of the effect strongly varies in tokamaks. Based on the available data, it was conjectured that the ratio of the ion Larmor radius to the turbulence scale length might be important for the strength of the observed isotopic effect. The absence of an isotopic effect in stellarators might as well be due to the smaller ion temperatures at which present stellarators are operated. It is worthwhile to resume the investigation of the isotopic effect in stellarators of the next generation.

In summary, transport in stellarators and tokamaks turns out to be more alike than it has previously appeared: Parameter dependences and absolute values of the energy confinement times are similar; the clear density dependence of stellarator confinement turned out to vanish above a critical density; in DIII-D it was found (LUCE *et al.*, 1995) that the electron thermal diffusivity follows, as in W7-AS, a gyro-Bohm-like scaling; like in W7-AS, in ASDEX Upgrade, heat pulse and power balance diffusivities with similar values were observed; and finally, discharge conditions were found in tokamaks, where profile consistency is violated, while there exists some evidence in W7-AS that the concept of a resilient electron temperature profile might be also relevant for stellarators. The remaining clear differences are the isotopic effect and some results connected with the investigation of power degradation.

Power degradation, transient transport, profile consistency and non-local effects are related problems. The common question is whether a temperature or temperature gradient dependent electron thermal diffusivity can explain the observations. At present, the results are contradictory: The existence of a heat pinch is indicated by the power modulation experiments in RTP and DIII-D. In the contrary, a strong pinch is in variance with the flat profiles observed in RTP and the ECH power modulation results from ASDEX Upgrade. If indications of profile consistency in W7-AS could be confirmed, this would also point to the importance of a pinch term or a critical temperature gradient. However, a strong pinch and a dependence on temperature gradient are in variance with the heat pulse experiments in the same device. Further experiments with ECH power modulation also at larger tokamaks and a stringent test of profile consistency on W7-AS should provide sufficient data for a more consistent picture in the near future.

There is some agreement between stellarators and tokamaks that strong dependences of the diffusivity on the temperature and the temperature gradient are not present. This must be concluded from the power scans in ASDEX, the power stepping experiments in RTP and W7-AS and the heat pulse experiments in ASDEX Upgrade, RTP and W7-AS. A variety of experiments in W7-AS can be consistently described by a non-local model for the diffusivity with a direct dependence on heating power. And also tokamak experiments revealed the importance of non-local effects in transport. It is too early for final conclusions, but it seems that a theory of anomalous transport should contain elements which can explain fast transport processes.

The similarity of the transport phenomena in the different devices indicates, that the strong toroidal plasma current, major rational q values inside the plasma or strong magnetic shear are possibly not central elements of a theoretical model for anomalous transport in fusion plasmas.

References

ALLADIO F., APRUZZESE G., BARBATO E., BARDOTTI G., BARTIROMO R., *et al.* (1991). Analysis of Saturated Ohmic Confinement in FT. In *Plasma Physics and Controlled Fusion Research (Proc. 13th Int. Conf., Washington, DC, 1990), IAEA, Vienna*, volume 2, page 153.

ATKINSON D. W., BRADLEY J., DELLIS A. N., GILL R. D., HAMBERGER S. M., *et al.* (1977). Confinement Studies in the Culham Stellarator with Ohmic Heating Currents. In *Plasma Physics and Controlled Fusion Research (Proc. 6th Int. Conf., Berchtesgaden, 1976), IAEA, Vienna*, volume 2, page 71.

BALET B., CORDEY J. G., MUIR D., and SCHMIDT G. (1992). *Nucl. Fusion* **32**, 1261.

BATHA S. H., LEVINTON F. M., ZARNSTORFF M. C., and SCHMIDT G. L. (1995). Supershot Performance with Reverse Magnetic Shear in TFTR. In *Proc. of the 22nd Europ. Conf. on Controlled Fusion and Plasma Heating, Bournemouth*, volume 2, page 113.

BESSENRODT-WEBERPALS M., WAGNER F., *et al.* (1993). *Nucl. Fusion* **33**, 1205–1238.

BLEUEL J. *et al.* (1996). The Edge-Turbulence in the W7-AS stellarator: 2D Characterization by Probe Measurements. In *Proc. of the 23rd Europ. Conf. on Controlled Fusion and Plasma Heating, Kiev.* to be published.

BRACCO G., BURATTI P., *et al.* (1993). Electron Heat Transport Analysis of FTU Ohmic Plasmas. In *Proceedings of the Varenna Meeting on Local Transport, Varenna*, page 63. Editrice Compositori, Bologna.

BURRELL K. H., AUSTIN M. E., CARLSTROM T. N., CODA S., DOYLE E. J., *et al.* (1995). H-mode and VH-mode confinement improvement in DIII-D: Investigations of Trubulence, Local Transport and Active Control of the Shear in the $E \times B$ Flow. In *Plasma Physics and Controlled Fusion Research (Proc. 15th Int. Conf., Seville, 1994)*, volume 1, page 221.

CALLEN J. D., CHANG Z., COFFEY R. L., GIANAKON T. A., HEGNA C. C., *et al.* (1993). Magnetic Island Effects, Interactions in Tokamaks. In *Proc. of the Varenna Meeting on Local Transport, Varenna*, page 243. Editrice Compositori, Bologna.

CALLEN J. D., CHRISTIANSEN J. P., CORDEY J. G., THOMAS P. R., and THOMSEN K. (1987a). *Nucl. Fusion* **27**, 1857–1875.

CALLEN J. D. and JAHNS G. L. (1976). *Phys. Rev. Lett.* **38**, 491–494.

CALLEN J. D., QU W. X., SIEBERT K. D., CARRERAS B. A., SHAING K. C., and SPONG D. A. (1987b). Neoclassical MHD Equations, Instabilities and Transport in Tokamaks. In *Plasma Physics and Controlled Fusion Research (Proc. 11th Int. Conf., Kyoto, 1986), IAEA, Vienna*, volume 2, page 157.

CARRERAS B. A. and DIAMOND P. H. (1989). *Phys. Fluids B* **1**, 1011.

CARRERAS B. A., GRIEGER G., HARRIS J. H., JOHNSON J. L., LYON J. F., *et al.* (1988). *Nucl. Fusion* **28**, 1613–1694.

CHALLIS D. D. *et al.* (1992). *Nucl. Fusion* **32**, 2217.

CHANDRASEKHAR S. (1961). *Hydrodynamic and Hydromagnetic Stability.* Oxford University Press.

CHRISTIANSEN J. P., DEBOO J., KARDAUN O. J., KAYE S. M., MIURA Y., *et al.* (1992). *Nucl. Fusion* **32**, 291–338.

COLCHIN R. J., MURAKAMI M., ANABITARTE E., ANDERSON F. S. B., BELL G. L., *et al.* (1990). *Phys. Fluids B* **6**, 1347.

CONNOR J. W. and TAYLOR J. B. (1977). *Nucl. Fusion* **17**, 1047–1055.

COOPER W. A. *Plasma Phys.* . submitted.

COPPI B. (1980). *Comments Plasma Phys. Controlled Fusion* **5**, 1305.

COPPI B., DETRAGIACHE P., MIGLINOLO S., NASSI M., ROGERS B., *et al.* (1993). Reconnection and Transport in High Temperature Regimes. In *Plasma Physics and Controlled Fusion Research (Proc. 14th Int. Conf., Würzburg, 1992)*, volume 2, page 131.

CORDEY J. G. *et al.* (1995a). *Nucl. Fusion* .

CORDEY J. G., MUIR D. G., PARAIL V. V., VAYAKIS G., ALI-ARSHAD S., *et al.* (1995b). *Nucl. Fusion* **35**, 505.

COTTRELL G. A., LOMAS P. J., MAY A. B., FIELDING S. J., and JOHNSON P. C. (1984). Analysis of High-Beta, Neutral-Beam Heated discharges in DITE Tokamaks. In *Heating in Toroidal Devices*, volume 1, page 105.

DOMINGUEZ R. R. and WALTZ R. E. (1987). *Nucl. Fusion* **27**, 65–79.

EJIMA S., OKABAYASHI M., and SCHMIDT J. (1974). *Phys. Rev. Lett.* **32**, 872.

EJIMA S., PETIRE T. W., RIVIERE A. C., ANGEL T. R., ARMENTROUT C. J., *et al.* (1982). *Nucl. Fusion* **22**, 1627–1649.

ENDLER M., NIEDERMEYER H., GIANNONE L., HOLZHAUER E., RUDYJ A., *et al.* (1995). *Nucl. Fusion* **35**, 1307.

ERCKMANN V., LAQUA H., MAASSBERG H., ROME M., STROTH U., *et al.* (1995). Response of the Plasma Confinement on Shear Modification by ECCD at W7-AS. In *Proc. of the* 21^{rst} *Europ. Conf. on Controlled Fusion and Plasma Physics, Montpellier*, volume 1, page 389.

ESIPTCHUK Y. V. and RAZUMOVA K. A. (1986). *Plasma Phys. Controlled Fusion* **28**, 1253.

FERRON J. R., LAO L. L., TAYLOR T. S., KIM Y. B., STRAIT E. J., *et al.* (1993). *Phys. Fluids B* **5**, 2532.

FONCK R. J., BTRETZ N., COSBY G., DURST R., MAZZUCATO E., *et al.* (1992). *Plasma Phys. Controlled Fusion* **34**, 1993.

FREDERICKSON E. D., CALLEN J. D., MCGUIRE K., BELL J. D., COLCHIN R. J., *et al.* (1986). *Nucl. Fusion* **26**, 849.

FREDRICKSON E. D., JANOS A. C., MCGUIRE K. M., SCOTT S. D., and TAYLOR G. O. (1993). *Nucl. Fusion* **33**, 1759.

FREDRICKSON E. D., MCGUIRE K. M., CAVALLO A., BUDNY R., JANOS A., *et al.* (1990). *Nucl. Fusion* **65**, 2869.

FREDRICKSON E. D., MCGUIRE K. M., GOLDSTON R. J., BELL M. G., GREK B., *et al.* (1987). *Nucl. Fusion* **27**, 1897–1904.

FUJIWARA M. *et al.* (1995). Present Status of Systems and their Prospects. In *Proc. of the* 6^{th} *Int. Toki Conf. on Plasma Phys. and Contr. Nuclear Fusion, Toki*, page 58.

GARBET X., CAPES H., CLAIRET F., COLAS L., DUBOIS M. A., *et al.* (1995). *Physica Scripta* **51**, 617.

GARBET X., PAYAN J., LAVIRON C., DEVYNCK P., SAHA S. K., *et al.* (1992). *Nucl. Fusion* **32**, 2147–2155.

GAUDREAU M., GONHALEKAR A., HUGHES M. H., OVERSKEI D., PAPPAS D. S., *et al.* (1977). *Phys. Rev. Lett.* **39**, 1266.

GENTLE K. W. (1988). *Phys. Fluids* **31**, 1105–1110.

GENTLE K. W., BRAVENEC R. V., CIMA G., GASQUET H., HALLOCK G. A., *et al.* (1995). *Phys. Fluids* .

GIANNONE L., BALBIN R., NIEDERMEYER H., ENDLER M., HERRE G., *et al.* (1994). *Plasma Phys.* **1**, 3614.

GIANNONE L., ERCKMANN V., GASPARINO U., HARTFUSS H.-J., KÜHNER G., *et al.* (1992). *Nucl. Fusion* **32**, 1985–1999.

GIANNONE L., STROTH U., KÖLLERMEYER J., ALEXANDER M., ERCKMANN V., *et al.* (1996). *Plasma Phys. Controlled Fusion* **38**, 477.

GIANNONE L., STROTH U., KÖLLERMEYER J., ALEXANDER M., ERCKMANN V., and OTHERS. (1995). Combined Analysis of Steady State and Transient Transport by the Maximum Entropy Method. In *Proc. of the* 22^{nd} *Europ. Conf. on Controlled Fusion and Plasma Physics, Bournemouth*, volume 4, page 265.

GOLDSTON R. J. (1984). *Plasma Phys. Controlled Fusion* **26**, 87.

GORINI G., MANTICA P., HOGEWEIJ G. M. D., DE LUCA F., JACCHIA A., KONINGS J. A., *et al.* (1993). *Phys. Rev. Lett.* **71**, 2038.

GREENWALD M., GWINN D., MILORA S., PARKER J., PARKER R., *et al.* (1984). *Phys. Rev. Lett.* **53**, 352–355.

GREENWALD M., GWINN D., MILORA S., PARKER J., PARKER R., *et al.* (1985). Pellet Fuelling Experiments in Alcator C. In *Plasma Physics and Controlled Fusion Research (Proc.* 10^{th} *Int. Conf., London, 1984), IAEA, Vienna*, volume 1, page 45.

GRIEGER G., BEIDLER C. D., MAASSBERG H., HARMEYER E., HERRNEGGER F., JUNKER J., *et al.* (1991). Physics and Engineering Studies for Wendelstein 7-X. In *Plasma Physics and Controlled Fusion Research (Proc.* 13^{th} *Int. Conf., Washington, DC, 1990), Vol. 3, IAEA, Vienna*, page 525.

GRISHAM L. R., SCOTT S. D., GOLDSTON R. J., BELL M. G., BELL R., *et al.* (1991). *Phys. Rev. Lett.* **67**, 66–69.

GRUBER O. (1984). Confinement Regimes in Ohmically and Auxiliary Heated Tokamaks. In *Plasma Physics (Proc. Int. Conf. Lausanne, 1984, Part 1,Commision of the European Communities, Brussels*, page 67.

H-MODE DATABASE GROUP (1993). ITER: Analysis of the H-Mode Confinement and Threshold databases. In *Plasma Physics and Controlled Fusion Research (Proc.* 14^{th} *Int. Conf., Würzburg, 1992)*, volume 3, page 251.

HARTFUSS H. J., ENDLER M., ERCKMANN V., GASPARINO U., GIANNONE L., *et al.* (1994). *Plasma Phys. Controlled Fusion* **36**, B17.

HARTFUSS H. J., MAASSBERG H., TUTTER M., *et al.* (1986). *Nucl. Fusion* **26**, 678.

HAWRYLUK R. J., ADLER H., ALLING P., ANCHER C., ANDERSON H., *et al.* (1994). *Phys. Rev. Lett.* **72**, 3530–3533.

HAWRYLUK R. J., ARUNASALAM V., BARNES C. W., BEER M., BELL R., *et al.* (1991). *Plasma Phys. Controlled Fusion* **33**, 1509–1536.

HOANG G. T., GIL C., JOFFRIN E., MOREAU D., BECOULET A., *et al.* (1994). *Nucl. Fusion* **34**, 75.

HOGEWEIJ G. M. D., DE LUCA F., GORINI G., JACCHIA A., KONINGS J. A., *et al.* (1994). Scaling of Incremental Heat Diffusivity with Heating Power, T and ∇T. In *Proc. of the* 21^{rst} *Europ. Conf. on Controlled Fusion and Plasma Physics, Montpellier*, volume 1, page 66.

HOGEWEIJ G. M. D., DE LUCA F., GORINI G., JACCHIA A., KONINGS J. A., *et al.* (1995). *Physica Scripta* **51**, 627.

HUGILL J. (1983). *Nucl. Fusion* **23**, 331.

HUGON M., P. M. B., SMEULDERS P., APPEL L. C., BARTLETT D. V., *et al.* (1992). *Nucl. Fusion* **32**, 33.

ITER DATABASE GROUP (1994). *nf* **34**, 131.

ITER DATABASE GROUP (1995). Projections of the ITER perfomance using the multi-machine L and H-mode databases. In *Plasma Physics and Controlled Fusion Research (Proc.* 15^{th} *Int. Conf., Seville, 1994)*, volume 2, page 525.

ITOH K., ITOH S.-I., FUKUYAMA A., YAGI M., and AZUMI M. (1994a). *Plasma Phys. Controlled Fusion* **36**, 279.

ITOH K., ITOH S.-I., FUKUYAMA A., YAGI M., and AZUMI M. (1994b). *Plasma Phys. Controlled Fusion* **36**, 1501.

JACCHIA A., DE LUCA F., GALLI P., GORINI G., and MANTICA P. (1995). *Phys. Plasmas* **2**.

JACCHIA A., DE LUCA F., HOGEWEIJ G. M. D., GORINI G., KONINGS N. J., *et al.* (1994). *Nucl. Fusion* **34**, 1629.

JACKSON G. L. *et al.* (1991). *Phys. Rev. Lett.* **67**, 3098.

JET TEAM (1995). Studies of Energy and Particle Transport in JET. In *Plasma Physics and Controlled Fusion Research (Proc.* 15^{th} *Int. Conf., Seville, 1994)*, volume 1, page 307.

KALLENBACH A., MAYER H. M., FUSSMANN G., MERTENS V., STROTH U., *et al.* (1991). *Plasma Phys. Controlled Fusion* **33**, 595–605.

KAMADA Y., USHIGUSA K., NAITO O., NEYATANI Y., OZEKI T., *et al.* (1994). *Nucl. Fusion* **34**, 1605.

KAUFMANN M., BÜCHL K., FUSSMANN G., GEHRE O., GRASSIE K., *et al.* (1988). *Nucl. Fusion* **28**, 827.

KAYE S. M. and GOLDSTON R. J. (1985). *Nucl. Fusion* **25**, 65–69.

KEILHACKER M., v. GIERKE G., MÜLLER E. R., MURMANN H., SÖLDNER F., *et al.* (1986). *Plasma Phys. Controlled Fusion* **28**, 29.

KESSEL C., MANICKAM J., REWOLT G., and TANG W. M. (1994). *Phys. Rev. Lett.* **72**, 1212–1215.

KISSICK M. W., FREDRICKSON E. D., CALLEN J. D., BUSH C. E., CHANG Z., *et al.* (1994). *Nucl. Fusion* **34**, 349.

KLÜBER, O. ENGELHARDT W., CANNICI B., GERNHARDT J., GLOCK E., *et al.* (1975). *Nucl. Fusion* **15**, 1194.

KÖLLERMEYER J. (1995). Untersuchungen von Sägezahnpulsen und ECRH-Modulation in ASDEX Upgrade. Master's thesis, Max-Planck-Institut für Plasma Physik, Garching.

LACKNER K. and GOTTARDI N. A. O. (1990). *Nucl. Fusion* **30**, 767–770.

LACKNER K., GRUBER O., WAGNER F., BECKER G., *et al.* (1989). *Plasma Phys. Controlled Fusion* **31**, 1629.

LAURENT L. and EQUIPE TFR (1986). *Plasma Phys. Controlled Fusion* **28**, 85–99.

LAZARUS E. A., LAO L. L., OSBORNE T. H., TYLOR T. S., TURNBULL A. D., *et al.* (1992). *Phys. Fluids B* **4**, 3644.

LIEWER C. (1985). *Phys. Fluids* **25**, 543–621.

LIU W. and TALVARD M. (1994). *Nucl. Fusion* **34**, 337.

LOPES CARDOZO N. J. (1995). *Plasma Phys. Controlled Fusion* **37**, 799–854.

LOPES CARDOZO N. J., DE HAAS J. C. M., HOGEWEIJ J., O'ROURKE J. O., SIPS A. C. C., and TUBBING B. J. D. (1990). *Plasma Phys. Controlled Fusion* **32**, 983–998.

LOPES CARDOZO N. J., HOGEWEIJ G. M. D., JASPERS R. J. E., KONINGS J. A., OOMENS A. A. M., *et al.* (1993). Transport Studies in the RTP tokamak. In *Plasma Physics and Controlled Fusion Research (Proc. 14th Int. Conf., Würzburg, 1992), IAEA, Vienna*, volume 1, page 271.

LUCE T. C., FOREST C. B., MAKOWSKI M. A., MEYER W. H., PETTY C. C., *et al.* (1993). Evidence from Modulated ECH for Convective-Like Transport. In *Proc. of the Varenna Meeting on Local Transport, Varenna*, page 155. Editrice Compositori, Bologna.

LUCE T. C. and PETTY C. C. (1994). *Nucl. Fusion* **34**, 121.

LUCE T. C., PETTY C. C., BURRELL K. H., FOREST C. B., GOHIL P., *et al.* (1995). Experimental Constraints on Transport. In *Plasma Physics and Controlled Fusion Research (Proc. 15th Int. Conf., Seville, 1994)*, volume 1, page 319.

MANTICA P., PETERS M., DE LUCA F., DE LAURINI A., GORINI G., *et al.* (1996). *Nucl. Fusion* . in press.

MANUEL M. E., RICE B. W., STRAIT E. J., LAO L. L., TAYLOR T. S., *et al.* (1995). Production and Stability of High-Beta DIII-D Discharges with Reversed Magnetic Shear. In *Proc. of the 22nd Europ. Conf. on Controlled Fusion and Plasma Heating, Bournemouth*, volume 4, page 137.

MCGUIRE K. M., ARUNSALAM V., BARNES C. W., BELL M. G., BITTER M., *et al.* (1988). *Plasma Phys. Controlled Fusion* **30**, 1391.

MEADE D. M., ARUNASALAM V., BARNES C. W., BELL M. G., BELL R., *et al.* (1991). Recent TFTR Results. In *Plasma Physics and Controlled Fusion Research (Proc. 15th Int. Conf., Washington, D.C., 1990), IAEA, Vienna*, volume 1, page 9.

MONTGOMERY D., PHILLIPS L., and THEOBALD M. L. (1989). *Phys. Rev. A* **40**, 1515.

MORITA S., YAMADA H., IGUCHI H., ADATI K., AKIYAMA R., *et al.* (1993). The Role of Neutral Hydrogen in CHS Plasmas with Reheat and Collapse, and Comparison with JIPP T-IIU Tokamak Plasmas. In *Plasma Physics and Controlled Fusion Research (Proc. 14th Int. Conf., Würzburg, 1992), IAEA, Vienna*, volume 2, page 515.

MÜLLER G. A., ERCKMANN V., HARTFUSS H., LAQUA H., MAASSBERG H., ROME M., STROTH U., and WELLER A. (1995). Shear Modification by ECCD and Related Confinement Phenomena in W7-AS. In *Proceedings of the 11th Topical Conference on Radio Frequency Power in Plasmas, Palm Springs.*

MURAKAMI M., ARUNASALAM V., BELL J. D., BELL M. G., BITTER M., *et al.* (1986). *Plasma Phys. Controlled Fusion* **28**, 17.

MURAKAMI M. *et al.* (1991). Energy Confinement and Bootstrap Current Studies in the Advanced Toroidal Facility. In *Plasma Physics and Controlled Fusion Research (Proc. 13th Int. Conf., Washington, DC, 1990), IAEA, Vienna*, volume 2, page 455.

MURMANN H., WAGNER F., *et al.* (1988). The Isotopic Dependence of Global Confinement in Ohmically and Auxiliary Heated ASDEX Plasmas. In *Proc. of the* 15^{th} *Europ. Conf. on Controlled Fusion and Plasma Heating, Dubrovnik*, volume 1, page 3.

NAVE M. F. F., EDWARDS A. W., HIRSCH K., HUGON M., JACCHIA A., *et al.* (1992). *Nucl. Fusion* **32**, 825.

NEUDATCHIN S. V., CORDEY J. G., and MUIR D. G. (1993). The Time Behaviour of the Electron Conductivity during L-H and H-L transitions in JET. JET report JET-P(93)58, JET Joint Undertaking, Oxon, OX143EA, UK.

NEVINS W. M., GOLDSTONE R. J., HILL D. N., JARDIN S. C., MEDLEY S. S., *et al.* (1993). Mission and Design of the Tokamak Physics Experiment TPX. In *Plasma Physics and Controlled Fusion Research (Proc.* 14^{th} *Int. Conf., Würzburg, 1992)*, volume 3, page 279.

NORDMANN H. *et al.* (1992). *Nucl. Fusion* **32**, 419.

NÜHRENBERG J., LOTZ W., MERKEL P., NÜHRENBERG C., SCHWENN U., STRUMBERGER, E. M., *et al.* (1995). Overview of Wendelstein 7-X Theory. In *Proc. of thr* 6^{th} *Int. Toki Conf. on Plasma Phys. and Contr. Nuclear Fusion, Toki*, page 71.

PARKER R. R., GREENWALD M., LUCKHARDT S. C., MARMAR E. S., PORKOLAB M., and WOLFE S. M. (1985). *Nucl. Fusion* **25**, 1127.

PEGOURIE B. and DUBOIS M. A. (1989). *Nucl. Fusion* **29**, 745.

PETERS M. (1995). *Electron Heat Transport in Current Carrying and Currentless Thermonuclear Plasmas.* PhD thesis, Technische Universiteit Eindhoven.

PETERS M., HARTFUSS H. J., STROTH U., DE LUCA F., ERCKMANN V., GIANNONE L., GORINI G., HOGEWEIJ G. M. D., JACCHIA A., KONINGS J. A., LOPEZ CARDOZO N. J., MAASSBERG H., and MANTICA P. (1994). A comparative heat pulse propagation study on RTP and W7-AS. In *Proc. of the* 21^{rst} *Europ. Conf. on Controlled Fusion and Plasma Physics, Montpellier*, volume 1, page 158.

REBUT P.-H., CHUYANOV V., HUGUET M., PARKER R. R., SHIMOMURA Y., *et al.* (1995). The ITER EDA Outline Design. In *Plasma Physics and Controlled Fusion Research (Proc.* 15^{th} *Int. Conf., Seville, Spain, 1994), IAEA, Vienna*, volume 2, page 451.

REBUT P. H., LALLIA P. P., and WATKINS M. L. (1989). The Critical Temperature Gradient Model of Plasma Transport: Applications to JET

and Future Tokamaks. In *Plasma Physics and Controlled Fusion Research (Proc. 12th Int. Conf., Nice, 1988), IAEA, Vienna*, volume 3, page 191.

RINGLER H., GASPARINO U., KÜHNER G., MASSBERG H., RENNER H., *et al.* (1990). *Plasma Phys. Controlled Fusion* **32**, 933–948.

ROMANELLI F. (1989). *Plasma Phys. Controlled Fusion* **31**, 1535.

ROMANELLI F. and BRIGUGLIO S. (1989). *Plasma Phys. Controlled Fusion* **31**, 1535–1549.

ROMANELLI F., TANG W. M., and WHITE R. B. (1986). *Nucl. Fusion* **26**, 1515–1528.

RUDYI, A. BENGTSON R. D., CARLSON A., GIANNONE L., KRÄMER M., *et al.* (1989). Investigation of low-frequency Fluctuations in the Edge Plasma of ASDEX. In *Proc. of the 16th Europ. Conf. on Controlled Fusion and Plasma Heating, Venice*, volume 1, page 27.

RYTER F., ALEXANDER M., BOSCH H. S., FUCHS J. C., GRUBER O., *et al.* (1995). H-Mode and L-Mode Confinement in ASDEX Upgrade: Comparison under conditions with low and high H-mode power threshold. In *Proc. of the 22nd Europ. Conf. on Controlled Fusion and Plasma Heating, Bournemouth*, volume 4, page 89.

RYTER F. *et al.* (1996). Confinement and Transport studies in Asdex Upgrade. In *Plasma Physics and Controlled Fusion Research (Proc. 16th Int. Conf.,Montreal, 1996), IAEA, Vienna.* to be published.

RYTER F. and THE H-MODE DATABASE WORKING GROUP (1996). *Nucl. Fusion* **36**, 1217.

SANO F., TAKEIRI Y., HANATANI K., ZUSHI H., SATO M., *et al.* (1990). *Nucl. Fusion* **30**, 81.

SATTLER S., HARTFUSS H. J., and W7-AS TEAM (1994). *Phys. Rev. Lett.* **72**, 653.

SCOTT B. D. (1992a). *Phys. Fluids B* **4**, 2468–2494.

SCOTT B. D. (1992b). *Plasma Phys. Controlled Fusion* **34**, 1977–1983.

SCOTT S. D., BARNES C. W., GRISHAM L. R., HAMMET G. W., HEIDBRINK W. W., *et al.* (1991). Local Transport Measurements During Auxiliary Heating in TFTR. In *Plasma Physics and Controlled Fusion Research (Proc. 15th Int. Conf., Washington, D.C., 1990), IAEA, Vienna*, volume 1, page 235.

SCOTT S. D., ERNST D. R., MURAKAMI M., ADLER H., BELL M. G., *et al.* (1995). *Physica Scripta* **51**, 394.

SEKI Y., KIKUCHI M., ANDO T., OHARA Y., NISHIO S., *et al.* (1991). The Steady State Tokamak Reactor. In *Plasma Physics and Controlled Fusion Research (Proc. 15th Int. Conf., Washington, D.C., 1990), IAEA, Vienna*, volume 3, page 473.

SIMMET E. E. (1994). *Ionenenergietransport in Elektronengeheizten Entladungen am Tokamak ASDEX.* PhD thesis, Max-Planck-Institut für Plasmaphysik, Garching.

SIMMET E. E. and STROTH U. Statistical Analysis of the Density and Energy Confinement Time at the Transition from Linear to Saturated Ohmic Confinement. to be published.

SIMMET E. E. and THE ADSEX TEAM (1996). *Plasma Phys. Controlled Fusion* **38**, 689.

SMEULDERS P. *et al.* (1995). *Nucl. Fusion* **35**, 225.

SÖLDNER F. X., BALET B., BARANOV Y., EKEDAHL A., FISCHER B., *et al.* (1995). Shear Reversal Experiments in JET. In *Proc. of the 22nd Europ. Conf. on Controlled Fusion and Plasma Heating, Bournemouth*, volume 4, page 113.

SÖLDNER F. X., MÜLLER E. R., WAGNER F., BOSCH H. S., EBERHAGEN A., *et al.* (1988). *Phys. Rev. Lett.* **61**, 1105.

STROTH U., BRANAS B., ESTRADA T., GIANNONE L., HARTFUSS H. J., HIRSCH M., KICK M., KÜHNER G., SATTLER S., BALDZUHN J., BRAKEL R., ERCKMANN V., JÄNICKE R., RINGLER H., and WAGNER F. (1995a). *Physica Scripta* **51**, 655.

STROTH U., FUSSMANN G., KRIEGER K., MERTENS V., WAGNER F., *et al.* (1991a). *Nucl. Fusion* **31**, 2291–2304.

STROTH U., GIANNONE L., ERCKMANN V., GEIST T., HARTFUSS H.-J., *et al.* (1993a). On the Diffusive Nature of W7-AS Transport. In *Proc. of the 20th Europ. Conf. on Controlled Fusion and Plasma Heating, Lisbon*, volume 1, page 349.

STROTH U., GIANNONE L., HARTFUSS H., *et al.* (1993b). Transient Transport Studies on W7-AS. In *Proc. of the Varenna Meeting on Local Transport, Varenna*, page 161. Editrice Compositori, Bologna.

STROTH U., GIANNONE L., and HARTFUSS H. J. (1996a). *Plasma Phys. Controlled Fusion* **38**, 1087.

STROTH U., KAISER M., RYTER F., and WAGNER F. (1995b). *Nucl. Fusion* **35**, 131–142.

STROTH U., KÜHNER G., RINGLER H., *et al.* (1993c). *Phys. Rev. Lett.* **70**, 936–939.

STROTH U., MURAKAMI M., YAMADA H., SANO F., DORY R. A., *et al.* (1996b). *Nucl. Fusion* **36**, 1063.

STROTH U., WAGNER F., GRUBER O., HERRMANN W., KALLENBACH A., *et al.* (1991b). On Temperature and Density Dependence of the ASDEX L-Mode Confinement. In *Proc. of the* 18^{th} *Europ. Conf. on Controlled Fusion and Plasma Heating, Berlin*, volume 1, page 101.

SUDO S., TAKEIRI Y., ZUSHI H., SANO F., ITOH K., *et al.* (1990). *Nucl. Fusion* **30**, 11–21.

SWAIN D. W., MURAKAMI M., BATES S. C., BUSH C. E., DUNLAP J. L., *et al.* (1981). *Nucl. Fusion* **21**, 1409.

TFR GROUP and FOM ECRH TEAM (1988). *Nucl. Fusion* **28**, 1995–2025.

TOI K., HAMADA Y., KAWAHATA K., WATARI T., ANDO A., *et al.* (1991). Study of Limiter H- and IOC-Modes by Control of Edge Magnetic Shear and Gas Puffing in the JIPP T-IIU Tokamak. In *Plasma Physics and Controlled Fusion Research (Proc.* 13^{th} *Int. Conf., Washington, DC, 1990), IAEA, Vienna*, volume 1, page 301.

TUBBING B. J. D., LOPES CARDOZO N. J., and VAN DER WIEL M. J. (1987). *Nucl. Fusion* **27**, 1843.

VLASES G., BÜCHL K., and CAMPBELL D. (1983). Studies of Tokamak Transport Based on Pellet Injection. In *Proc. of the* 11^{th} *Europ. Conf. on Controlled Fusion and Plasma Physics, London*, volume 1, page 127.

W7-A TEAM (1977). Ohmic Heating in the W7-A Stellarator. In *Plasma Physics and Controlled Fusion Research (Proc.* 6^{th} *Int. Conf., Berchtesgaden, 1976), IAEA, Vienna*, volume 2, page 81.

WAGNER F., BECKER G., BEHRINGER K., CAMPBELL D., EBERHAGEN W., *et al.* (1982). *Phys. Rev. Lett.* **49**, 1408–1412.

WAGNER F., BESSENRODT-WEBERPALS M., GIANNONE L., KALLENBACH A., MCCORMICK K., SÖLDNER F. X., and STROTH U. (1990). The Isotope Dependence of Confinement in ASDEX: Part 2. In *Proc. of the* 17^{th} *Europ. Conf. on Controlled Fusion and Plasma Heating, Amsterdam*, volume 1, page 58.

WAGNER F., GRUBER O., LACKNER K., MURMANN H. D., SPETH E., *et al.* (1986). *Phys. Rev. Lett.* **56**, 2187–2190.

WAGNER F. and STROTH U. (1993). *Plasma Phys. Controlled Fusion* **35**, 1321–1371.

WALTER H. *et al.* Cold Pulse Experiments in W7-AS. to be published.

WALTZ R. E. and BOOZER A. H. (1993). *Phys. Fluids B* **5**, 2201.

WALTZ R. E., DEBOO J. C., and ROSENBLUTH M. N. (1990). *Phys. Rev. Lett.* **65**, 2390–2393.

WEILAND J. and NORDMAN H. (1993). *Phys. Fluids B* **5**, 1669.

WOBIG H., MAASSBERG H., RENNER H., *et al.* (1987). Plasma Confinement in the W7-A Stellarator. In *Plasma Physics and Controlled Fusion Research (Proc.* 11^{th} *Int. Conf., Kyoto, 1986), IAEA, Vienna*, volume 2, page 367.

YUSHMANOV P. N., TAKIZUKA T., RIEDEL K. S., KARDAUN O. J. W. F., CORDEY J. G., *et al.* (1990). *Nucl. Fusion* **30**, 1999–2006.

ZARNSTORFF M. C., BARNES C. W., EFTHIMION P. C., HAMMETT G. W., HORTON W., *et al.* (1991). Advances in Transport Understanding using Perturbative Techniques in TFTR. In *Plasma Physics and Controlled Fusion Research (Proc.* 13^{th} *Int. Conf., Washington, DC, 1990),IAEA, Vienna*, volume 1, page 109.

ZARNSTORFF M. C., BATHA S., JANOS A., and LEVINTON F. L. (1993). Search for Radial Structures on TFTR. In *Proceedings of the Varenna Meeting on Local Transport, Varenna*, page 257. Editrice Compositori, Bologna.

ZARNSTORFF M. C., SCOTT S. D., BARNES C. W., BELL R., BUSH C. E., *et al.* (1995). Heating and Transport in TFTR D-T Plasmas. In *Plasma Physics and Controlled Fusion Research (Proc.* 15^{th} *Int. Conf., Seville, Spain, 1994), IAEA, Vienna*, volume 1, page 183.

ZUSHI H., SATO M., MOTOJIMA O., SUDO S., MUTOH T., *et al.* (1988). *Nucl. Fusion* **28**, 1801.

Danksagung

Einem Fusionsplasma lassen sich seine Geheimnisse nur entlocken, wenn viele gemeinsam an einem Strang ziehen. Das Experiment muß in gutem Zustand sein, es braucht erfahrene Operateure, das Plasma braucht zuverlässige Heizungen und es muß von Diagnostikern beobachtet werden. Die vorliegende Arbeit ist zustande gekommen, weil die vielen Kollegen, die diese Aufgaben betreuen, mich tatkräftig unterstützt haben. Es ist mir eine Freude, mich dafür bei meinen Kollegen am Wendelstein VII-AS zu bedanken. Dabei möchte ich die Bedeutung herausheben, die Herrn Hartfuß ECE-Diagnostik und Herrn Giannones Analysen für diese Arbeit haben.

Mein Dank gilt insbesondere Herrn Wagner, der diese Arbeit über die Jahre hinweg, zuerst an ASDEX und dann an W7-AS, mit zahlreichen Anregungen und großer Sachkenntnis unterstützt und gefördert hat.

Weiterhin danke ich Herrn Hübner für sein Interesse an dieser Arbeit und für Diskussionen mit ihm und seiner Gruppe, sowie für die anregenden Diskussionen mit meinen Kollegen von ASDEX Upgrade, vom FOM-Institut in Rijnhuizen und vom IFP in Milano.

Nicht zuletzt möchte ich Frau Dreier, Frau Eggeling und Frau Volkenandt für die freundliche Stimmung und die Unterstützung in verschiedensten Belangen danken.